REPUBLIC OF TURKEY

YILDIZ TECHNICAL UNIVERSITY

GRADUATE SCHOOL OF NATURAL AND APPLIED SCIENCES

DEVELOPMENT OF NANO PARTICLE REINFORCED ABRASION RESISTANT GLASS-CERAMICS

Nurullah ÇÖPOĞLU

MASTER OF SCIENCE THESIS

Department of Metallurgical and Materials Engineering

Material Program

Advisor

Assist. Prof. Dr. Buğra ÇİÇEK

July, 2020

REPUBLIC OF TURKEY

YILDIZ TECHNICAL UNIVERSITY

GRADUATE SCHOOL OF NATURAL AND APPLIED SCIENCES

DEVELOPMENT OF NANO PARTICLE REINFORCED ABRASION RESISTANT GLASS-CERAMICS

A thesis submitted by Nurullah ÇÖPOĞLU in partial fulfillment of the requirements for the degree of MASTER OF SCIENCE is approved by the committee on 21.07.2020 in Department of Metallurgical and Materials Engineering, Material Program.

Assist. Prof. Dr. Buğra ÇİÇEK

Yıldız Technical University

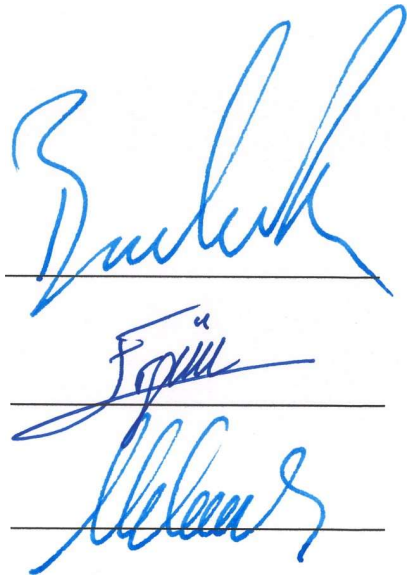
Advisor

Approved By the Examining Committee

Assist. Prof. Dr. Buğra ÇİÇEK, Advisor
Yıldız Technical University

Assoc. Prof. Dr. Ergün KELEŞOĞLU, Member
Yıldız Technical University

Prof. Dr. Mehmer SOMER, Member
Koc University



I hereby declare that I have obtained the required legal permissions during data collection and exploitation procedures, that I have made the in-text citations and cited the references properly, that I haven't falsified and/or fabricated research data and results of the study and that I have abided by the principles of the scientific research and ethics during my Thesis Study under the title of Development Of Nano Particle Reinforced Of Nano Particle Reinforced Abrasion Resistant Glass-Ceramics supervised by my supervisor, Assist. Prof. Dr. Buğra ÇİÇEK. In the case of a discovery of false statement, I am to acknowledge any legal consequence.

Nurullah ÇÖPOĞLU



Dedicated to my family and

my beautiful nieces

ACKNOWLEDGEMENTS

First of all, I would like to express my sincere appreciation to my advisor Assist. Prof. Dr. Buğra ÇİÇEK, who supported and guided me through my master studies and thesis studies with everything he can. This thesis would not be possible without his endless help, tireless support and patience.

I would like to thank Gizem Seramik Frit ve Glazür Co. Enamel R&D team for their endless support, all the information they did not hesitate to share, and industrial guidance. I would like to thank all the members of this valuable team, for whom I enjoyed working together, for their contributions.

My special thanks are for Gülfikar KOTAN and Ömer Burak YEL who were always with me in all my life and encouraged me during my master's education and thesis studies.

Finally, my deepest gratitude is definitely for my family for supporting me in this process, not leaving me alone and always being behind me. This thesis would not have accomplished without them.

Nurullah ÇÖPOĞLU

TABLE OF CONTENTS

LIST OF SYMBOLS XI

LIST OF ABBREVIATIONS XIII

LIST OF FIGURES XIV

LIST OF TABLES XVIII

ABSTRACT XIX

ÖZET XXI

1 INTRODUCTION 1

1.1 Literature Review 1

1.2 Objective of the Thesis 3

1.3 Abrasion Resistance 111

2 GLASS-CERAMICS 5

2.1 Definition of Glass-Ceramics 5

2.2 Properties of Glass-Ceramics 6

2.3 Application of Glass-Ceramics 7

3 ENAMEL 9

3.1 Definition of Enamel 9

3.2 Chemical Composition of Enamel 10

3.2.1 Fluxes 11

3.2.2 Refractories 11

3.2.3 Adhesion Agents 12

3.2.4 Opacifiers 12

3.2.5 Color Agents 12

3.3 Types of Enamel 12
3.3.1 Ground Coat 12
3.3.2 Cover coat 13
3.4 Properties of Enamel 14
3.4.1 Thermal Properties 14
3.4.2 Physical and Mechanical Properties 20
3.4.3 Chemical Properties 22
4 ENAMEL COATED METAL SURFACES 24
4.1 Cast Iron 24
4.2 Decarburized Steel 25
4.3 Low Carbon Steel 25
4.4 Interstitial Free Steel 25
4.5 Stainless Steel 26
5 ENAMEL COATING 27
5.1 Frit Production 27
5.2 Milling 29
5.2.1 Batch Amount 30
5.2.2 Mill Speed 30
5.2.3 Mill Additives 30
5.2.4 Milling Methods 32
5.3 Metallic Surface Preparation 33
5.3.1 Mechanical Cleaning 33
5.3.2 Chemical Cleaning 33
5.4 Coating Methods 35
5.4.1 Spraying Technique 35
5.4.2 Dipping 36

5.4.3 Flow Coating 36
5.4.4 Electrostatic (Wet) Spraying 36
5.4.5 Electrostatic Powder Spraying 37
5.4.6 Electrophoretic Coating 37
5.4.7 Thermal Spray Coating 37
5.5 Coating Process 38
5.5.1 One Coat One Fire 38
5.5.2 Two Coat Two Fire 38
5.5.3 Two Coat One Fire 38
5.5.4 Three Coat Two Fire 38
5.5.5 Three Coat Three Firing 399
5.6 Enamel – Metal Interface Relation 40
5.6.1 Mechanical Theory 40
5.6.2 Chemical theory 41
5.6.3 Electrolytic Theory 42
5.6.4 Diffusion Theory 43
6 TUNGSTEN (WOLFRAM) CARBIDE (WC) 44
6.1 Structure of Tungsten Carbide 44
6.1.1 Phase Equilibria of Tungsten Carbide 44
6.1.2 Crystal Structure of Tungsten Carbide 46
6.2 Physical Properties 47
6.2.1 Density and Melting Point 47
6.3 Mechanical Properties 47
6.3.1 Hardness 47
6.3.2 High Temperature Hardness of Tungsten Carbide 48
6.4 Thermal Properties 49

6.4.1 Thermal Conductivity 49
6.4.2 Thermal Expansion 49
6.5 Electrical and Magnetic Properties 50
7 ABRASION RESISTANCE 52
7.1 Abrasion Mechanism of Glass-Ceramic Structures 52
7.2 Abrasion standards 53
7.3 Improving Abrasion Resistance 54
8 EXPERIMENTAL STUDIES 58
8.1 Materials 58
8.2 Frit Preparation 58
8.3 Preparation of The Samples 58
8.4 Coating Process 60
9 CHARACTERIZATION STUDIES 61
9.1 Chemical Analysis 61
9.2 Microstructural Analysis 61
9.3 Phase Analysis 61
9.4 Thermal Analysis 61
9.5 Impact Resistance Analysis 62
9.6 Acid Resistance Analysis 62
9.7 Coating Thickness 62
9.8 Color Measurement 62
9.9 Gloss Measurement 63
9.10 Surface Roughness Analysis 63
9.11 Abrasion Resistance 63
10 RESULTS AND DISCUSSION 64
10.1 Chemical Analysis 64

10.2 Microstructural Analysis 67
10.2.1 Surface Analysis Before Abrasion Test 67
10.2.2 Cross-Section Analysis Before Abrasion Test 84
10.2.3 Surface Analysis After Abrasion Test 85
10.2.4 Cross-Section Analysis After Abrasion Test 103
10.3 Phase Analysis 65
10.4 Thermal Analysis 104
10.5 Impact Resistance Analysis 106
10.6 Acid Resistance Analysis 107
10.7 Coating Thickness 108
10.8 Color Measurement 108
10.9 Gloss Measurement 109
10.10 Surface Roughness Analysis 110
10.11 Abrasion Resistance 111
10.12 Conclusion and Recommendation 111
REFERENCES 118
PUBLICATIONS FROM THE THESIS 126

LIST OF SYMBOLS

A	Ampere
Ra	Arithmetic Average of the Roughness Profile
at. %	Atomic Percent
atm	Atmospheric Pressure
°C	Celsius Degree
cm	Centimeter
cm^3	Centimeter Cube
cm^2	Centimeter Square
GPa	Gigapascal
T_g	Glass Transition Temperature
g	Gram
A	Hall Coefficient
h	Hour
K	Kelvin
kg	Kilogram
kJ	Kilojoule
kV	Kilovolt
L	Lighness – Darkness in Color Values
α	Linear Thermal Expansion Coefficient
lt	Liter
MPa	Megapascal
m	Meter

m^3	Meter Cube
m^2	Meter Square
mg	Milligram
ml	Milliliter
µm	Micrometer
µΩ	Microohms
N	Newton
±	Plus – Minus
pH	Potential Hydrogen
a	Redness – Greenness in Color Values
sec	Second
c	Specific Heat
P	Tensile Strength
λ	Thermal Conductivity Coefficient
K	Thermal Shock
V	Volt
β	Volume Thermal Expansion Coefficient
W	Watts
wt. %	Weight Percent
b	Yellowness – Blueness in Color Values

LIST OF ABBREVIATIONS

DIN	Deutsche Institut für Normung
DTA	Differential Thermal Analysis
DSC	Differential Scanning Calorimetry
DSP	Disodium Phosphate
EDS	Energy-Dispersive X-Ray Spectroscopy
EN	European Norm
IEI	International Enamellers Institute
ISO	International Organization for Standardization
IF	Interstitial Free
PEI	Porcelain Enamel Institute
POESTA	Powder Electrostatic Application
RTU	Ready to Use
RT	Room Temperature
SEM	Scanning Electron Microscopy
STTP	Sodium Tripolyphosphate
D65	Standard Illuminant
TSP	Trisodium Phosphate
TSSP	Tetrasodium Pyrophosphate
VEA	Vitreous Enamel Association
XRD	X-Ray Diffraction
XRF	X-Ray Fluorescence

LIST OF FIGURES

Figure 2.1 From glass to glass-ceramic. (a) nuclei formation, (b) crystal growth on nuclei, and (c) glass-ceramic microstructure 5

Figure 2.2 The effect of temperature on nucleation and crystal growth in glasses 6

Figure 3.1 Viscosity – Temperature curve for a theoretical glass 18

Figure 3.2 Rate – Viscosity and Temperature graph of the enamels during firing process 19

Figure 5.1 Production steps of the frit production 27

Figure 5.2 Illustration of dendrite formation in the surface of the enamel coating during firing process 40

Figure 5.3 Ellingham Diagram 41

Figure 5.4 Electrolytic cells between molten enamel and cast iron 42

Figure 6.1 Generalised phase diagram of the W–C system 45

Figure 6.2 Hexagonal structure of higher δ-WC (WC) tungsten carbide: (•) C and (O) W 46

Figure 6.3 Hardness' of carbides as a function of temperature 48

Figure 6.4 Hot Knoop hardness of single crystal tungsten carbide of several alignments and polycrystalline tungsten carbide 49

Figure 7.1 Relationship of gloss and roughness according to the used mill additives 54

Figure 7.2 Mass loss graph of the studied mill additives with respect to the wt.% mill additive 55

Figure 7.3 Mass loss graph of the studied samples with the content of 1 wt. % particle addition after the Taber abrasion test 56

Figure 7.4 Gloss change percentage of the different particle added samples after the Taber abrasion test 56

Figure 7.5 Mass loss graph of the studied samples with different content of SiC particles after the Taber abrasion test 57

Figure 8.1 Flow chart of the experimental procedure done for this study 60

Figure 10.1 XRD patterns of the studied samples 65

Figure 10.2 Surface SEM image of the studied reference sample without nano-WC particles 67

Figure 10.3 EDS analysis results of the reference sample's shown surface 67

Figure 10.4 EDS mapping results of the reference sample 68

Figure 10.5 Surface SEM image of the studied W10 sample with 1 wt. % nano-WC particles addition 69

Figure 10.6 EDS analysis of the studied W10 sample with 1 wt. % nano-WC particles addition 70

Figure 10.7 EDS mapping results of the W10 sample with addition of 1 wt. % nano-WC particle addition 71

Figure 10.8 Surface SEM image of the studied W25 sample with 2.5 wt. % nano-WC particle addition 72

Figure 10.9 EDS analysis of the studied W25 sample with 2.5 wt. % nano-WC particles addition 72

Figure 10.10 EDS mapping results of the W25 sample with 2,5 wt. % nano-WC particles addition 74

Figure 10.11 Surface SEM image of the studied W50 sample with 5 wt. % nano-WC particle addition 75

Figure 10.12 EDS analysis of the studied W50 sample with 5 wt. % nano-WC particles addition 75

Figure 10.13 EDS mapping results of the W50 sample with 5 wt. % nano-WC particles addition 77

Figure 10.14 Surface SEM image of the studied W75 sample with 7.5 wt. % nano-WC particles addition 78

Figure 10.15 EDS analysis of the studied W75 sample with 7,5 wt. % nano-WC particles addition 78

Figure 10.16 EDS mapping results of the W75 sample with 7.5 wt. % nano-WC particle addition 80

Figure 10.17 Surface SEM image of the studied W100 sample with 10 wt. % nano-WC particles addition 81

Figure 10.18 EDS analysis of the studied W100 sample with 10 wt. % nano-WC particles addition 81

Figure 10.19 EDS mapping results of the W100 sample with 10 wt. % nano-WC particles addition 83

Figure 10.20 Cross-sections of the studied samples after the coating process; (a) reference sample, (b) W10, (c) W25, (d) W50, (e) W75 and (f) W100 84

Figure 10.21 Surface SEM image of the studied reference sample without nano-WC particles after the abrasion test. 85

Figure 10.22 EDS analysis of the reference sample without nano-WC particles after the abrasion test 85

Figure 10.23 EDS mapping results of the reference sample without nano-WC particles after the abrasion test 87

Figure 10.24 Surface SEM image of the studied W10 sample with addition of 1 wt. % nano-WC particles after the abrasion test 88

Figure 10.25 EDS analysis of the W10 sample with addition of 1 wt. % nano-WC particles after the abrasion test 88

Figure 10.26 EDS mapping results of the W10 sample with addition of 1 wt. % nano-WC particles after the abrasion test 90

Figure 10.27 Surface SEM image of the studied W25 sample with addition of 2.5 wt. % nano-WC particles after the abrasion test 91

Figure 10.28 EDS analysis of the W25 sample with addition of 2.5 wt. % nano-WC particles after the abrasion test 91

Figure 10.29 EDS mapping results of the W25 sample with addition of 2.5 wt. % nano-WC particles after the abrasion test 93

Figure 10.30 Surface SEM image of the studied W50 sample with addition of 5 wt. % nano-WC particles after the abrasion test 94

Figure 10.31 EDS analysis of the W50 sample with addition of 5 wt. % nano-WC particles after the abrasion test 94

Figure 10.32 EDS mapping results of the W50 sample with addition of 5 wt. % nano-WC particles after the abrasion test 96

Figure 10.33 Surface SEM image of the studied W75 sample with addition of 7.5 wt. % nano-WC particles after the abrasion test 97

Figure 10.34 EDS analysis of the W75 sample with addition of 7.5 wt. % nano-WC particles after the abrasion test 97

Figure 10.35 EDS mapping results of the W75 sample with addition of 7.5 wt. % nano-WC particles after the abrasion test 99

Figure 10.36 Surface SEM image of the studied W100 sample with addition of 10 wt. % nano-WC particles after the abrasion test 100

Figure 10.37 EDS analysis of the W100 sample with addition of 10 wt. % nano-WC particles after the abrasion test 100

Figure 10.38 EDS mapping results of the W100 sample with addition of 10 wt. % nano-WC particles after the abrasion test 102

Figure 10.39 Cross-sections of the studied samples after the abrasion test; (a) reference sample, (b) W10, (c) W25, (d) W50, (e) W75 and (f) W100 103

Figure 10.40 Sintering behavior graph of the studied samples 104

Figure 10.41 Dilatometer results of the studied frit composition 105

Figure 10.42 Color change of the studied sample at every 250 cycles of abrasion in terms of ΔE 111

Figure 10.43 Gloss change of the studied samples during the abrasion test 112

Figure 10.44 Mass loss of the studied samples during abrasion test.....113

Figure 10.45 Surface roughness (Ra) values of the studied samples at every abrasion cycles 115

LIST OF TABLES

Table 2.1 The main crystalline phases, properties and application areas of some glass-ceramic systems 7

Table 3.1 The classification of oxides according to their functions in the glass structure 10

Table 3.2 Cubical thermal expansion coefficients of some enamels and some metals 15

Table 3.3 Bulk densities and coefficient of thermal expansions of some enamel types 17

Table 4.1 Limit composition of cast iron for enameling applications 24

Table 4.2 Chemical composition of a commercial IF steel 26

Table 5.1 Some cleaner components and their function in chemical surface cleaning before the enamelling application 34

Table 5.2 Coating process techniques for some industrial application areas 39

Table 6.1 Density and Melting Point of WC, W and C 47

Table 6.2 Electrical Properties of WC 50

Table 6.3 The general properties of WC 51

Table 8.1 Studied enamel mixture composition 59

Table 8.2 Sample codes and nano-WC addition content in this study 59

Table 10.1 Chemical composition of the studied frit composition 64

Table 10.2 Sintering, softening, half sphere, sphere and melting temperatures of studied samples 105

Table 10.3 Impact resistance test results of the studied samples 106

Table 10.4 Acid resistance of the studied samples 107

Table 10.5 Coating thicknesses of the studied samples 108

Table 10.6 Color values of the studied samples in terms of D65 SCE 108

Table 10.7 Gloss values of the studied samples 109

Table 10.8 Surface roughness results of the studied samples 110

ABSTRACT

Development of Nano Particle Reinforced Abrasion Resistant Glass-Ceramics

Nurullah ÇÖPOĞLU

Department of Metallurgical and Materials Engineering

Master of Science Thesis

Advisor: Assist. Prof. Dr. Buğra ÇİÇEK

Glass-ceramic materials are inorganic materials that show a high similarity to the glasses in terms of chemical composition and the produced by the process of controlled crystallization with different methods. The properties of glass-ceramics are characterized as high strength, high impact resistance, low coefficient of thermal expansion, good resistance to thermal shock and a range of optical properties. Vitreous (porcelain) enamelling technology is a branch of glass-ceramic materials, which is used to protect the metallic substrates to bring aesthetical appearance owing to enamels' glass-ceramic structure.

Enamel coatings are subject to abrasion depending on the place of use, for example, metallic abrasion during cooking and cleaning. With abrasion, degradation occurs in the surface properties of enamels and at first they lose their aesthetic properties. The abrasion resistance property of enamel coatings is weak due to their high hardness and low fracture toughness properties.

The nano-WC hard ceramic particles used in the study were designed to remove stress points in the vitreous matrix and locally as nano particles, thereby increasing the abrasion resistance across the entire surface. 1, 2.5, 7.5 and 10 wt. % nano-WC

particles were added to the coating as a mill additive. All enamels were applied to cast iron surfaces by water spray method and fired at 770 °C for 12 min. Acid resistance, impact resistance and coating thickness of the enamel coatings obtained were analyzed. In addition, the abrasion resistance of the samples was tested with Taber abrasion device and H18 wheels. The changes in SEM, EDS, color, gloss, mass loss and surface roughness values were analyzed before and after the abrasion test of the samples.

According to the results obtained, the abrasion test W25 sample, with the addition of 2.5 wt. % nano-WC, showed the lowest mass loss and the lowest change in the surface properties. The lowest amount and the lowest size in the pores were also observed in the W25 sample and the sample had high abrasion resistance. It was observed that agglomeration occurred with the increase of nano-WC ratio in the samples and the abrasion resistance decreased. Thus, glass-ceramic coatings with a high abrasion resistance that do not distort the enamel coating surface properties were obtained by the addition of nanoparticles.

Keywords: Glass-ceramics, vitreous enamel coating, abrasion resistance, nano particle

ÖZET

Nano Partikül Takviyeli Aşınma Direnci Yüksek Cam-Seramiklerin Geliştirilmesi

Nurullah ÇÖPOĞLU

Metalurji ve Malzeme Mühendisliği Bölümü

Yüksek Lisans Tezi

Danışman: Dr. Öğr. Üyesi Buğra ÇİÇEK

Cam-seramik malzemeler, kimyasal bileşim açısından camlara yüksek benzerlik gösteren inorganik malzemelerdir ve kontrollü kristalizasyon adı verilen proses ile çeşitli yöntemlerle üretilmektedir. Cam seramiklerin özellikleri, yüksek mukavemet, yüksek darbe direnci, düşük termal genleşme katsayısı, yüksek termal şok direnci ve bir dizi optik özelliklerle karakterize edilir. Vitröz (porselen) emaye teknolojisi, metal substratları korumak ve emayelerin cam-seramik yapısı sayesinde estetik görünüm kazandırmak için kullanılan cam-seramik malzemelerin bir dalıdır.

Emaye kaplamalarda aşınma direnci özelliği, kaplama ömrü ve insan sağlığı endişeleri nedeniyle önemli bir mekanik özelliktir. Emaye kaplamalar, kullanım yerine göre, örneğin pişirme ve temizleme sırasında metalik aşınma, aşınmaya maruz kalır. Aşınma ile emayelerin yüzey özelliklerinde bozulma meydana gelir ve önce estetik özelliklerini kaybederler. Emaye kaplamaların aşınma direnci özelliği, yüksek sertlikleri ve düşük kırılma tokluğu özellikleri nedeniyle zayıftır.

Çalışmada kullanılan nano-WC sert seramik parçacıkları, vitröz matristeki ve lokal olarak nano parçacıkları olarak stres noktalarını gidermek, böylece tüm yüzey

boyunca aşınma direncini arttırmak için tasarlanmıştır. Ağırlıkça % 1, 2.5, 5, 7.5 ve 10 nano-WC partikülleri değirmen katkı maddesi olarak kaplamaya ilave edilmiştir. Bütün emayeler dökme demir yüzeylere sulu sprey yöntemi ile uygulanmıştır ve 770 °C'de 12 dakika pişirilmiştir. Elde edilen emaye kaplamaların asit direnci, darbe direnci ve kaplama kalınlığı analiz edilmiştir. Ayrıca, numunelerin aşınma direnci Taber aşınma cihazı ve H18 tekerleri ile test edilmiştir. SEM, EDS, renk, parlaklık, kütle kaybı ve yüzey pürüzlülük değerlerindeki değişiklikler, numunelerin aşınma testinden önce ve sonra analiz edilmiştir.

Elde edilen sonuçlara göre, aşınma testi W25 numunesi, ağırlıkça % 2.5 nano-WC ilavesi, en düşük kütle kaybını ve yüzey özelliklerinde en düşük değişikliği gösterdi. Gözeneklerdeki en düşük miktar ve en düşük boyut W25 numunesinde gözlenmiştir ve numune yüksek aşınma direncine sahiptir. Numunelerde nano-WC oranının artması ile aglomerasyonun meydana geldiği ve aşınma direncinin azaldığı gözlenmiştir. Böylece, yüzey özelliklerini bozmayan ve yüksek aşınma direncine sahip cam-seramik kaplamalar, nano partikül takviyesi ile elde edilmiştir.

Anahtar Kelimeler: Cam-seramikler, vitröz emaye kaplama, aşınma direnci, nano partikül

1
INTRODUCTION

1.1 Literature Review

Glass-ceramic materials are defined as materials produced by controlled crystallization and nucleation of glasses. Its first production is found in the Li_2O-SiO_2 (lithium silicate) glass structure by the formation of $Li_2Si_2O_5$ (lithium disilicate) crystals on the Ag (silver) precipitates due to the furnace's overheating. It is understood that when the formed material accidentally falls to the ground and does not break, it has different mechanical properties than glasses [1]. As its structure implies, it contains the properties of glass and ceramic materials. Oxides used in its structure provide glass-ceramic materials with high mechanical resistance, thermal resistance and chemical resistance. Thanks to these superior properties, glass-ceramic materials are used in many different fields such as industrial kitchen equipment, telescope mirrors, radar heads, electrotechnology, dentistry, prostheses, building materials and architectural panels [2].

Vitreous (porcelain) enamels are inorganic coatings with a glass-ceramic structure. Its production is based on the principle of making amorphous structures ready for coating suitable for controlled crystallization called frit. Many oxides SiO_2 (silicon dioxide), B_2O_3 (boron oxide), Al_2O_3 (aluminum oxide), Na_2O (sodium oxide), K_2O (potassium oxide), Li_2O (lithium oxide), as well as smaller amounts of BaO (barium oxide), SrO (strontium oxide), CaO (calcium oxide), CuO (copper oxide), MgO (magnesium oxide), CoO (cobalt oxide), NiO (nickel oxide), TiO_2 (titanium dioxide), ZrO_2 (zirconium dioxide), etc. are combined to produce the frit and the batch is melted at 1200 - 1500 °C temperatures. The molten material is fritted with water-cooled rollers or poured directly into water. The frit structures formed are grinded and made ready for the coating process. The critical point in the coating process is the application parameters. Mill additives vary depending on whether the application is water-based or electrostatic. While organosilicon oil is used in

electrostatic applications, clay, sodium nitrite ($NaNO_2$), boric acid (H_3BO_3) etc. are used in wet applications. Enamel coating is obtained by firing electrostatic or wet applied enamel at 720 – 850 °C. The resulting coating has high thermal resistance, mechanical resistance and chemical resistance. Another property of enamel coating is their aesthetic appearance. Smooth, glossy or matt and desired color surfaces can be obtained with enamel coating. Thanks to the superior properties obtained, it is widely used in many fields such as heaters, fireplaces, gas and electric cookers, clock faces, cookware, hot water services, etc. [3].

Enamels show a brittle fracture mechanism against mechanical effects due to their glass-ceramic structures. Cracks and micro voids in the structure show low resistance against mechanical effects since they have high stress. Abrasion resistance is the ability of materials to withstand the effects of abrasion. The abrasion process may include the surface layer of the coating (surface abrasion) or the material beneath it (sub-surface surface abrasion). Surface abrasion can simply be understood from the loss of gloss on the surface. Sub-surface abrasion is larger scale damage and includes degradation of the metal substrate [4, 5]. Abrasion resistance property increases with hardness. Enamels exhibit optimum corrosion resistance and high hardness, but low fracture toughness weakens the abrasion resistance. In addition, the high number of pores in the structure weakens the abrasion resistance. Since the abrasion mechanism is based on brittle fracture, the degradation starts from weak points. Particle agglomeration and pores are weak points and areas for the onset of nucleation and cause crack formation. Abrasion resistance provides resistance against mechanical abrasions and scratches [6]. Micro and macro abrasions create a path between the enamel layer and the metal. This path causes the substrate metal to corrode and the coating to lose its function completely. In addition, element migration occurs from the abraded surface to the food contact surfaces. The level of migration increases gradually and in the following years, it causes fatal diseases due to the accumulation of harmful elements in the body.

In order to increase the abrasion resistance of enamel coatings, ideas to increase mechanical strength have been proposed [7]. The first studies aim to increase

strength with the use of mill additives. Another thought suggests that by adding hard particles into the enamel matrix, mechanical strength can be increased. During the grinding processes, the particles are coated with the injection of additives. The aim is to reduce the pore sizes by obtaining a composite enamel. In the literature, feldspar [$K(AlSi_3O_8)$], zircon (ZrO_2), corundum (Al_2O_3), spodumene [$LiAl(Si_2O_6)$] and quartz (SiO_2) additives have been studied and it has been demonstrated that quartz and spodumene particles increase the abrasion resistance. As their usage increases, they increase frit viscosity and decrease the pore size [8]. Another method used to increase enamel abrasion resistance is the advanced particle addition method. The particles to be added are expected to withstand enamel firing temperature and show good affinity with the vitreous matrix. Since it is a new research area, limited information is available about the compatibility between particles and the vitreous matrix. The particles should be well connected and bonded to the vitreous matrix. Because the particles are required not to form weak spots and pores. The particles used in the literature are tungsten carbide (WC), silicon carbide (SiC) and graphite (C)[9, 10].

1.2 Objective of the Thesis

The first objective of the study is to investigate the effect of nano particle addition on enamel coating. Due to the complex oxide structure in enamel coatings, it does not always respond positively to mill additives added. There are certain indispensable properties required from enamel coatings and they are impact resistance, acid resistance, surface roughness, color and gloss properties. It is aimed that the mill additives added as the first purpose do not distort the structure.

The second objective of the study is to increase the mechanical resistance in enamel coating, on the surface and under the surface by adding nano particles. The brittle fracture mechanism of enamels is effective in stress areas within the structure. It is aimed to remove the stress areas in the structure with nanoparticles and provide mechanical resistance both locally and throughout the structure.

1.3 Hypothesis

Enamel coatings have low resistance against scratches and abrasion. It is necessary to increase the wear resistance of the enamel coated products to increase the usage time and to minimize their health effects. Accordingly, it is envisaged to increase the abrasion resistance by adding high hardness WC particles as a mill additive to the enamel composition. In addition, it has been suggested that the particles used should be nano-sized due to the homogeneous distribution in the structure and the removal of micro stresses in the structure.

It is also expected that with increasing concentration of nano-WC particles used, the abrasion resistance will increase up to a point and then decrease. The increase is expected to continue until the nano-WC particles remove stress points such as microcracks and micro voids in the structure. Then, it is thought that agglomeration may occur in the structure with increasing nano-WC ratio and thus the structure may be distorted. An optimum nano-WC concentration can be obtained in the study.

Another prediction is that the nano-WC particles used can provide an advantageous change in enamel surface properties. It is thought that the opacity can develop with the increase of the roughness on the surface in micro size.

2
GLASS-CERAMICS

2.1 Definition of Glass-Ceramics

Glass-ceramics are defined as inorganic materials produced by controlled nucleation and crystallization of glasses [1, 11]. More precisely, they are polycrystalline materials that replace nucleation and crystal growth processes with controlled heat treatment of glasses suitable for crystallization. The crystallization procedure takes place by adding nucleating agents to the glass matrix. Nucleating agents are mainly TiO_2 (titanium dioxide), Cr_2O_3 (chromium (III) oxide), ZrO_2 (zirconium dioxide) and P_2O_5 (phosphorus pentoxide) oxide groups and fluorides. These oxides act as nucleation centers within the matrix. Thus, in the controlled heat treatment step, these nuclei grow and form crystals. Crystallization generally does not take place entirely, meaning that the crystal structure still has an amorphous structure. One or more crystalline phases precipitate in crystallization, and these crystals can be of various shapes, generally rods, sheets, spherical. Generally, the size of the crystals formed is less than 1 μm and these crystals provide properties such as superior toughness, impact resistance and wear resistance to the glass-ceramic structures [1, 2]. Formation of glass-ceramics is shown in Figure 2.1.

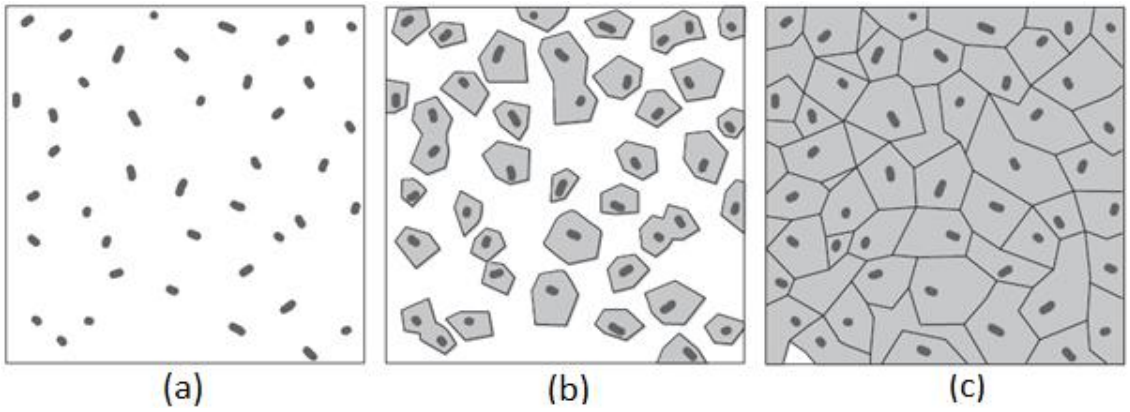


Figure 2.1 From glass to glass-ceramic. (a) nuclei formation, (b) crystal growth on nuclei, and (c) glass-ceramic microstructure [1]

In crystallization heat treatment or controlled crystallization process, which is the main stage of glass-ceramic production, the aim is to transform the amorphous glass into microcrystalline ceramic. The effect of temperature on nuclei formation and crystal growth is shown in Figure 2.2. The crystallization of any glass can be explained by its tendency to nucleation and crystal growth. Below the equilibrium melting temperature, if a sufficient number of nuclei (at least 10^{12} – 10^{15} nuclei in 1 cm^3 volume) is achieved by heterogeneous nucleation, a semi-stable region temperature range occurs where crystal growth can occur [12, 13].

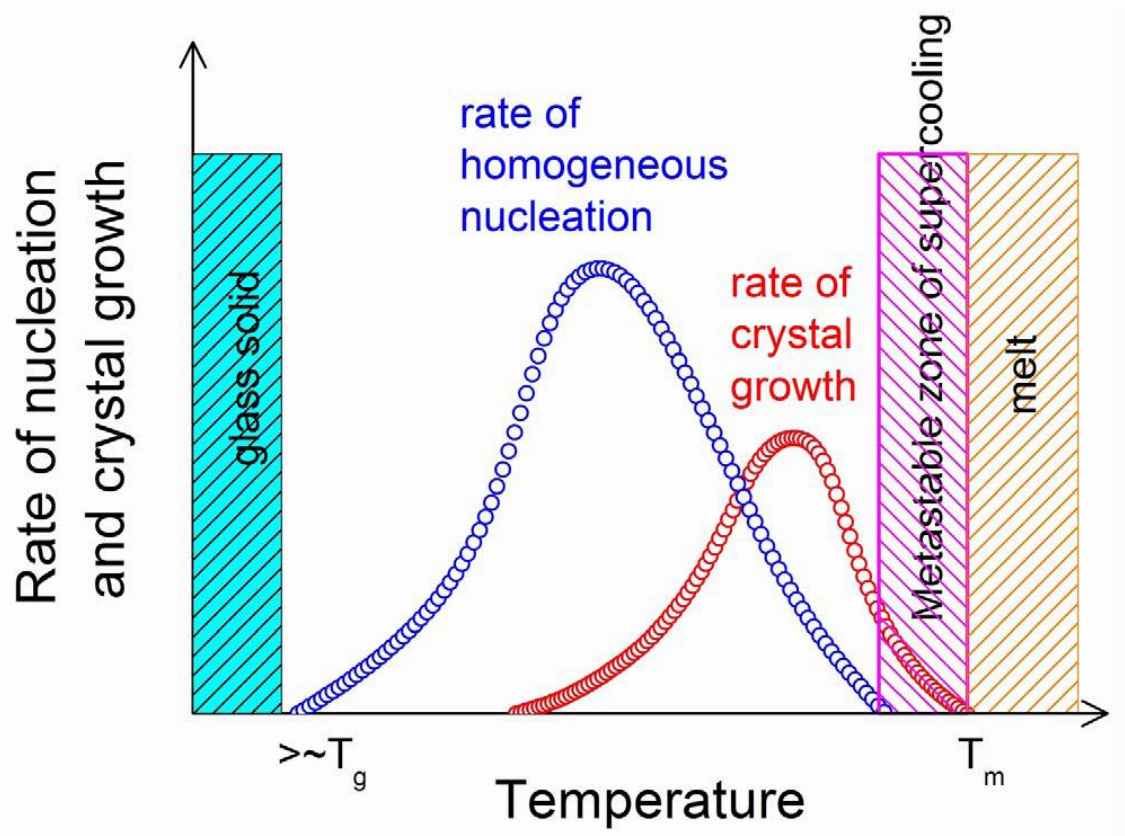


Figure 2.2 The effect of temperature on nucleation and crystal growth in glasses [14]

2.2 Properties of Glass-Ceramics

Glass-ceramic materials do not show any shrinkage during their production due to their thermal properties. In this way, they can be widely used in industrial and technological applications, especially in kitchenware. Owing to their glassy phase and nonporous structure, the desired transparency values and opacity values can be achieved with the use of crystals and microstructure control. Another optic property is that all desired colors can be obtained in glass-ceramic applications. When the

chemicals interact with glass-ceramics, thanks to the crystal structure, glass structure and chemical durability property, they have superior chemical properties. Mechanically, flexural strengths can reach up to 500 MPa and toughness values were obtained more than 3 MPa.$m^{1/2}$ with the developments [1, 11, 15 – 18].

2.3 Application of Glass-Ceramics

Glass-ceramics can be used in many fields industrially thanks to their superior engineering properties. Some of these application areas are given in Table 2.1.

Table 2.1 The main crystalline phases, properties and application areas of some glass-ceramic systems [2]

System	Main Crystalline Phase	Property	Application Area
$Li_2O.Al_2O_3.SiO_2$ (ZrO_2, TiO_2)	β-quartz β-spodumene β- eucryptite	Low thermal expansion High temperature resistance Transparency	Kitchenware Telescope Mirrors Oven Tops
$Li_2O.Al_2O_3.SiO_2$ (P_2O_5)	$Li_2O.Al_2O_3.SiO_2$	Dielectric properties Chemical resistance	Electronic Insulation Optical Coding Magnetic Recording Head Electric Sleeve
$MgO.\ Al_2O_3.SiO_2$ (P_2O_5, TiO_2)	Cordierite ($Mg_2Al_4Si_5O_{18}$)	Radar permeable Low expansion High strength	Missile Cap Radar Dome
$PbO.ZnO.\ B_2O_3.SiO_2$ (F)	Rankinite ($3CaO.SiO_2$)	Heat and vacuum insulation	Electrotechnology Microelectronic Circuits Capacitor

Table 2.2 The main crystalline phases, properties and application areas of some glass-ceramic systems [2] (continue)

$BaO.Al_2O_3.SiO_2$ (TiO_2)	Celsian ($BaAl_2Si_2O_8$) Barium Titanate ($BaTiO_3$)	High strength Thermal shock resistance	Kitchenware Cookware
$SiO_2.Al_2O_3.MgO.\ K_2O$ (F)	Phlogopite [$KMg_3AlSi_3O_{10}(F, OH)_2$]	Turning ability Dielectric properties	Electrotechnology Insulator Hermetic Seals
$SiO_2.CaO.NaO_2$ (P_2O_5)	Apatite [$Ca_5(PO_4)_3(F,Cl,OH)$]	Biocompatibiliy Resistance Chemical resistance	Dentistry Prostheses
$SiO_2.Al_2O_3.MgO$ (TiO_2)	Mg-Al titanate [$Mg_xAl_{2(1-x)}Ti_{(1+x)}O$]	Hardness Resistance Abrasion resistant	Construction Material
$SiO_2.Al_2O_3.CaO$ (ZnO)	Wollastonite ($CaSiO_3$)	Hardness Resistance Chemical resistant	Exterior Architectural Materials
$SiO_2.Al_2O_3.MgO.\ CaO$ (sulphide, fluoride, oxide)	Wollastonite ($CaSiO_3$), anorthite ($CaAl_2Si_2O_8$), pyroxene [$(Na,Ca)(Mg,Fe,Al)(Al, Si)_2O_6$], diopside ($MgCaSi_2O_6$)	Hardness Resistance Abrasion and chemical resistant	Floor Tile Exterior Arhitectural Material Pump Pipe

3
ENAMEL

3.1 Definition of Enamel

The word enamel comes from the word "smelzan" as the word of high German and then the word "esmail" in the old french language [19]. The current usage of the word enamel is “smalto” in Italian, “email” in French and German [20].Enamel is an inorganic glass-ceramic coating that has high heat capacity owing to the silicates in their chemical structure, high hardness and durability owing to their amorphous structure, chemical resistance and abrasion resistance. Enamel is obtained by grinding the frits, which is raw material of the enamels, into powder and applying them to metallic surfaces such as steel, cast iron, copper or aluminum and firing at temperatures of 500 - 870 °C. The application methods are generally electrostatic, spraying, electrophoretic, dipping and more recent thermal spray applications. Enamel coatings have superior engineering properties such as high temperature resistance, chemical resistance and mechanical strength, as well as aesthetic properties, so that application examples can be observed in many areas such as heaters, fireplaces, gas and electric cookers, clock faces, cookware, hot water services etc. [3] When combined with the superior technical features, aesthetic appearance and numerous color options of enamel coatings, it is an indispensable coating for cookware [21 – 23].

Although many authors and institutions make different definitions about the definition of enamel, basically the same explanation is accepted. For instance, while ISO (International Standards Organization) defines enamel in 25.220.50 coded title as “substantially vitreous, or glassy, inorganic coating bonded to metal by fusion at a temperature above 500 °C [24]”, VEA (Vitreous Enamel Association) defines enamel as “simply a thin layer of glass fused at high temperature on to the surface of a metal” [19], PEI (The Porcelain Enamel Institute, Inc.) defines enamel as “substantially vitreous or glassy inorganic coating bonded to metal by fusion at a

temperature above 800°F [25]" and IEI (The International Enamellers Institute) defines enamel as "A natural material that is born from fire, is immune to corrosion and as pure as glass, comes in a huge range of colours that remain unaffected by time and atmospheric conditions, can always be recycled... A coating that offers a global, utterly versatile response to the requirements of all sorts of industrial sectors" [26].

3.2 Chemical Composition of Enamel

The raw material of enamel coatings are structures called "frit". In order to obtain the frit structure, the raw materials are melted at 1200 - 1400 °C which are SiO_2 (silicon dioxide), Al_2O_3 (aluminum oxide), TiO_2 (titanium dioxide), ZrO_2 (zircon dioxide), P_2O_5 (phosphorus pentoxide), and F (fluorine) according to the place and feature of various oxides such as sodium, potassium and barium. The particles sizes of the used raw materials have a great importance before melting in terms of melting regime and homogeneity. Fast cooling is made by passing the melt coming out of the furnace through the cooled steel rollers. The amorphous structure suitable for the controlled crystallization obtained is called "frit" [3].

Table 3.1 The classification of oxides according to their functions in the glass structure

Glass Former	Glass Modifier (R_2O)	Glass Modifier (RO)	Glass Former (RO_2, R_2O_3)	Adhesion Promoter
SiO_2	Li_2O	MgO	TiO_2	CaF_2
B_2O_3	Na_2O	CaO	ZrO_2	MnO_2
	K_2O	SrO	SnO_2	CoO
		BaO	Fe_2O_3	NiO
		ZnO	Al_2O_3	

The structures that make up the frit structure may be too many or too few. Depending on the properties expected from the structure, the amount and variety

of oxides used may vary. However, these oxides can be classified according to their functions in the glass structure as shown in Table 3.1.

Silica is the most important oxide in glass-ceramic structures. It forms a glass structure on its own when enough high temperature (above 1700 °C) is given. Most enamel coating formulations have more silica compared to other compounds. One way to look at vitreous coatings is to see them as a silica tetrahedra network, where other materials are added as modifiers. Low melting point compositions melt at temperatures of 1050 °C or lower, have one or two parts of silica per part of other components. Compositions with higher melting points melt at 1250 °C or higher, have three to five parts of silica per part of other oxides. The most serious disadvantage of silicon dioxide as the coating component is its very high melting point (above 1700 °C) [27].

The oxides used in the enamel chemical composition are examined under 5 headings according to their function in the chemical structure: fluxes, refractories, adhesion agents, opacifiers and color agents.

3.2.1 Fluxes

The main task of oxides in this group is to reduce the melting temperature of silicon dioxide, the basic glass-making oxide in the enamel composition. Oxides in this group also increase the consistency of the enamel. The composition of suitable consistency increases the bonding between enamel and metal, but also has a positive effect on surface quality. Also, these basic characteristic oxides react with the acidic refractories to form the glass structure. The man raw materials in this group can be listed as: borax, soda ash, soda nitrate ($NaNO_3$), fluorspar (CaF_2), cryolite (Na_3AlF_6), barium carbonate ($BaCO_3$), magnesium carbonate ($MgCO_3$), litharge (lead (II) oxide), red lead (lead (II, IV) oxide) and zinc oxide (ZnO) [3].

3.2.2 Refractories

The materials in this group contribute to the formation of the glass structure and support the acidic part of the melt. The most important materials in this group are quartz, feldspar and clay. It is a quartz glass maker and is responsible for providing mechanical and chemical properties for the final product [3].

3.2.3 Adhesion Agents

Enamel coatings are very important to bond with the metal as they are applied to the metal surface. For this reason, oxides such as cobalt oxide, nickel oxide and copper oxide in the melt are used. The most important adhesion agent is CoO, not only provides adhesion but also acts as a colorant in blue color [3].

3.2.4 Opacifiers

The main task of oxides in this group is to opaque enamel coating, as mentioned in the title. Oxides in this group generally consist of antimony oxide, sodium antimonate ($NaSbO_3$), titanium dioxide, zirconium silicate ($ZrSiO_4$) and zirconium oxide. The common point of these oxides is their refractory properties. There are also auxiliary opacifiers such as cryolite and fluorspar, and these materials increase the fluidity of the melt [3].

3.2.5 Color Agents

Enamels are the coating type that is at the forefront with its aesthetic features as well as its superior technical features. For this reason, different colors and shades should be applicable in coatings. The most commonly used oxides in this context are cobalt oxide, copper oxide, iron oxide and nickel oxide. These oxides can be used as colorants by themselves, and coloring can be done by adding pigment to the frits that are formed [3].

3.3 Types of Enamel

Enamel coatings may differ depending on the method of application as well as depending on the place of application. For this reason, the terms ground coat and cover coat are introduced in this manner.

3.3.1 Ground Coat

The main purpose of ground coat enamel coating is the perfect adhesion between metal and enamel. Enamel coatings are exposed to impacts within the scope of the application. For this reason, the impact resistance should be high, that is, the ground coat should be strong to adhere to the metal.

Metal surfaces before application generally go through pre-processes such as degreasing, acid bath, hot water rinsing, cold water rinsing and drying. In this way, enamel powder or slurry is provided to cover the entire metal surface before firing. In addition, substances such as dirt, oil or scale on the surface cause faults in the coating and decrease the quality of the coating [28].

In addition, the ground coat enamel composition is prepared by considering the cover coat applications as well as ensuring adhesion. The difference of thermal expansion coefficient in the upper layer tile lining layer decreases the quality of the upper layer applications. Expansion by heat can cause cracking or shrinkage during cooling. However, cover coat application is not a mandatory choice. With the new generation enamels developed, the desired technical and visual features can be provided to enamel coatings only with a ground coat [28].

3.3.2 Cover coat

Cover coat enamel applications are generally carried out in order to provide the desired technical properties. It is difficult to provide other properties (acid resistance, alkali resistance, boiling water resistance, easy cleaning, abrasion resistance, color, etc.) since the main purpose of ground coat applications is to be able to provide adhesion as stated. One of the most important parameters in cover coat applications is the thermal expansion coefficient to ensure compliance with the ground coat. It is imperative that the thermal expansion coefficients of the ground and cover coat enamel compositions are close to each other. Otherwise, cracking may occur after application step. Color is an important factor here even though the cover coat applications contain technical specifications. For example, it is a problem to see the color of the ground coat in white cover coat enamel coatings. For this reason, the hiding power of the cover coat applications should also be relatively high [28].

In enamel applications, there are also applications called as three coatings. In cases where the one cover coat is not sufficient alone, the second cover coat application can be used. In this case, the middle coat is called the intermediate layer. However, in three coat applications, the thermal expansion coefficient is very important

because of the increasing cystallization. In each firing phase, amorphous structure decreases within the coating as a result of the growth of the ceramic crystals in the glass-ceramic structure. Also, during the firing process the hydrogen solubility inside the metal substrate increases and hydrogen tries to escape from the surface and this behavior can be observed only in steel sheets. This greatly increases the probability of cracking and defects (most importantly re-boiling) on the enamel surface [28].

3.4 Properties of Enamel

3.4.1 Thermal Properties

3.4.1.1 Thermal Expansion

Thermal expansion is the increase in the volume or length of the materials along with the temperature increase. In other words, at 1 unit temperature change, the volume or length changes occurring in the substance are obtained by observing. Thermal expansion coefficient a coefficient obtained by the ratio of unit shape change to the temperature difference. The change in the length of the material when the temperature of 1 °C increases is explained by the linear thermal expansion coefficient. The linear thermal expansion coefficient (α) is calculated by the following equation:

$$\alpha = \frac{1}{l} \times \frac{\Delta l}{\Delta t} \tag{3.1}$$

where l is the length of the material, and Δl is the elongation obtained by means of heating through Δt °C.

The change in the volume of the material when the temperature of 1 °C increases is explained by the volume thermal expansion coefficient. The relationship between the volume thermal expansion coefficient (β) and the linear thermal expansion coefficient (α) is explained as follows in isotropic bodies such as amorphous structures and glasses:

$$\beta = 3 \,.\, \alpha \tag{3.2}$$

The importance of the thermal expansion coefficient in enamels is related to the bonding of enamel and metal. It is a necessity in enamel technology that the thermal

expansion coefficients of enamel and substrate metal are close to each other. If the thermal expansion coefficient of the enamel coating is less than metal, the enamel will shrink rapidly during cooling after firing as the enamel cools faster. When the bond between enamel and metal is particularly good according to enamel adhesion parameters (Section 5.6), the metal surface resists the enamel shrink. In this case, when the tensile strength of the enamel is exceeded, stress-developing cracks remain in the structure. However, if the metal's thermal expansion coefficient is less than enamel, chipping defects occur because the enamel's compressive strength is higher. Since the compressive strength is 15-20 times more dangerous than the tensile strength, in the enamel coating applications, the expansion coefficient of the enamel is desired to be less than the metal [29, 30]. Volume thermal expansion coefficients of some metals and enamels are given in the Table 3.2.

Table 3.2 Cubical thermal expansion coefficients of some enamels and some metals [30]

Material	**Cubical Thermal Expansion Coefficient ($3.\alpha \times 10^{-7}$)**	**Temperature Range (°C)**
Iron	426	0 – 500
Low Carbon Steel	465	27 – 760
Cast Iron	378 – 390	20 – 500
Ground Coat for Steel	240 – 300	0 – 100
Cover Coat for Steel	280 – 360	0 – 100
Ground Coat for Cast Iron	250 – 300	0 – 100

3.4.1.2 Thermal Shock

The thermal shock resistance in enamel coatings indicates the behavior of the enamel in sudden temperature changes and is calculated mathematically according to the proposal of Winklemann and Schott:

$$K = \frac{P}{\alpha.E}\sqrt{\lambda/_{c}.d} \quad (3.3)$$

where P is tensile strength, α is the linear expansion coefficient, E is the elasticity modulus, λ is thermal conductivity coefficient, c is the specific heat and d is the density.

Thermal shock resistance depends not only on certain thermal properties, but also on many other parameters. The most important role here is internal strains. Since the coefficient of thermal expansion of the enamel is lower than that of the metal, it creates compressive strains in rapid heating and creates tensile strains in rapid cooling. Enamels show better thermal shock resistance in rapid heating as compressive forces are weaker than tensile forces. Also, the magnitude of the strains is important here. Since the convex surfaces have more tension than concave surfaces, the thermal shock resistance of the convex surfaces is lower. In addition, enamel thickness and substrate metal thickness are also important in thermal shock resistance [29].

As mentioned above, the thermal shock resistance of enamels is weaker in rapid cooling. However, the cooling environment is also important. Thermal shock action with cold air is weaker than thermal shock with cold water. For this reason, thermal shock resistances of enamel coatings are analyzed by tests with cold water [31].

3.4.1.3 Thermal Conductivity

The thermal conductivity of enamels is an important property in industrial and scientific terms. It is an important requirement that heat is transmitted through enamel in kitchen equipment. It is a desired property in military, construction, refrigerator and oven applications as a reflector or emitter. Increasing thermal conductivity in enamels can occur by addition of oxides with high thermal conductivity (metal powders) to the recipe.

Thermal conductivity is a magnitude of the thermal conductivity coefficient and is calculated as follows:

$$\lambda = p_1.\lambda_1 + p_2.\lambda_2 + p_3.\lambda_3 \quad (3.4)$$

where λ is thermal conductivity, p represents percentage of oxide and λ_i represents factor for the oxide.

Depending on the enamel composition, the thermal conductivity ranges from 0.84 to 1.26 watts/m.deg. Bubble structures in enamel have a great effect on thermal conductivity. As the bubble structure in the enamel structure increases, the thermal conductivity decreases. This can be explained by the thermal conductivity of oxygen (O) is 28.5 and nitrogen (N) is 27.7 milliwatts/m.deg (at 50 °C) [29]. This relationship is also shown in the Table 3.3. Also, low thermal conductivity adversely affects thermal expansion.

Table 3.3 Bulk densities and coefficient of thermal expansions of some enamel types [32]

Enamel Type	**Bulk Density (kg/dm^3)**	**Coefficient of Thermal Conductivity (watt/m.deg at 40 °C)**
Ordinary	2.48	1.17
With some bubbles	2.45	1.09
With many small bubbles	2.36	1.05
Slightly foamed	2.28	0.8
Foamed	2.16	0.46

3.4.1.4 Fusibility and Fluidity

Fusibility and fluidity properties are important properties related to the molten state that comes to the fore during melting the enamel raw material and firing it after application. It is controlled by the chemical composition, but its calculation has generally not gone beyond being experimental. Most of the calculation attempts made were valid for certain composition range. For this reason, certain tests have become important for each enamel composition: cone fusion test, fusion flow test,

fusion block test, bead test and interferometer test. Cone fusion test gives information about deformation intervals, fusion flow test gives information about frit's temperature-related hardness and softness, fusion block test is about fusion temperature of enamel compositions, bead test is about frit's fusibility, fluidity and surface tension properties, and interferometer test provides measurement of expansion coefficient [29].

3.4.1.5 Viscosity

Enamel coatings viscosity property is a valid parameter as for all glassy materials and it is highly affected by temperature, hence a low change in temperature can cause a high change in viscosity. In the Figure 3.1, T_g temperature is the temperature at which the material becomes brittle and reaches viscosity of 10^{12} N.sec/m_2. Ts indicates the melting temperature and the viscosity value was 10 N.sec/m^2.

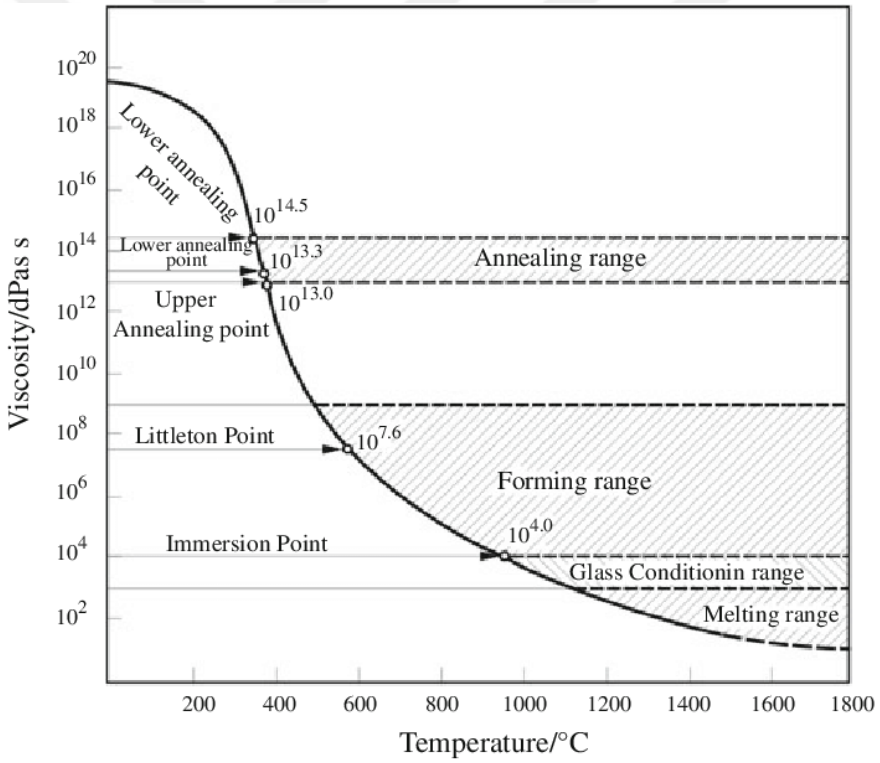


Figure 3.1 Viscosity – Temperature curve for a theoretical glass [33]

These values can be determined from the chemical composition. T_g temperature is usually below 500 °C and T_s temperature is approximately 1400 °C in enamels. Also, as the viscosity increases, the firing temperature of the enamel increases, the gas evolution decreases and the flatness of the surface increases. In contrast, low

viscosity values cause enamel defects and uneven coating thickness. During firing process, the viscosity of enamels is in the range of $10^2 – 10^3$ N.sec/m^2 [29].

In wet applications of enamel coating process, the viscosity values of the prepared enamel slurry can be easily adjusted with materials such as boric acid, clay and sodium nitrite.

3.4.1.6 Crystallization

The ability to give the desired physical and chemical properties to enamels is highly dependent on the crystallization process and this process can be understood via nuclei, crystal growth, solubility and supercooling terms. In enamel coatings, crystal formation is observed in the melt process as in glass and ceramic production processes. However, the frit structure formed by the rapid cooling step is completely in amorphous form. Crystal formation is then observed during the firing process. Nucleus is formed primarily for crystal formation. Approximately 25 atoms or molecules come together to form the nucleus, forming the first aggregation. However, this requires energy and mobility.

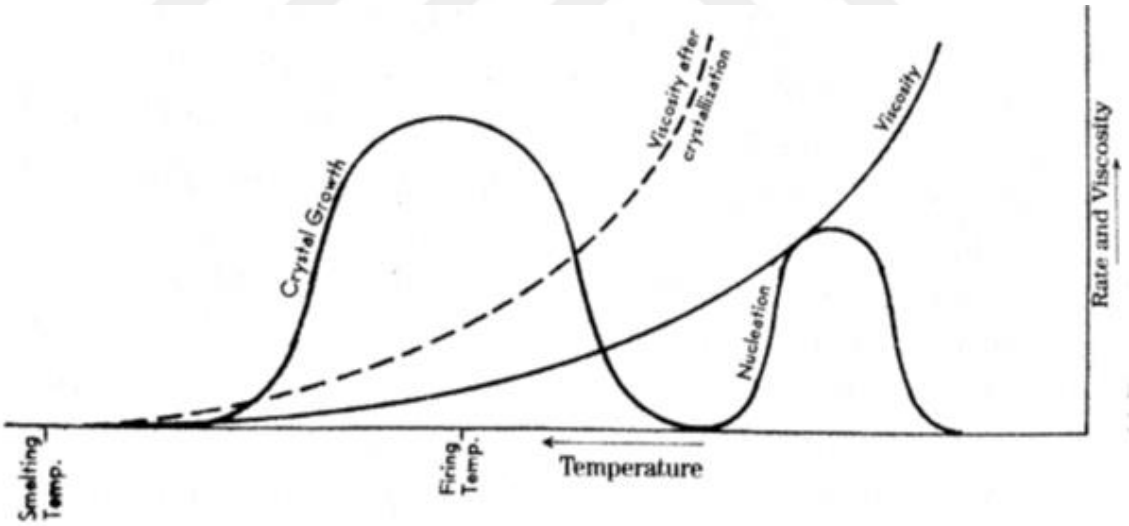


Figure 3.2 Rate – Viscosity and Temperature graph of the enamels during firing process [29]

If the viscosity is not sufficient, nuclei formation cannot start. Nucleus formation is an endothermic reaction since the nucleus have a greater binding energy thank the nuclei, while crystal formation is an exothermic reaction since the attaining of stable state requires energy release [29, 34]. The figure 3.2 shows the crystal formation of titanium, zircon and fluoride enamels.

3.4.2 Physical and Mechanical Properties

3.4.2.1 Density

Density (specific gravity) property is generally used to control the fluidity of the sample in wet applications. Enamels should be diluted in the concept of density measured with the help of a pycnometer. The density of enamels is measured by the formula:

$$S = (w - p)/[(w - p) - (w_2 - w_1)] \quad (3.5)$$

where S is specific gravity of enamel, w is the weight of the tapered pycnometer and sample, w_1 is the weight of the tapered pycnometer filled with water, w_2 is the weight of tapered pycnometer, sample and water and p is the weight of the tapered pycnometer [30].

3.4.2.2 Specific Heat

Specific heat is the amount of heat required to increase the temperature of the material weighing 1 kg in constant pressure and constant volume by 1 ° C. Specific heat of the enamels can be calculated with the following formula:

$$S = p_1.s_1 + p_2s_2 + p_3s_3 \ldots \quad (3.6)$$

where S is the specific heat of the enamel, p is the percentage of the oxide and s is the factor for the oxide [30].

3.4.2.3 Hardness

The hardness values of enamels do not vary greatly according to the chemical composition and according to the Mohs scale, enamels' hardness values are between 5 and 6. Hardness measurement methods such as Rockwell, Brinell and Knopp are not generally used because they give insufficient results for enamels. Mohs scale is also used to measure the scratch resistance of enamels [30].

3.4.2.4 Elasticity

Although the elasticity property is an important feature in materials, its use in enamel field is not common. It can be analyzed by mechanical and sonic methods. The mechanical method uses the following mathematical formula:

$$E = 4PL^3/bd^3\Delta \quad (3.7)$$

where P is the load, L is the length of the material, b is the width, d is the thickness and Δ is the deflection [30].

3.4.2.5 Compressive Strength

The compressive strength property of enamels is usually an unanalyzed property and is an auxiliary parameter that can affect other features. It has a value between 77 - 81 kg/mm^2 for standard enamels and can be calculated Winkelmann and Schott's by factor [30].

3.4.2.6 Tensile Strength

Although the tensile strength of enamels is an important property, it is very difficult to analyze. Enameled materials are very suitable for breaking due to their brittle fracture property. For this reason, many different methods have been proposed for its analysis. Although it is not a property that is desired or analyzed directly, it affects the thermal properties especially thermal expansion of enamels [30].

3.4.2.7 Abrasion Resistance

The abrasion resistance property of enamels is a very important mechanical feature and can determine the life of the material. Enamels are constantly exposed to different types of abrasion depending on their location, for instance, in kitchenware enamel coatings constantly exposed to metallic spoon, scoop, knife, wire etc. This causes the enamels' important surface properties to deteriorate. When the scratches on the surface increase, the loss of color and gloss occurs first and enamels lose their aesthetic properties. When the abrasion progresses more, it can progress to the metal interface with enamel. When the enamel is completely deformed as a result of abrasion (even in a very small place), the metal and the outdoor environment become open to interaction. Thus, metal corrosion begins. As the corrosion progresses over time, it can completely remove the coating. In addition, a process that can lead to fatal errors starts in kitchen applications. For example, when food comes into direct contact with metal as a result of abrasion on food contact surfaces, the elements in the metal enter the human body through food, but can cause illness. For this reason, abrasion resistance property in enamels is an important property.

The abrasion resistance property depends on the chemical composition of the enamel, the glass-ceramic structure it has, the surface roughness and the bubble structures in the material. Taber branded abrasives and falling abrasive tests can be used to test the abrasion resistance property [35].

3.4.3 Chemical Properties

3.4.3.1 Acid Resistance

In many areas of use, especially in kitchenware, enamels are constantly exposed to acid attack. One of the important oxides affecting acid resistance is SiO2 because the continuity of the structure [SiO_4] in the enamel determines the acid resistance of the enamel. [SiO_4] terahedrons covers the surroundings of {[AlO_4] - R^+} and {[BO_4] - R^+]} in the structure to resist the corrosive effect of acid. That is, as the SiO2 content increases in the enamel recipe, acid resistance increases. Conversely, with the increase of the R_2O group in the structure, the continuity of the [SiO_4] tetrahedrons is disturbed by the Si-R-O structure formed by ions such as Li^+, Na^+ and K^+, and the acid resistance decreases [36, 37].

3.4.3.2 Alkali Resistance

Enamels may also exposed an alkaline attack depending on the area of use. However, the alkali attack is slower compared to the acid attack. For this reason, the alkali tests of the enamel last longer. In addition, when acid and alkaline solutions are compared, the effect of corrosive materials that will cause ion exchange leach in the enamel structure is lower. It is usually tested in sodium pyrophosphate, sodium hydroxide and sodium bicarbonate solutions.

The ion exchange leach of enamel is made with hydrogen ions in the solution, which reacts with the enamel matrix and causes the ionization of the alkaline ions in the enamel. This reaction is pH related and usually takes place at pH <9 [37].

The reaction between hydrogen ions and a silica network with two non-bridging oxygen produces alkaline ions in the solution. This means that hydrogen will be easily replaced by any of the alkali metal ions bound by non-bridged oxygen and will form an aqueous surface layer.

The dissolution of the silicate structure usually takes place at pH> 8 initially and increases as the pH increases. At these pHs, the OHs react with the hydrated layer or glass matrix. Further reactions of hydroxyl groups with the first product will lead to the formation of Si(OH), the molecules that enter the alkaline solution. The second product SiO^- reacts with water to $SiO^- + H_2O \rightarrow Si\text{-}OH + OH^-$ reaction. As a result, enamel is eroded as a result of repeated reactions with hydroxyl groups [37].

3.4.3.3 Water Resistance

Enamels have resistance to water at room temperature and do not lose anything from their structure. In addition, hot water does not have a major effect on the enamel structure. However, losses from the enamel structure begin with constant exposure to high temperature and pressure at the place of use [37]. Enamel coatings in tests performed according to the DIN EN ISO 4753-3 standard indicate that the enamel should not exceed 8 mg/m^2 after the test in the tests performed as 21 + 21 days (total 42 days) [38]. Water resistance is important in thermosiphon, valve and boiler applications.

4
ENAMEL COATED METAL SURFACES

Enamel coatings can be applied to many metal surfaces, such as aluminum, gold, copper, cast iron, low carbon steel, decarburized steel, interstitial-free steel, titanium-stabilized steel, cold rolled steel and hot rolled steel. However, there are differences in firing temperatures, melting temperatures and chemical composition during enameling process of these metal substrates. For this reason, only the types of steel which are mostly used in the industry for enameling are included.

4.1 Cast Iron

Cast iron is a widely used enameling substrate since the adherence is caused by adhesive environment of oxide layer and mechanical interlocking between cast iron and enamel. Grey cast iron is mostly preferred in enameling industry with different compositions [39]. Limit chemical composition of cast irons for enameling are shown in Table 4.1.

Table 4.1 Limit composition of cast iron for enameling applications [40].

Element	**Percentage (%)**
Total C	3.25 – 3.60
Graphitic C	2.80 – 3.20
Si	2.25 – 3.00
Mn	0.45 – 0.65
P	0.60 – 0.95
S	0.05 – 0.10

With these respects cast iron enamels differ from steel enamels since cast iron – enamel adhesion mechanism mostly mechanical due to the penetration of the enamel into the pores of the rough surface of the cast iron while steel – enamel adhesion mechanism is mostly chemical [41]. Also, the components of cast iron have influence on the adherence. For example, phosphorus (P) and silicon (Si) increase adherence between cast iron and enamel indirectly with the positive effects in cast iron solidification process. The reason of this is either explained by the carbon equivalent (Eq. 4.1) or the good chemical relationship of phosphorus and silicon with the enamel structure [42].

$$C_{eq.} = C_{total} + \frac{Si+P}{3} \quad (4.1)$$

4.2 Decarburized Steel

Decarburized steels are the most suitable steels for enamelling process and can be used even for direct cover coat applications. Boiling defects, carbon gases formations and fish scale defects that occur after enamelling and during firing do not occur in this type of steel [40].

4.3 Low Carbon Steel

These steels have low carbon content (0.002 to 0.004%) and are aluminum killed steels containing 0.15 - 0.30 wt. % Mn, maximum 0.015 wt. % P, maximum 0.015 wt. % S, maximum 0.015 wt. % Si. Up to 0.006 wt. % boron can also be used to eliminate the fish scale defect that occurs when enamel is coated and control the grain size. It generally has a yield strength between 172 - 221 MPa, a tensile strength of 303 - 338 MPa and an elongation between 38 - 46%. The important point is that there are no faults on the steel surface and the surface is suitable for acid washing [40].

4.4 Interstitial Free Steel

It is the steels in which all carbon and nitrogen in the structure are bonded with the alloying element. For this purpose, titanium, niobium or titanium and niobium are used together as alloy elements. It generally has a yield strength between 138 – 165 MPa, a tensile strength of 290 – 317 MPa and an elongation between 41 – 45 % [40]. The chemical composition of an IF Steel is shown in Table 4.2. However, the titanium

ratio has a negative effect on the adhesion of the enamel to the steel, the enamel composition to be prepared must be prepared by considering this concept.

Table 4.2 Chemical composition of a commercial IF steel [43]

Generic Name	**Max. Content (%)**								
	C	Si	Mn	P	S	Al	Ti	Nb	Cu
IF180	0.01	0.3	0.7	0.06	0.025	≥ 0.01	0.12	0.09	0.2

4.5 Stainless Steel

Stainless steels are among the most used steel types with 18 wt. % Cr content and 8 wt. % Ni content average. Since its corrosion resistance properties are magnificent, it has a large area of application. While 400 series (Cr) stainless steels are ferrite and allow easy application of low temperature enamels, 200 series (Cr-Ni-Mn) and 300 series (Cr-Ni) stainless steels are austenitic and their high thermal expansion coefficient makes the enamelling process very difficult and special enamel studies needs to be done. It has been observed in studies on this subject that adhesion with mechanical activation of the surface can be achieved in 316L stainless steels and has been successful in enamel coating in order to prevent oxidation of stainless steel at high temperature [44, 45].

5
ENAMEL COATING

5.1 Frit Production

Although the method used in frit production is the same in enterprises, with the changing technology, the production stage is technological and economical. Steps like raw material preparation, weighing, mixing and loading are now technologically more systematic and economical. Control is required at every step, and this is achieved through computer-aided systems. Frits that require uniform chemical and physical properties can be produced according to any enamel type desired. However, companies prefer to buy them from large-scale producers for economic reasons rather than producing them themselves. The production phase is divided into subtitles as raw material supply and storage, weighing, mixing, melting, quenching, drying and storage as shown in Figure 5.1.

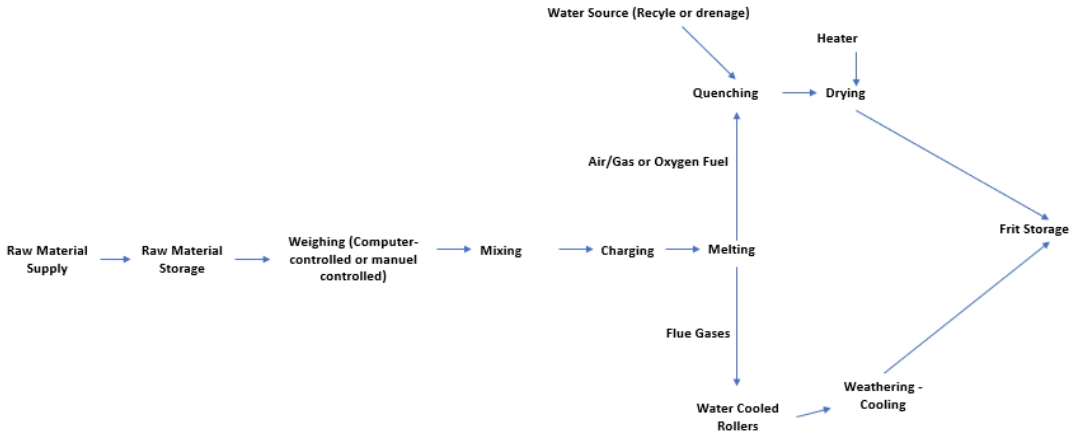


Figure 5.1 Production steps of the frit production [46]

Due to transportation costs and economic considerations in supplying the product, factories are usually located close to raw material producers or close to transportation centers such as ports. The raw materials received are usually sent with prescriptions indicating their chemical composition, but most manufacturers still conduct chemical analysis of the raw materials. Raw materials are kept in large and covered structures. Today, although raw material transportation is carried out

with scoops, this process is made more economical with modern robotic methods and the confidentiality of the recipe is protected [46].

Making enamel batch is a step that requires careful, disciplined and rational workers. Weighing equipment in modern organizations are made with computer aided systems. In these systems, weights are automatically measured and brought to the desired level. Given that small changes in prescriptions have huge consequences, computer systems eliminate human errors. Weighing chambers are usually made of square or round steel plates. The raw blend can be conveyed to the mixing area either pneumatically or with a feeder. The most important point here is that the computer-aided automatic weighing machine loads all the raw materials to the same place in different ways, while the impurities from the previous raw material can cause defects or production faults [46].

Since raw materials are generally of high quality, they do not require pre-separation and magnetic separation for contaminants and foreign parts. Mixing process is done with horizontal rotary mixers or high speed pan type mixers. It is important that the blending must be homogeneous due to the refractories and fluxes in the blend. If there is no good mixing, a longer time and energy is required for melting. (The reaction rate depends on the contact surface.) Better mixing also helps with uniform color and opacity. Enamels are very viscous; therefore, the distribution of different materials after melting is slow and often incomplete [46].

Melting process aims to heat the raw materials in the enamel composition in a uniform heat distribution. Some materials in the blend evaporate, some are ready to melt, some are ready to decompose and some are refractory. Those which are ready to melt first, melt and wet the blend. In this way, rapid gas formation is prevented and the loss of volatiles is reduced. Volatiles are sealed with melt and added to the solution formed with refractories. Sufficient time and sufficient temperature must be given to the furnace in order to complete the melting. Once the appropriate viscosity is reached, the melt is ready to be removed from the furnace [46].

The purpose of quenching or rapid cooling is to rapidly cool the formed structure into amorphous form and form the structure called frit. Rapid cooling structure is also resistant to cracking and breaking because it accumulates intense stress and

tension. Cracking occurs due to thermal gap, severe thermal change and expansion. In contact with water, the molten mass begins to solidify, but also crack formation begins. A good frit is not only the structure in small pieces, it is the frit that contains many cracks in its structure. In this way, a better grinding is provided. Technologically water - air atomizing devices have been developed. These devices, which use less energy, form smaller grains and reduce the cost of the grinding process. In addition, frit production is possible just with air-jet devices. The frit formed takes up more space, but it has been reported to have better acid resistance and opacity. Also, in water atomization technique, the frits were become micron sized and the morphologies are very close to each other with more contact time with device and each other [46, 47].

When frit from production is stored, it contains 5 - 15% water in its structure after the quenching step. This step is necessary if the desired frit will be processed dry. It is not required in wet applications. Generally, cleaned flue gases coming out of the furnace are sent to fixed or rotary type dryers for heating. However, it is not necessary in cases where water-cooled rollers are used since the frits are already dry [46].

5.2 Milling

Enamels must be powdered in any case before application and mills are used for this. These mills have a steel body, cylindrical shape and balls of different sizes. With the rotational movement, the balls inside fall over each other and grind the enamel frits. The important point for the mill is that the inner surface and the balls must be the same material, otherwise the mill may abrade itself. Suspension does not occur in the slurry prepared in wet applications when no floaters are available. In order for the frits to suspend in the water, it must be grinded together with the appropriate clay and mill additives. Although the size of the balls in the mill varies according to the mill, in general, balls of different sizes between 20 mm and 80 mm are used in order to increase the total grinding surface and reduce the grinding time [48].

5.2.1 Batch Amount

The frits reaching the desired grain size depend on the weight of the frit loaded on the mill during grinding, while excess frit loading increases the grinding time, less frit loading causes the abrasion of the balls and the inner surface of the mill [48].

The amount of frit to be milled is obtained theoretically by multiplying the internal volume of the mill by the coefficient of 0.8.

$$\text{Frit Weight (kg)} = (\text{Internal volume of the mill} \times 0.8)/\ 2 \qquad (5.1)$$

5.2.2 Mill Speed

The rotational speed of the mill determines the quality of the powder because the milling process is basically based on the principle that the balls are fall on the frits and bring the frits into powder form. When the mill speed is slow, the balls slide over each other and cannot complete the milling process, and on the contrary, when the mill speed is too fast, the balls get steady by sticking to the inner surface of the mill, under the influence of centrifugal forces and the milling process cannot be completed. Although the speed of the mill varies according to the size of the mill so an appropriate speed is not specified, but the most appropriate speed in the literature specified as 80 - 90 m/min [48].

5.2.3 Mill Additives

Mill additives are of great importance in end product properties and application parameters and vary depending on wet or dry application. From dry application, intent is electrostatic powder applications and requires only pigment and organosilicon compound as a mill additive. While the desired color properties are provided with the pigment, organosilicon compound is used to adhere and hold the powder electrostatically. In wet applications, many contributions are required. The quality of the water used in wet applications is also important because the waters containing dissolved salt (sodium, calcium, magnesium sulfate, chloride and carbonate) have a negative effect on enamel quality. Although it has the best effect in distilled water applications, its industrial use is not feasible [48].

5.2.3.1 Floating Agents

Floating agents are essential for the ground frit particles to remain suspended in water. Clay comes first in this group of materials. Although the properties of the clays vary depending on the region from which they are extracted, they can be used in general from 4 % to 8 %. Another one, bentonite (montmorillonite clay), is a better floating agent than clay, but it cannot be preferred much because of its high cost. Generally, it can be used in clay stabilization or in environments where clay cannot be used much. Bentone is artificial bentonite and it is a more floater material. Due to its cost, it can be used in mill amount in low quantities. CMC (carboxy methyl cellulose), another material, swells in water and increases its texture, but since it is a very strong material, it is sufficient to use it under 0.1% [48].

5.2.3.2 Color Agents

They are high temperature resistant inorganic materials used to change the color of the enamel and obtain the desired color tone. Color is an important property in enamels because there are specific color values desired according to the application place. For this reason, colors can be obtained from frits as well as pigments. Pigments are organic and inorganic based materials. In enamel applications, inorganic pigments are used because of high temperature firing. Since it is desired that pigments do not disturb their chemical stability at enamel firing temperature, spinel pigments are generally used. It is determined by the raw materials in the pigment color and is usually Fe-Cr-Co and Fe-Cr-Cu-Mn complexes for black color, Co-Si and Co-Al complexes for blue color, Sb-Cr and Ti-Sb-Ni complexes for yellow color are used [48].

5.2.3.3 Electrolytes

The purpose of the materials in this group is to ensure that the frit particles, in which suspended by floating agents, are placed in the slurry in a certain sequence. These are the materials that provide the fluidity, consistency, flow rate and infiltration balance of the enamel slurry. Sodium nitrite ($NaNO_2$), boric acid (H_3BO_3), potassium carbonate (K_2CO_3), borax penta hydrate ($B_4H_{10}Na_2O12$), potassium nitrite (KNO_2),

magnesium sulfate ($MgSO_4$) and sodium aluminate ($NaAlO_2$) are examples of materials in this group [48].

5.2.3.4 Others

The use of quartz in the mill increases acid resistance and firing temperature, but excess use weakens the adhesion between enamel and metal. Also, sodium molybdate (Na_2MoO_4) and molybdenum trioxide (MoO_3) can be used at a low rate in order to increase the adhesion of the enamel. In addition, materials such as citric acid and sodium gluconate can be used to change the fluidity value without changing the density of the slurry [48].

5.2.4 Milling Methods

5.2.4.1 Dry Milling

In order to make the frits suitable for powder electrostatic application (POESTA), extra surface active materials are used during milling. The chemical materials used (silicon components, silizanes and alkylsilanoles) react with hydroxyl groups on the frit surface and form an almost hydrophobic surface. The purpose of these applications is to bring the electrical resistances of frits with resistances of 10^8 - 10^9 ohms to 10^{14} ohms. Because frits applied directly in electrostatic application cannot hold onto the metal surface during application and the after the firing process coating fails due to the insufficient coating thickness [48].

5.2.4.2 Wet Milling

The mill additive and frit mixture prepared for wet applications can be diluted differently. For example, RTU (Ready-to-Use) enamels can be diluted and applied directly. However, in order to ensure homogeneous distribution, it can be rotated in the mill filled with water for a few minutes. In addition, powder can be removed and mixed in a separate place, for example with a large drum, with a mechanical mixer and made homogeneous. With the appropriate mill additive and suitable frit mass, there are also compositions that are milled directly with the water in the mill [48].

5.3 Metallic Surface Preparation

5.3.1 Mechanical Cleaning

Mechanical cleaning is generally done by abrasive action to the surface. In this way, some of the impurities on the surface are adhered to the impacted particles, away from the metal surface and the surface roughness of the metal surface is increased. Increased surface roughness increases the specific surface area to react between the enamel and the metal surface, creating more possibilities for adhesion. Important parameters in the sandblasting technique, which is mostly used in mechanical cleaning, are particle size, particle size difference and applied pressure [49, 50].

5.3.2 Chemical Cleaning

Chemical cleaning includes several steps which are depending on each other. The first step is degreasing which is done in order to remove the oil, rust preventing oil and various rust types. Several parameters are important in the degreasing process which are:

- Type of degrasing agent
- Degreasing temperature (must be between 60 °C – 90 °C)
- Concentration of the agent (must be between 45 – 50 g/lt)
- pH of the baths
- Treatment time (approximately 15 min)
- Mechanical action (spraying pressure)

After this process, hot water rinsing, cold water rinsing and final rinsing with demineralized water steps must be done before pickling step [49]. The purpose of pickling with acid is to generally remove rust and scale on the metal surface. The way to do this is to make the acid react with rust on the metal surface. Between the reacted acid and rust, hydrated ferric oxide ($Fe_2O_3.2H_2O$), anhydrous ferric oxide (Fe_2O_3) and magnetic iron oxide (Fe_3O_4) are formed as products. In addition, the acid solution on the surface allows the release of hydrogen gases that remain dissolved in the metal. One of the acids used in this context is sulfuric acid (H_2SO_4). The metal surface is cleaned slowly with the process performed with 6% H_2SO_4 solution at 66

°C. However, H^+, SO_4^- and SO_4^{-2} ions, which are produced by low ionization of H_2SO_4, react faster with the surface. Temperature is important here for reaction mobility and rate. As the acid solution will decrease as the process is repeated, the solution must be changed after certain pickling process. Hydrochloric acid (HCl) can be used during pickling, but its use is rare due to the requirement of heating and high concentration. Phosphoric acid (H_3PO_4) is the acid that has the best effect on the enamel quality used in this context, but since it is expensive, it is available in one coat – one fire white enamel applications [50]. Cleaning can be done via several cleaner components and listed in Table 5.1.

Table 5.1 Some cleaner components and their function in chemical surface cleaning before the enamelling application [50]

Component	**Function**
Silicates • Sodium metasilicate (Na_2SiO_3) • Sodium orthosilicate (Na_4SiO_4)	Softening the water by precipitation Good dispenser and saponifier Inhibition of Al and Zn dissolution High alkalinity property
Phosphates • Trisodium phosphate (TSP - Na_3PO_4) • Sodium tripolyphosphate (STPP - $Na_5P_3O_{10}$) • Tetrasodium pyrophosphate (TSPP – $Na_4P_2O_7$) • Disodium phosphate (DSP - Na_2HPO_4)	Softening the water Improving rinsing

Table 5.1 Some cleaner components and their function in chemical surface cleaning before the enamelling application [50] (continue)

Carbonates • Sodium carbonate (Na_2CO_3)	Good buffering Good alkalinity property
Hydroxides • Potassium hydroxide (KOH) • Sodium hydroxide (NaOH)	Source of alkalinity
Nitrites • Sodium nitrite ($NaNO_2$)	Prevents the oxidation due to drying process
Chelants • Ethylenediaminetetraacetic acid ($C_{10}H_{16}N_2O_8$)	Softening the water Prevention of metal ion deposition

After cleaning, metal surfaces must enter the rinsing process. The chemicals or their by-products used can remain as thin layer on the metal surface or remain in the pores on the surface. Rinsing must be done after each washing step. Rinsing process continue as hot water rinsing and cold water rinsing. After the rinsing step, the metals are introduced into the neutralization bath. In this bath, the last traces of acid are completely removed with alkaline solution (soda ash, borax or trisodium phosphate and water). It is preferred that the solution temperature is at 60 - 70 °C. In the last step, the metals enter the drying step and are quickly dried and become free of dust and scale [50].

5.4 Coating Methods

5.4.1 Spraying Technique

This technique consists of manual or fully automatic coating systems with a spray gun and a booth. It is based on the principle of throwing enamel slurry particles from a thin opening (nozzle) to the opposite side (metal plate) with air pressure. The

important point is that the slurry particles sent are not too fast or too slow and there are no air gaps inside. Generally, the air pressure ranges from 4.1 atm to 6.8 atm [51].

An ideal spray gun has the following properties;

- Nozzle hole: 1.8 - 2.4 mm
- Spray Pressure: 2.8 - 3.5 atm.
- Enamel Flow: 36 - 48 lt/h
- Air Consumption: 30 - 35 m^3/h
- Optimum distance to enamel parts: 30 - 50 cm

5.4.2 Dipping

It is based on the principle of immersion, removal and filtering of the workpiece to be coated in a tank filled with enamel slurry. Although material loss is very low, defects may occur when coating large or shaped parts. In addition, the slurry in the tank tends to settle after a while and accumulate water on it. For this reason, it is necessary to mix the bottom of the tank with a mechanical mixer in order to obtain a uniform slurry for application [51].

5.4.3 Flow Coating

The parts to be coated in the process with a constantly flowing enamel slurry are generally smaller and less shaped. It is generally used for the application of the ground coat in 2C1F applications. It is preferred for cover coat required ground coat applications since the water on the surface will cause water trace defect in the ground coats [51].

5.4.4 Electrostatic (Wet) Spraying

Although its application is not preferred very much, it is formed by the transfer of enameled slurry particles that are technically electrostatically charged to the metal sample charged with the opposite electric charge. It is not favored to do it manually because the electric current is too much. In addition, the coating can be made homogeneously and without defects [51].

5.4.5 Electrostatic Powder Spraying

Enamel powder taken from the mill or frit composition is loaded negatively by passing near the high potential electrode. This creates an electric field between the high-potential spray gun and the workpiece, causing local ionization of the air in the environment. In this way, oxygen ions in the environment are loaded negatively. Enamel powder also take on the negative charge in the air. With the direction of the electric field formed in the environment, enamel powder and air go towards the workpiece. In this process, 4 different forces affect enamel powders: electrical force, mechanical force, air resistance and gravity. The operation is at 100 kV voltages and very low amperes. At the end of the process, enamel coating is generally homogeneous. The smaller the powder particles, the easier it is for these particles to be charged with electric charge, and the adhesion of the metal to the surface increases. In addition, dust particles that do not be on the part or scattered in the ether can be reused in this method [51].

5.4.6 Electrophoretic Coating

In this method, the metal plate to be coated is the positive electrode. Both positive and negative electrodes are found in the enamel slurry bath. When the metal substrate is exposed to 50 V and 50-300 A/m^2 potential in the enamel sludge, it attracts the charged frit particles collected in the coating layer. The most important parameters affecting coating quality are density of enamel, particle size and amount of power applied. The enamel density should be approximately 1.5 g/cm^3. Coating thickness increases as the voltage to be applied increases, but surface defects may occur due to the gas evolution at very high voltages [51].

5.4.7 Thermal Spray Coating

Powder frits or enamel powder are injected into the plasma jet, melted and applied on a material to be coated in this coating type. The melted frit is sent to the surface at a speed of 100-200 m/sec approximately through the spray gun. The distance between the surface and the gun is between 100 and 150 mm. Frits come out of the gun at a temperature close to 1500 °C and when they stick to the surface, their temperature decreases to 270 °C due to the sudden direct cooling, the temperature

drops to 90 °C and then to 40 °C. It is an application that requires attention hence when done properly, it gives the best results compared to other methods [52].

5.5 Coating Process

5.5.1 One Coat One Fire

This method, abbreviated as 1C1F, is used for ground coat applications. It states that the enamel is applied to the surface once and fired once. It is the most basic method. Wet or electrostatic powder methods can be used [51].

5.5.2 Two Coat Two Fire

It is shortened as 2C2F and it specifies the applications of cover coats. It indicates that the first coat, that is, the ground coat is applied and fired, and then the second coat, the cover coat, is applied and fired. Wet and powder methods may vary among themselves. In other words, after applying ground coat as powder, the cover coat application can be applied wet method and vice versa. It is a technique frequently used in industry [51].

5.5.3 Two Coat One Fire

It is called 2C1F it states that the ground coat is not fired after the application, but that the cover coat is applied, then the two layers are fired together. For this reason, it is an important process. It is a method to be used in the industry because it greatly reduces energy use. Generally, after ground coat is applied with wet application method in a thickness of 40 - 80 μm, it is not fired but only dried and thus has a form called biscuit. Although the biscuit form looks hard, it has no resistance to impacts. The cover coat of the biscuit form is usually applied by powder method and the coating is fired at the firing temperature. Important points are that the gorund coat must not be visible from the cover coat or must not cause black dot defects [51].

5.5.4 Three Coat Two Fire

The 3C2F system is generally based on the principle of bringing the ground or intermediate layer (first cover coat) into biscuit form and then firing it. This process is made by optimizing the 2C1F system. However, the thermal expansion

coefficients of the layers applied to the important note are very close to each other. Otherwise, cracking may occur in the coating [51].

5.5.5 Three Coat Three Firing

The 3C3F system mentions the firing method after each application. The important point here is that the thermal expansion coefficients of the enamel compositions coated are very close to each other and do not allow crystal growth within their body during reheating much. Otherwise, the material may lose its glassiness. In addition, internal stresses and the release of hydrogen and other gases from the metal surface have a negative effect on the coating quality [53]. Some of the industrially applied methods are given in the Table 5.2.

Table 5.2 Coating process techniques for some industrial application areas [53]

Processes	**Boiler**	**Cookware**	**Kitchenware**	**Sanitaryware**
1 coat / 1 fire dry	Yes	Yes	No	No
1 coat / 1 fire wet	Yes	Yes	Yes	No
2 coat / 1 fire dry/dry	No	Yes	No	Yes
2 coat / 1 fire wet/dry	Yes	Yes	No	Yes
2 coat / 1 fire wet/wet	No	Yes	No	Yes
2 coat / 2 fire dry/dry	Yes	Yes	No	Yes
2 coat / 2 fire dry/wet	Yes	Yes	No	Yes
2 coat / 2 fire wet/wet	Yes	Yes	Yes	Yes
3 coat / 2 fire wet/wet/wet or dry/wet/wet or dry/wet/dry or wet/wet/dry	No	No	No	Yes

5.6 Enamel – Metal Interface Relation

5.6.1 Mechanical Theory

The mechanical theory mechanically examines the connection between the enamel and the metal surface and is therefore based on the surface area where the enamel contacts with the metal surface. Metal is roughened mechanically by surface preparation methods applied before application and also surface roughness increases with chemical solutions. Increased surface roughness increases the specific surface area of the metal surface, thereby increasing the surface that the metal surface contacts with enamel.

When the metal surface to be enamelled is fired, an oxide layer forms on the surface as the temperature increases. Although this oxide layer is a very thin layer, the oxide layer thickness increases as the ambient temperature increases. However, when the enamel reaches the softening temperature, the enamel coating wets the metal surface and prevents oxidation. But the oxide layer on the surface remained. As the temperature increases, the oxide layer on the metal surface diffuses into the enamel and forms dendrite structures [54]. The dendrite structures formed allow the metal and enamel to hold together mechanically (Figure 5.2). However, this theory is an

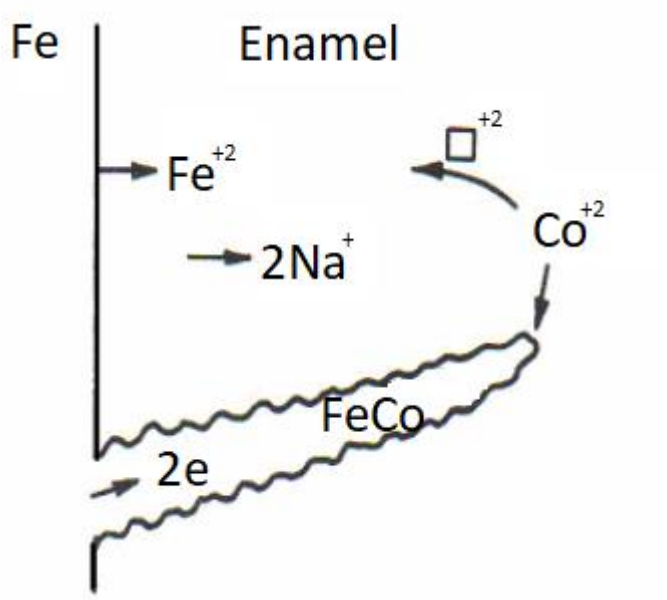


Figure 5.2 Illustration of dendrite formation in the surface of the enamel coating during firing process [54]

auxiliary theory that supports other theories since the mechanical bonding alone does not increase the adhesion between enamel and metal. When chemical bonding and mechanical bonding are compared, it can be observed that chemical bonding is much more important.

5.6.2 Chemical theory

The theory states that dissolution, redox, precipitation and interface diffusion reactions occur at the interface where enamel and metal be in contact, and a transition layer occurs. The iron oxide (FeO) compound, which is made up of oxidized metal as it rises to the enamel firing temperatures, is reduced by NiO and CoO compounds in the enamel and initiates redox reactions. The reason why is cobalt and nickel oxides are important is the Ellingham Diagram indicated in the Figure 5.3 [55 – 57].

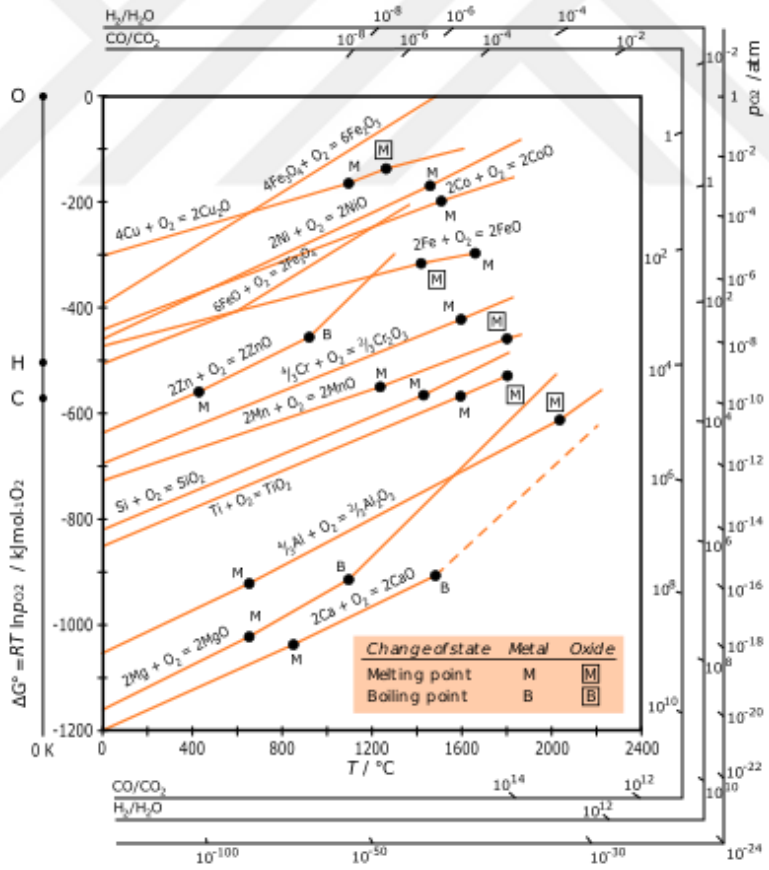


Figure 5.3 Ellingham Diagram

During the firing of enamel, iron in the base material changes to oxidic form and forms Fe^{+2} [55].

$$Fe_3O_4 \rightarrow Fe^{+2} + 2Fe^{+3} + 4O_2 \quad (5.1)$$

$$2Fe^{+3} + Fe \rightarrow 3Fe^{+2} \quad (5.2)$$

Subsequently, metallic iron in the substrate metal material reduces cobalt oxide and nickel oxide in enamel to metallic cobalt and iron [55].

$$Fe + CoO \rightarrow FeO + Co \qquad \Delta G = -36893\ J \quad (5.3)$$

$$Fe + NiO \rightarrow FeO + Ni \qquad \Delta G = -52988\ J \quad (5.4)$$

5.6.3 Electrolytic Theory

The theory is based on the galvanic element that occurs between cobalt and iron when the enamel starts melting at enamel firing temperatures. In the galvanic element, cobalt becomes a positive pole and iron becomes a negative pole. Thus, during melting process, a galvanic current from iron to cobalt forms and angled grooves occur with this current. Softened enamel enters the formed cavities and clings mechanically [58].

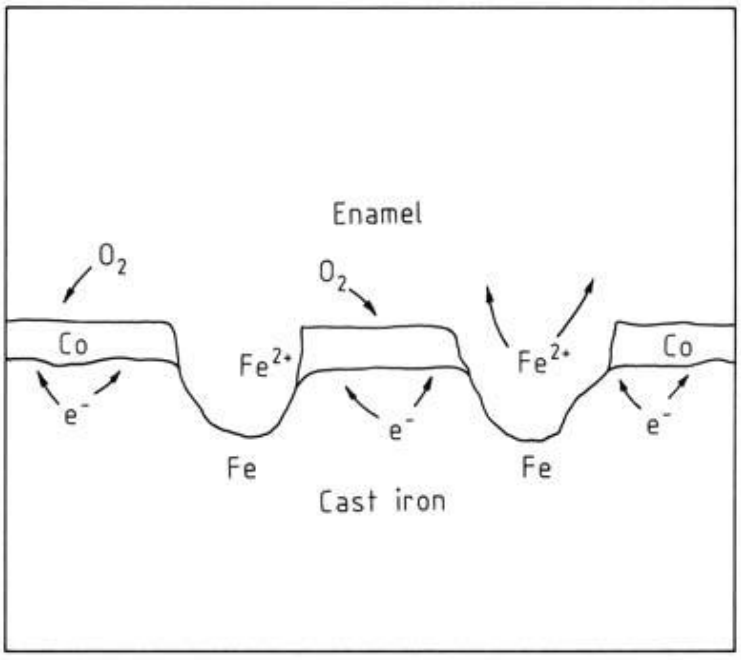


Figure 5.4 Electrolytic cells between molten enamel and cast iron [59]

5.6.4 Diffusion Theory

Ion exchanges occur between the metal ions in the enamel and the atoms in the metal at the enamel firing temperature. When the metal ions in the enamel spread on the metal surface, they become metal atoms by taking electrons. The atoms in metal are dispersed in enamel and ionized. Thus, a continuous diffusion situation occurs. If the enamel coating at the metal – enamel interface is not saturated with the appropriate oxide of the metal, an unstable balance occurs. In the interfaces, it was concluded that the situation caused by the presence of metallic iron in the enamel and the silicon in the substrate metal is diffusion and that diffusion helps adhesion [60].

6
TUNGSTEN (WOLFRAM) CARBIDE (WC)

6.1 Structure of Tungsten Carbide

This chapter aims to provide fundamental and practical information about the structure of tungsten carbide in three subtitles: crystal structure, phase diagram and nanocrystalline structure.

The crystal structure is a repetitive order in material science, macroscopically observed between the surfaces of crystalline minerals and microscopically between atoms of most layers. So, crystal structure shows that elements have very different properties depending on how they are stacked together or what other elements they are stacked together with.

The phase diagram is a chart that describes equilibrium conditions of distinct thermodynamic phases in specific conditions (temperature, pressure and volume).

6.1.1 Phase Equilibria of Tungsten Carbide

The compounds existing in the W–C system are W_2C (hexagonal close packed) and WC(simple hexagonal) [61]. There are some researchers who adds WC_{1-x} to this system and make these compounds three and some researchers take into account WC_{1-x} as a polymorphic compound [61, 62]. Both of WC and W_2C have several polymorphic compounds and they are stable in different composition and temperature values. The phase diagram of W-C system is divided into lower tungsten carbide and higher tungsten carbide because of their place in the phase diagram as shown in Figure 6.1. There are four modifications for lower tungsten carbide (W_2C) which are low temperature β''-W_2C, intermediate β'-W_2C and high temperature β-W_2C which are also designated in literature as α-,β- and γ-W_2C [63]. Nevertheless, these modifications were only in the limited experimental data from the literature. The other lower tungsten carbide (W_2C) designated as ε-W_2C which was revealed sufficiently reliably in neutron diffraction studies. The researchers investigated carbon-rich sourced tungsten with different compositions,

temperatures and cooling rates. This ε-W_2C has given a chemical analysis of $W_2C_{0,86}$ composition with barely significantly different from the other carbon-rich preparations and traces of α-W [64]. Distribution of carbon atoms effects the ordering at high and low temperatures. In lower carbide case W_2C can be disordered at high temperatures and ordered at low temperatures. Also, the different types of carbon atoms distribution can cause formation of above-mentioned modifications of W_2C.

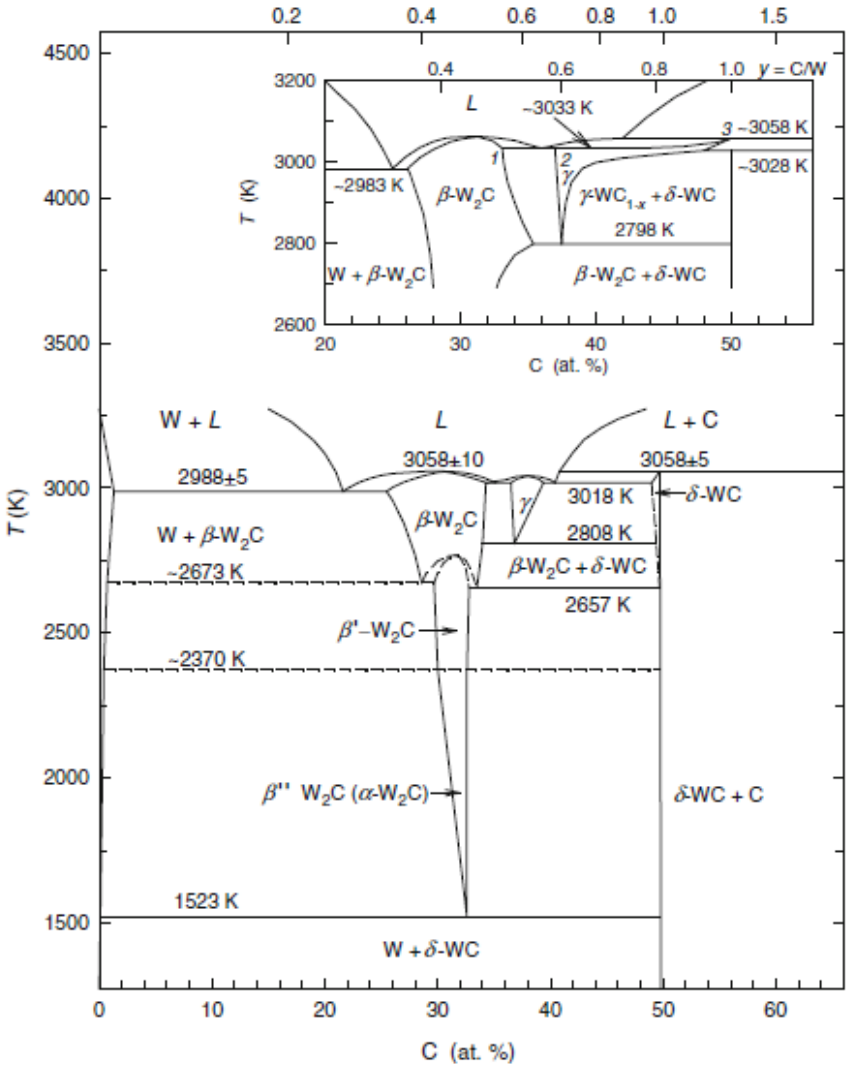


Figure 6.1 Generalised phase diagram of the W–C system [65]

The maximum solubility of carbon in tungsten is 0.3 at. % at 2400°C [66], and it decreases rapidly with falling temperature, being 0.05 at. % 2000°C and only traces at lower temperatures.

The tungsten-rich solid solution and the lower 'carbon carbide W2C form a eutectic containing 2 wt.% C and melting at 2710°C [67]. At 3.5 wt.% C the eutectic W_2C + WC is formed, which melts at 2760°C. In addition, a second modification of the carbide β-WC has been found; it crystallizes in a cubic lattice and is stable at temperatures above 2525°C [68].

6.1.2 Crystal Structure of Tungsten Carbide

The crystal structure of tungsten monocarbide WC is a simple hexagonal structure with AAAAAA metal atom packing, which is not detected for the pure metal. It results from the introduction of planes of carbon atoms. It can also be noted that the reaction WC ↔ W_2C + graphite is primarily redistribution of hexagonal planes. The segregation of carbon atoms during conversion from WC to W_2C transforms a simple hexagonal structure to a close packed structure [69]. The reaction is;

$$WC \leftrightarrow W_2C + \text{graphite} \quad [ACACAC \leftrightarrow A^{1/2}CB^{1/2}CA^{1/2}CB^{1/2}C + \text{graphite}] \qquad (6.1)$$

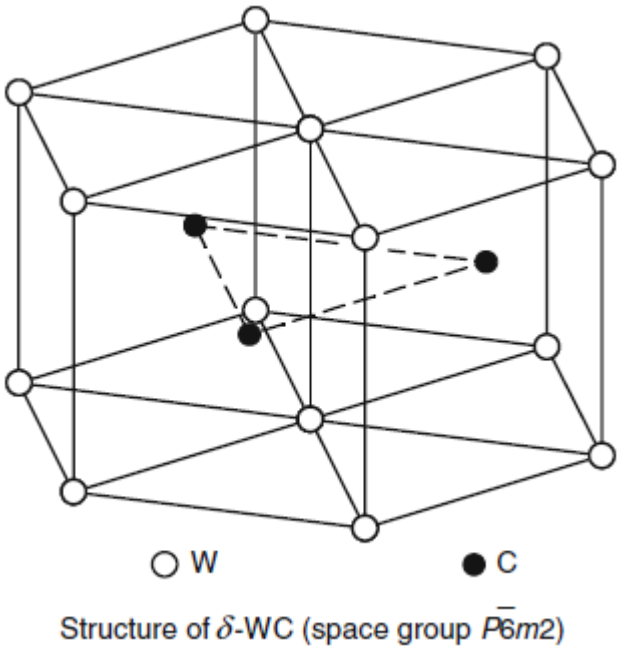


Figure 6.2 Hexagonal structure of higher δ-WC (WC) tungsten carbide: (•) C and (O) W [61]

Higher tungsten carbide δ-WC (WC) has an unimportantly small homogeneity region or negligible at all. Since the tungsten metal has its own structural type the

higher tungsten carbide δ-WC has hexagonal crystal lattice with own structural type B_h (the WC-type) and with the unit cell constants a = 0.2906 and c = 0.2837 nm [69, 70]. In this structure (Figure 6.2), tungsten atoms W occupy sites 1(*a*) with coordinates (000). Also, the carbon atoms are located in sites 1(*d*) with coordinates (1/32/31/2) [71].

Tungsten and carbon atoms in higher δ-WC (WC) carbide form simple hexagonal sublattices, in which C atoms are located in the centers of trigonal prismatic interstitials of the tungsten sublattice [61]. The estimated unit cell constants a = 0.288 and c = 0.281 nm [72].

6.2 Physical Properties

6.2.1 Density and Melting Point

As could be expected, the density increases considerably with the increasing atomic number of the metal. Unlike the carbides of Groups IV and V, the carbides of Group VI have melting points that are lower than those of their respective host metals [73].

Table 6.1 Density and Melting Point of WC, W and C

	Density (g/cm^3)	**Melting Point (°C)**
WC	15,8	2870
W	19,3	3422
C	2267	4227

6.3 Mechanical Properties

6.3.1 Hardness

Hardness is the resistance of a tunsgten carbide to penetration by a diamond driller under a specific load. It is measured on the Rockwell A scale in the US and on the Vickers (HV10 or HV30) scale in Europe and elsewhere.

Carbides of Group VI are not as hard as the carbides of Groups IV and V. This may be caused by the lower strength of their M-C bonds. The hardness decreases with temperature as shown in Figure 6.3. To compare, among the carbides, WC retains its hardness up to approximately 800 °C and, above 400 °C, also it is the hardest carbide [74, 75].

Hardness is mainly a function of composition and grain size. So, with the coarser tungsten carbide grain sizes produce lower hardness values. Conversely, fine grain sizes produce high hardness values. Hardness is directly related to abrasion resistance.

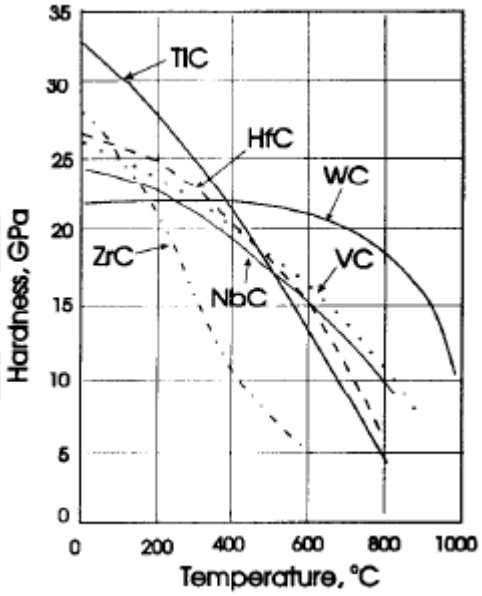


Figure 6.3 Hardness' of carbides as a function of temperature [73, 76]

6.3.2 High Temperature Hardness of Tungsten Carbide

In the hardness of WC single crystals, the effect of crystallographic alignment, carbide grain size and test temperature are investigated along with the hot hardness of polycrystalline tungsten carbide. The hot hardness of single crystal WC on all major crystallographic alignments evaluated decreases very rapidly for increasing temperature, and the single crystal hardness on its hardest alignment is only about half of the polycrystalline material depending on the test temperature. Because of its polycrystalline character, some cobalt bonded cemented tungsten carbides can be harder than single crystal WC over some intermediate temperature range [77].

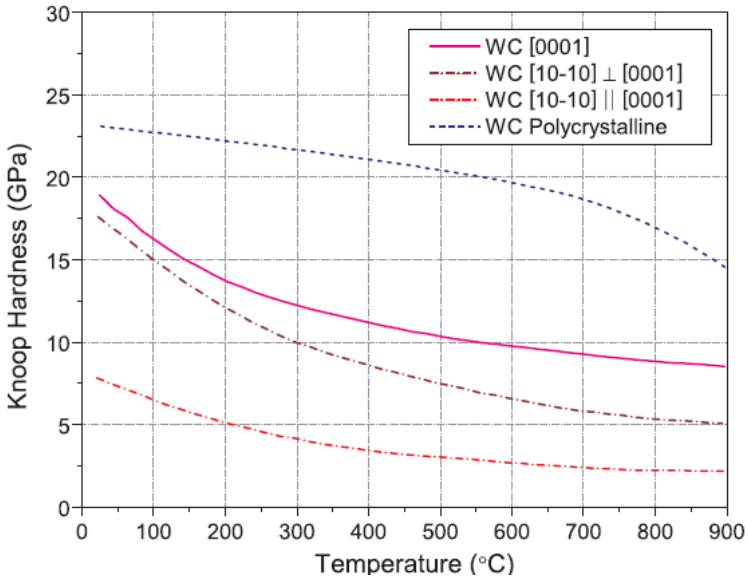


Figure 6.4 Hot Knoop hardness of single crystal tungsten carbide of several alignments and polycrystalline tungsten carbide [77]

The hardness value decrease of both polycrystalline samples with and without binder is not as extreme as the single crystals under 500 °C. Hardness of the polycrystalline samples, however, decreases rapidly as the temperature exceeds 600 °C as shown in Figure 6.4. Also, the hardness of polycrystalline WC is significantly higher than the single crystals [78].

6.4 Thermal Properties

6.4.1 Thermal Conductivity

Like the other interstitial carbides, the carbides of Group VI are good thermal conductors. This property comes from their metallic character. This is especially true for WC, which has the highest thermal conductivity of any of the transition-metal carbides, and so WC can be considered as an excellent thermal conductor [79, 80].

6.4.2 Thermal Expansion

Thermal expansion is important for predicting residual stresses in films, composites, and bonded hard materials. Tooling often requires bonding to materials that have either lower or higher thermal expansion. Difference with reduction that occurs when a material is cooled after high temperature bonding results in residual

stresses. Consequently, stresses occur if a low-temperature bond is put into high-temperature service. Thermal expansion is a fundamental property that is relevant for determining interatomic potentials and the equation of state of materials. It provides a stringent test for evaluating atomic potentials and equation-of-state concepts. At low and intermediate temperatures, thermal expansion can be reproducibly measured by using a variety of techniques. Theoretical calculations of thermal expansion have many assumptions which are both characteristic and exact. Tungsten carbide (α-WC) is an important industrial material that has a melting point of >3000 K and hexagonal symmetry. Limited thermophysical and mechanical property measurements are available for well-characterized samples. Currently, the thermal expansion coefficients for WC at temperatures 1300+ K (in some papers the values is dictated by Debye temperature) are limited and not very reliable however it can be said that the exact value for the room temperature for the tungsten carbide's coefficient of thermal expansion is 5.5 $\mu m.m^{-1}.K^{-1}$ [61].

6.5 Electrical and Magnetic Properties

The hexagonal tungsten carbide WC in the coarse grained and nanocrystalline states is a weak paramagnetic material at 300 –1250 K. The size of the particles in the n-WC nano powder remains unchanged during annealing in the temperature range from 300 to 1200 K, whereas the complete relaxation of micro strains occurs at 600 – 900 K. The features manifested in the temperature dependence of the magnetic susceptibility of nanocrystalline tungsten carbide are associated with the relaxation annealing of micro strains, which reduces the contribution of the orbital paramagnetism to the susceptibility of n-WC carbide and initiates the precipitation of iron and cobalt impurities in the form of superparamagnetic particles.

Table 6.2 Electrical Properties of WC

Material	**Electrical Resistivity at 20°C (μΩ.cm)**	**Hall Constant ($10^{-4}.cm^3/A.s$)**	**Magnetic Susceptibility (10^{-6} emu/mol)**
WC	22	-21,8	10

The direct effect of the small size of the particles of nanocrystalline tungsten carbide on its magnetic susceptibility has not known yet [81]. Electrical properties of WC are shown in Table 6.2. Like the carbides of Groups IV and V, the tungsten carbide is a good electrical conductor. WC has the lowest resistivity of any of the interstitial carbides. The Hall constant is negative [79].

The general properties of the WC are given in Table 6.3.

Table 6.3 The general properties of WC [82]

Property	**Value**	**Conditions**
Density	15800 kg/m^3	Ceramic
Knoop Hardness (KH)	1880 kg/mm/mm	100g, Ceramic
Vickers Hardness (VH)	2400 kg/mm/mm	50g, Ceramic
Vickers Hardness (VH)	1730 kg/mm/mm	100g, Ceramic
Modulus of Rupture	0.3838 - 5793 GPa	Ceramic, at RT
Poisson's Ratio	0.24	Ceramic
Tensile strength	0.3448 GPa	Ceramic
Thermal conductivity	84.02 W/m/K	Ceramic, at RT
Thermal Expansion	4.42 × 10^{-6} °C^{-1}	25 – 500 °C
	4.84–4.92 × 10^{-6} °C^{-1}	25 – 1000 °C
	5.35–5.8 × 10^{-6} °C^{-1}	25 – 1500 °C
	5.82–7.4 × 10^{-6} °C^{-1}	25 – 2000 °C
Young's Modulus	668.35 - 713.82 GPa	Ceramic, at RT

7
Abrasion Resistance

7.1 Abrasion Mechanism of Glass-Ceramic Structures

Abrasion resistance is the ability of materials to withstand the effects of wear. The abrasion process may include the surface layer of the coating (surface abrasion) or the material underneath (bottom surface abrasion). Surface abrasion can be easily understood from the loss of gloss or color change on the surface. Sub-surface abrasion, on the other hand, is larger scale damage, causing the metal substrate to deteriorate [4]. Abrasion resistance feature increases with hardness. Enamels exhibit optimum corrosion resistance and high hardness, but low fracture toughness weakens their abrasion resistance property. In addition, the high number of pores in the structure weakens the abrasion resistance. In enamel coatings, pores arise due to gases formed during firing such as hydrogen, water vapor, carbon dioxide, carbon monoxide and nitrogen. Although it is definitely present in wet applications, it can be used for resistance in some applications. The viscosity of the slurry is effective in the formation of pores, that is, low-viscosity slurries allow bubble formation, while not allowing gas evolution, thus large bubbles are formed. On the contrary, many small bubbles are formed while allowing the gas to escape in high viscosity enamel slurries. Mill additives also affect the viscosity of the slurry, as mentioned earlier. In general, the presence of alkali and alkaline earth oxides or silicates reduces the viscosity. Enamel slurries without additives have a low viscosity, thus allowing large bubbles to form, while not allowing the evolution of gaseous products [4, 6 – 8].

Since the abrasion mechanism of glass-ceramic materials is based on brittle fracture mechanism, it starts from weak points in the glass-ceramic structure. Particle agglomeration and pores are weak spots for the onset of nucleation and cause crack formation. It can be said that abrasion takes two steps. In the first step, a surface abrasion occurs, which eliminates the very thin shiny layer on the surface of the

enamel coating. Then the pores appear with sub-surface abrasion. Small pore sizes are a desirable feature for abrasion resistance in this context [4].

Abrasion resistance provides resistance against mechanical abrasions and scratches. Micro and macro abrasions create a path between the enamel coating and the metal substrate. This way causes corrosion of the bottom metal and the coating to deteriorate. In cookware, it causes the metal atoms to enter the food, which causes the migration of metal ions to the cooked food during cooking with the effect of temperature and pH of the processed food and has a very harmful effect on human health. The intake of these elements in the body for a longer period of time than required leads to diseases and can be fatal. The excess copper element accumulates in the cell core fluid and causes oxidative stress, thus affecting many immune functions [83]. Nausea, vomiting and diarrhea occur when excess iron increases in the body. Chronic or prolonged iron accumulation occurs in the body, while liver failure, diabetes, testicular atrophy, arthritis, cardiomyopathy, peripheral neuropathy and hyperpigmentation diseases occur [84]. Prolonged exposure to chromium causes chronic ulcers of the skin [85]. Manganese increasing in the body over an extended period of time causes anorexia, apathy, headache, leg cramps, speech disorder, encephalitis syndrome and Parkinson syndrome [86].

In order to protect the health of the human body at first, then to protect the coating quality and to prevent industrial loss, it is imperative that the abrasion resistance of glass-ceramic materials, especially enamels, are high.

7.2 Abrasion standards

In the literature, there are 2 standards specified for the abrasion resistance of enamels. The first of these is ASTM C488-88 (2016) The Tentative Method of Test for Abrasion Resistance of Porcelain Enamels standard. This method uses -70 + 100 mesh (+210 to -149 μm) glass sand for surface abrasion analysis and 180 μm electric corundum for sub surface abrasion analysis. For surface abrasion, 2 lt abrasive is released from a certain height with 30 ° and 45 ° degrees. The coating thickness and gloss values of the coating are measured and analyzed. The hard particles used in the sub-surface abrasion are released for 15 min. and mass changes in the enamel coated metal are observed. Then the abrasion indices are determined with the

formulations specified in the standard. The other method is the test for Taber Abraser device. The test involves the rotation of two abrasive stones under a certain mass and the enamel coated metal underneath. In this way, abrasion of the sample is provided. Typically, the abrasion process is completed with CS17F abrasive and 1 kg load. However, since the surface abrasion of the enamels did not change significantly against these abrasion systems, the researchers tested the enamel coatings in harsher environments [7, 87, 88].

7.3 Improving Abrasion Resistance

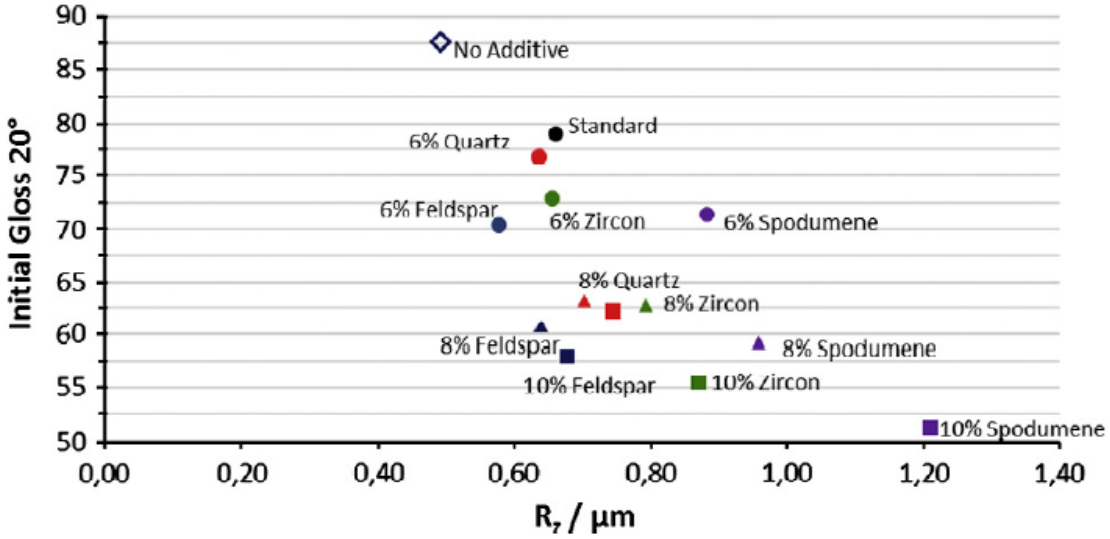


Figure 7.1 Relationship of gloss and roughness according to the used mill additives [8]

Rossi and Scrinzi studied on mill additions in order to investigate their effect on abrasion resistance of the vitreous enamel coatings [8]. The gloss depends to some extent on the surface roughness as shown in Figure 7.1. On a flat mirror-like surface, parallel light beams are projected in the same direction, while light beams are scattered on an irregular surface and the surface looks opaquer. The addition of milling additives leads to a reduction in gloss, since a certain amount remains undissolved in the glass-ceramic matrix. Therefore, it creates surface irregularities that lead to increased roughness and also a different light reflection. With the first addition of mill additives, the brightness decreases a lot, but with the increase of the addition the amount of increase decreases. Spodumene is the type of additive that leads to the highest roughness due to the size of large particles and low resolution.

Feldspar has a roughness value similar to a standard sample without additive because it has good solubility and low viscosity in the enamel matrix. However, the

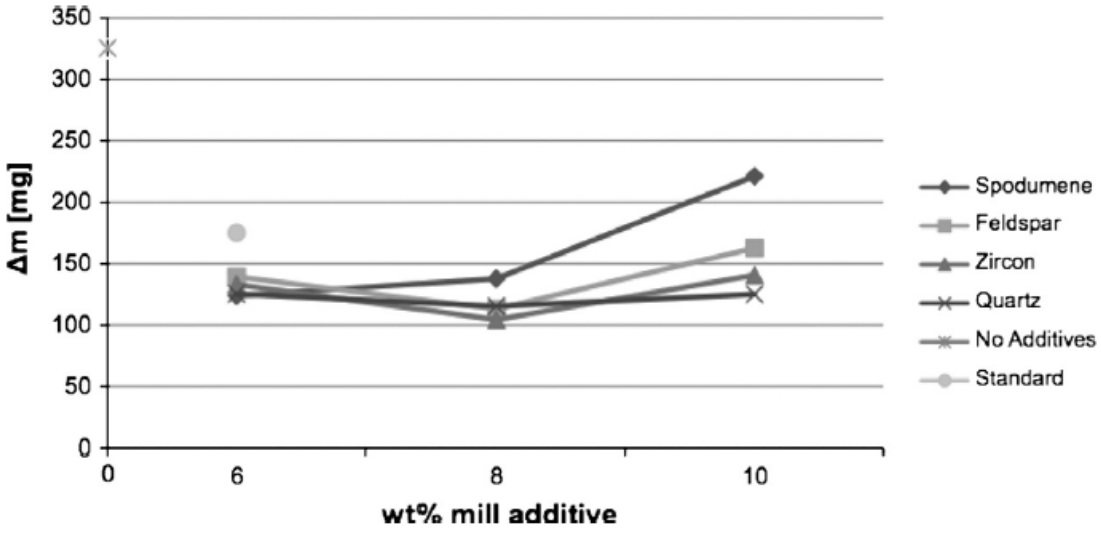


Figure 7.2 Mass loss graph of the studied mill additives with respect to the wt.% mill additive [8]

brightness decreases with increasing additives because the matrix composition changes with dissolution. Quartz and zircon have a roughness and luster similar to the standard sample without addition. Quartz provides the best brightness compared to the other three additives. Adding mill additives clearly increases the abrasion resistance of the enamel compared to the additive-free sample. In addition of 6% weight, all samples show a slight increase compared to the standard sample. Only a small difference in mass loss can be seen by increasing the mill additive content as shown in Figure 7.2. The mill additive has a threshold value. As the addition increases, the number of undissolved and large particles increases. This makes it easier to remove these particles from the surface by abrasion.

Again, Rossi, Parziani and Zanella have a study to investigate the effect of carbide particles on the abrasion resistance of enamels. In this study, 1% SiC, WC and graphite were added to the standard enamel coating [6]. All samples showed more mass loss than the reference sample. This is because the particle addition is insufficient to increase the abrasion resistance or larger pores are formed as a result of particle agglomeration. Particle agglomeration and pores are weak spots that initiate nucleation and crack formation and reduce abrasion resistance. Particles

such as WC, which are high in density, suffer greater mass loss during abrasion. For this reason, although mass loss is an important parameter, it is not the only parameter that determines the strength.

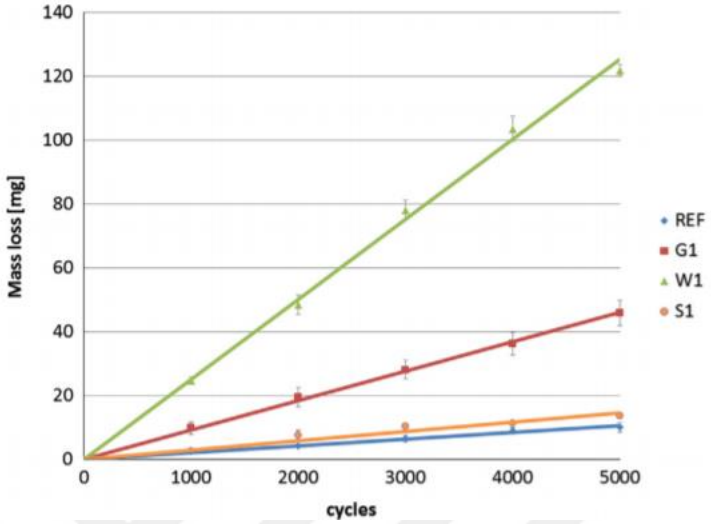


Figure 7.3 Mass loss graph of the studied samples with the content of 1 wt. % particle addition after the Taber abrasion test [6]

The abrasive effect causes the enamel surface gloss to decrease due to the removal of the coating parts and surface damage in all samples studied as shown in Figure 7.4. Specular reflection light value decreases with more diffuse reflection of light.

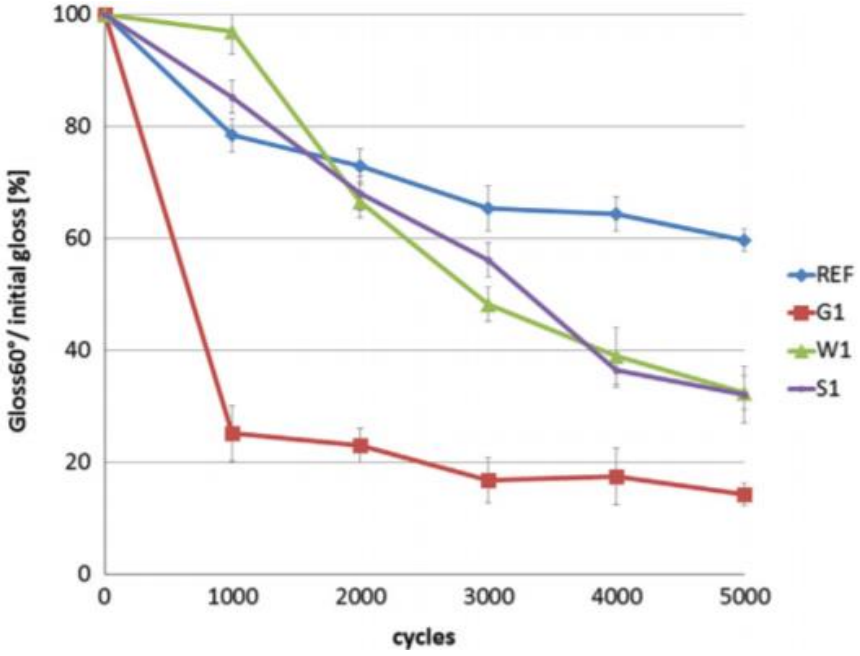


Figure 7.4 Gloss change percentage of the different particle added samples after the Taber abrasion test [6]

The sample containing 1% graphite particles has a rapid decrease in brightness values. This behavior stems from the tendency of lamellar graphite to produce flakes during the mechanical damage process. WC and SiC samples show a gradual change in brightness similar to the reference sample in the first 2000–3000 cycles. Then, a larger decrease from the reference is observed due to the high damage caused. Although there was an increase in abrasion resistance with the increase of WC amount used in the study, there was no major change in studies using graphite.

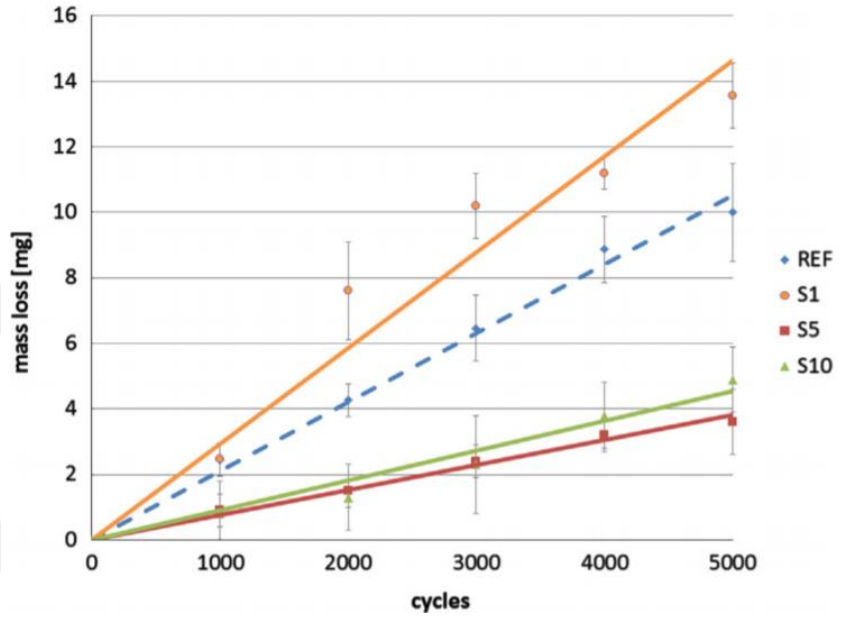


Figure 7.5 Mass loss graph of the studied samples with different content of SiC particles after the Taber abrasion test [6]

At the end of the study, mass loss shows excellent behavior by increasing the SiC amount in the samples containing SiC. The abrasion resistance is greatly increased by increasing the amount of particles between 1% and 5%. Increasing the particle content by 10% does not provide further improvement as shown in Figure 7.5.

Also in the study of Rossi et. al. with corundum particles, it has been reported that the abrasion resistance of the enamel can be increased with a high proportion of corundum particles with a low grain size [10]. In addition, it has been stated in the studies on aluminum enamels, WC and SiC particles have a positive effect on abrasion resistance [9].

8
EXPERIMENTAL STUDIES

8.1 Materials

Starting the study, the required mill additives for the coating application (black pigment, clay, boric acid and sodium nitrite) were provided by Gizemfrit Ceramic and Glaze San. Tic. A.Ş. The nano tungsten carbide (nano-WC) particles that were used in this study were purchased from Global Tungsten & Powders Corp. with particle size of 50 nm to 200 nm and with the purity of 99,99 %.

8.2 Frit Preparation

Seger formulation was prepared according to the desired properties and a recipe suitable for the formulation was prepared (Table 10.1). The weighed raw materials were placed in corundum pots, and the melting process was completed by melting them in the pot smelter at 1300 °C for 45 min. In order to obtain the frit structure after melting, the melt product is poured into water and the quenching process is completed. The resulting granular frit compositions were filtered, then dried at 100 °C for 24 h. The dried frit is thus made ready for milling step.

8.3 Preparation of The Samples

Alumina – zirconia ball mills with a capacity of 300 g were used in the milling procedure. Prepared frit composition and black pigment additive were ground in the mill for 12 min. Then, the grinding process was continued for another 3 min. by adding floaters and electrolyte additives. The recipe used in the study is given in Table 8.1.

In this study, nano tungsten carbide (WC) particles in different ratios were added to the samples as a mill additive. The ratios and sample codes of the nano WC particles used in the mill are shown in the Table 8.2.

Table 8.1 Studied enamel mixture composition

Material	**Content**
Frit Composition	100 %
Black Pigment	4 %
Clay	5 %
Acid Boric	0,25 %
Sodium Nitrite	0,25 %

Table 8.2 Sample codes and nano-WC addition content in this study

Sample Code	**Addition**
Reference	None
W10	1 wt. % nano WC
W25	2.5 wt. % nano WC
W50	5 wt. % nano WC
W75	7.5 wt. % nano WC
W100	10 wt. % nano WC

The powder enamel composition taken from the mill is sieved through a 60-mesh sieve. Then 40% (120 - 150 mL) of water of total frit composition was added. The slurry was mixed in the mill for two minutes in order to distribute the water and to distribute the floats and electrolytes homogeneously in the water. The slurry was filtered and made ready for application.

8.4 Coating Process

Cast iron was used as a metal substrate in the study. Cast iron pieces measuring 10 cm x 10 cm x 0,5 cm were subjected to surface cleaning before coating process. Samples were first subjected to sandblasting within the scope of mechanical cleaning and then they were cleaned with an industrial degreaser. After cleaning, the surface was subjected to hot water rinsing, cold water rinsing, neutralization and drying steps. Coating process was done by manual wet spraying method. Since the study was carried out on a laboratory scale, several furnaces were used in the firing process. The samples were first dried in an oven at 100 °C in order to evaporate the water inside and not distort the structure while evaporating. Then it was kept in the furnace at 550 °C for 5 min. The firing process was conducted in the furnace at 770 °C for 12 min. Samples were kept at room temperature after taken from the furnace.

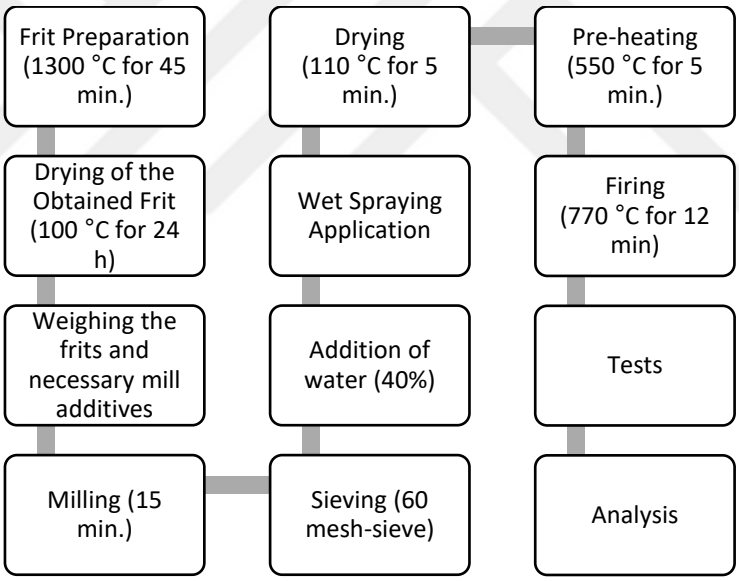


Figure 8.1 Flow chart of the experimental procedure done for this study

9
CHARACTERIZATION STUDIES

9.1 Chemical Analysis

The chemical composition analysis of the prepared frit was analyzed with the Bruker S8 Tiger X-ray fluorescence (XRF) device. Oxide percentages of frit were observed to see if the desired composition was obtained and to make a more accurate interpretation of the study.

9.2 Phase Analysis

Crystal phase analysis was carried out to examine the crystal structure formation and amorphous structure of enamels before and after firing and the behavior of nano WC particles during the enamel firing temperatures. XRD analysis with CuKα radiation, scanning range (2θ) of 15°–70° (Rigaku Miniflex 600) performed on pellets powders.

9.3 Microstructural Analysis

Microstructure of enamel before and after abrasion test, was observed by Jeol JSM-6060LV scanning electron microscopy/SEM equipped with EDS. For scanning electron microscopy (SEM) analysis, an acceleration voltage of 20 kV was used at working distances of 9.5 and 10 mm.

9.4 Thermal Analysis

The sintering behavior of the prepared frit composition was analyzed with the optical dilatometer (Misura 3.32) device. The sintering, softening, sphere, halfsphere, and melting temperatures of frit was determined by heating the frit sample to the melting temperatures at a rate of 10 °C/min. Linear thermal expansion coefficient of the frit composition studied in this study were determined using Netch thermal dilatometer (Model: 402EP) at a heating rate of 10°C/min to 550 °C.

Differential thermal analysis (DTA) was performed to evaluate the thermal expansion coefficient and glass transition temperature of the obtained frit via Netzsch STA 409 PC device.

9.5 Impact Resistance Analysis

Impact resistance (adhesion ability) of enamels is measured by releasing a 22 mm diameter cylinder apparatus weighing 1.5 kg from a height of 75 cm on an enamel coated metal surface as specified in BS EN ISO 10209: 2013 standard. As a result, the effect of a 15 kJ energy on the enamel surface is analyzed according to the standard [89].

9.6 Acid Resistance Analysis

For the acid resistance test of enamel coating, a solution is prepared with 10 g citric acid monohydrate and 100 mL distilled water which is based on ISO 28706-2 standard. 4 mL of the solution from the prepared solution is applied on the enamel surface and kept for 15 minutes on the enamel. The acid tested area is covered with a cap to prevent evaporation of the solution [90].

9.7 Coating Thickness

After the coating application and the firing process, the coating thickness of the enamel coating were analysed in order to investigate homogeneous coating thickness distribution and the changes in the coating thickness after the abrasion test with DeFelsko Positest DFT Combo model coating thickness gage according to ISO 2178:2016 standard [91].

9.8 Color Measurement

Color values and the color change after the abrasion of the studied samples were evaluated with Konica Minolta CM-700d Spectrophotometer in terms of L*, a* b* and ΔE [92].

9.9 Gloss Measurement

Gloss is evaluated with TQC Sheen Polygloss glossmeter device in 60° in five different points. The results are the mean of 5 measurements. Also, the gloss change of the samples after the abrasion test was analysed [93].

9.10 Surface Roughness Analysis

Roughness of samples after coating and rougness changes of the samples after the abrasion test were measured with Time TR200 Roughnessmeter device. Analyzes of 0.8 mm x 5 mm dimensions were made from 5 different regions.

9.11 Abrasion Resistance

The abrasion resistance of the samples were analyzed with Taber 5135 Rotary Platform Abraser. As abrasives, wheels of H18 type inelastic medium thickness containing vitreous clay and silicon carbide (SiC) or aluminum oxide (Al_2O_3) were used [94]. Samples were abraded under 250 g weight. After the abrasion process, the samples mass analyzes were performed in order to obtain the weight loss of the samples.

10
RESULTS AND DISCUSSION

10.1 Chemical Analysis

XRF analysis of the obtained frit composition is given in Table 10.1. The prepared frit composition contains high concentrations of SiO_2, B_2O_3 and Na_2O. A high proportion of SiO_2 and a relatively high proportion of B_2O_3 indicate that the frit is a thermally soft frit. As mentioned earlier, the concentration of CoO added to ensure adhesion between enamel and cast iron is 1.4 wt. %. It was observed that the frit composition was at the desired level.

Table 10.1 Chemical composition of the studied frit composition

Oxides	**Percentage (wt. %)**
Na_2O	11.67
K_2O	1.15
Li_2O	2.85
CaO	6.08
MgO	0.11
CoO	1.40
Fe_2O_3	2.01
Sb_2O_3	0.45
Al_2O_3	0.25
B_2O_3	17.99

Table 10.1 Chemical composition of the studied frit composition (continue)

SiO_2	52.94
TiO_2	1.60
ZrO_2	0.05
MoO_3	0.25
F	1.20

10.2 Phase Analysis

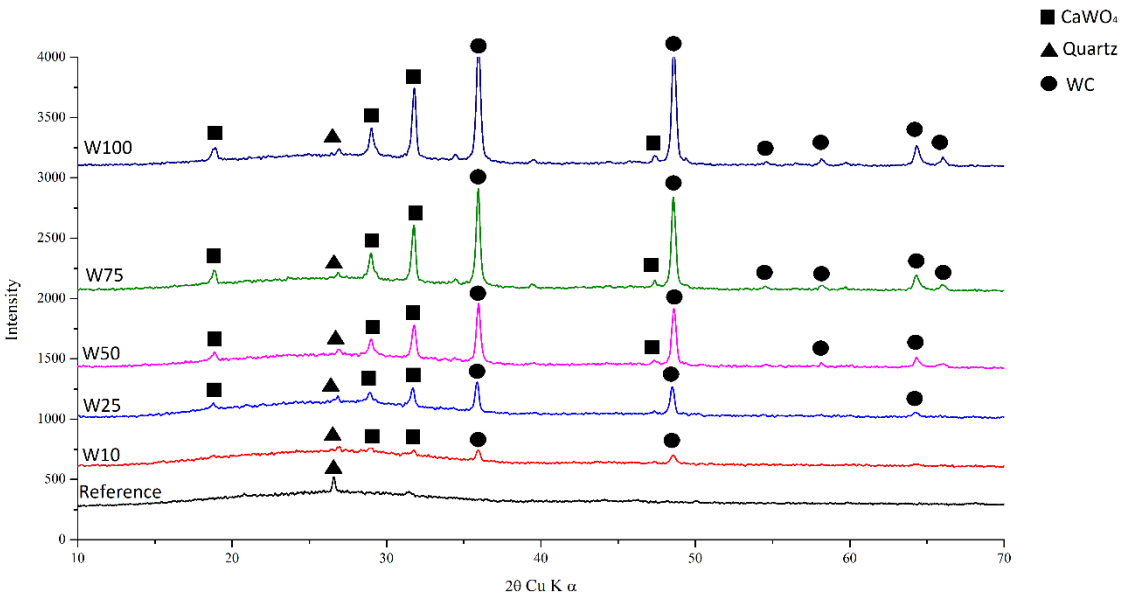


Figure 10.1 XRD patterns of the studied samples

Enamel coatings are in glass-ceramic structure, although the crystals formed can be of different crystal structure depending on the amount of oxide in the structure. In enamel coatings, the structure is generally β-Quartz or amorphous. In Figure 10.1, the quartz phase is observed, but the quartz phase in the structure may have been formed due to the clay used in the mill additive or the quartz phase may have formed in the crystal structure during the frit formation process. The nano tungsten carbide particles used in the study have WC peaks observed from the W10 sample in the structure. As can be seen from the increase in the peak size, there is an increase in the amount of WC. The important point here is the resulting $CaWO_4$ compound.

$CaWO_4$ peaks are observed in samples with WC added. This is explained by the oxidation of WC particles at enamel firing temperatures. The WC compound starts to oxidize from 500 °C. Oxidation products usually occur as WO_3 and WO_2 forms. The formation of these compounds depends on the amount of oxygen in the environment during oxidation [95 – 97]. The reactions that occur are given below:

$$WC + O_2 = WO_2 + C \quad (10.1)$$

$$WC + (3/2)\ O_2 = WO_2 + CO \quad (10.2)$$

$$WC + (3/2)\ O_2 = WO_3 + C \quad (10.3)$$

$$WC + 2O_2 = WO_2 + CO_2 \quad (10.4)$$

$$WC + 2O_2 = WO_3 + CO \quad (10.5)$$

$$WC + (5/2)\ O_2 = WO_3 + CO_2 \quad (10.6)$$

Since the furnace environment used in the study contains high oxygen, WO_3 compound is formed at the end of the firing process. The WO_3 compound formed reacts with CaO [98, 99]. The reaction that occurs is given below:

$$WO_3 + CaO = CaWO_4 \quad (10.7)$$

The reaction formation temperature is 550 °C and the name of the compound formed is the scheelite compound. The WO_3 compound forms a compound with Be, Mg, Ca, Sr, Na, and Ba from alkali oxides. However, the oxide structure of the enamel contains only MgO and Na_2O from these oxides. Since the MgO content in the structure is very low, they cannot form a compound. Although Na_2O is in high concentration, the compound is not formed because the reaction temperature is higher than 1000 °C [99, 100]. In this case, only scheelite compound was formed.

10.3 Microstructural Analysis

10.3.1 Surface Analysis Before Abrasion Test

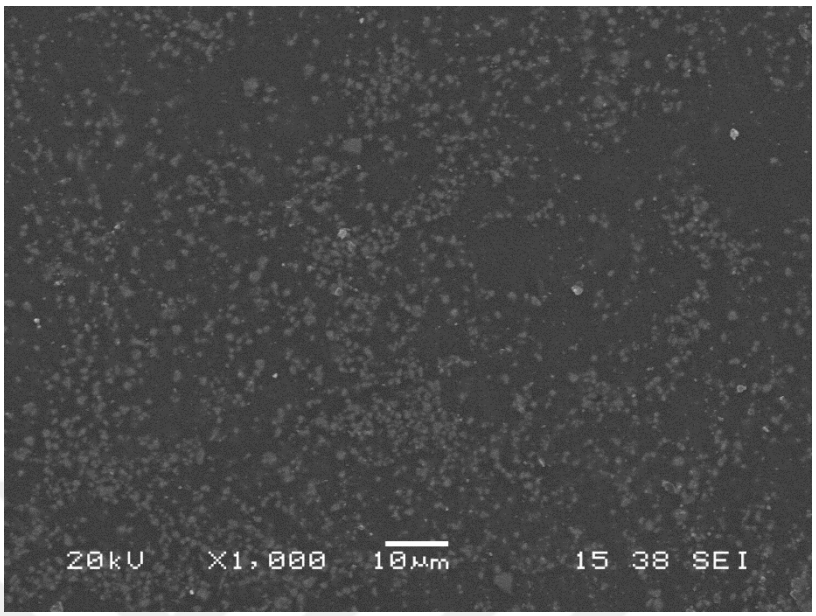


Figure 10.2 Surface SEM image of the studied reference sample without nano-WC particles

Figure 10.2 shows the surface SEM image of the reference sample without nano-WC particles. When the surface is examined, it is observed that the glass-ceramic structure is provided. The crystals formed are embedded in the structure and spread on the surface in the added pigment. The image examined shows the standard enamel coating image.

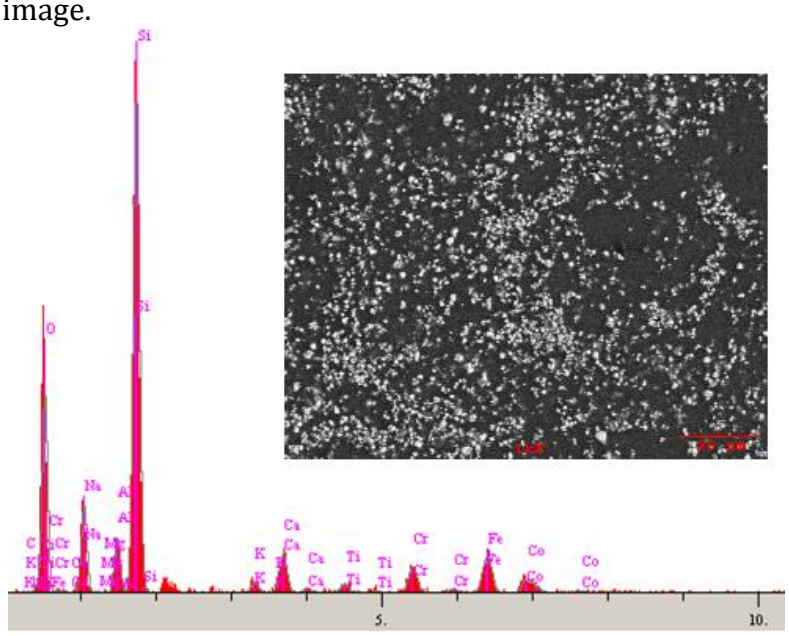


Figure 10.3 EDS analysis results of the reference sample's shown surface

EDS analysis was done regionally and expresses the element density in the whole region (Figure 10.3). As expected, there are mostly Si and O elements on the surface. Si and O elements that make up the half of the glass-ceramic structure were expected in this context. Other elements analyzed had different amounts and oxide forms. For this reason, it is observed that the EDS analysis is at the desired level, that is, the enamel coating structure that should be.

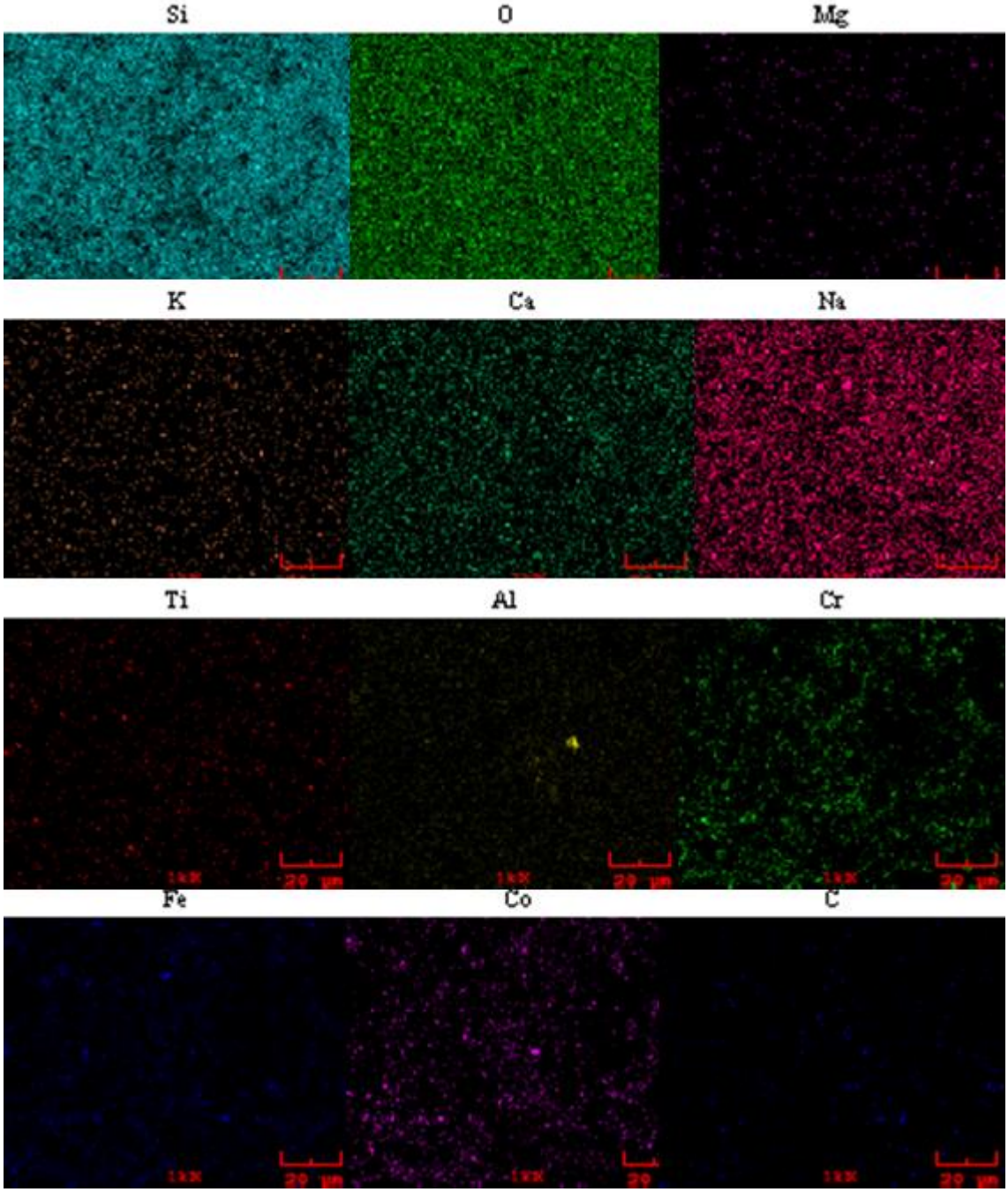


Figure 10.4 EDS mapping results of the reference sample

Figure 10.4 shows the EDS mapping results of the reference sample. After mapping analysis, it is observed that Si, O, Na and Ca elements are high on the surface in terms of peaks. It can be stated that these elements, which are also present in the glass-ceramic structure, are homogeneously distributed over the surface. It is observed that the white area in the middle of the surface is aluminum. It can be seen that aluminum is homogeneously distributed in the structure but accumulates at a certain rate. Although this is a common occurrence in enamel coating, it did not cause a defect on the surface since a large amount of accumulation did not occur. Afterwards, it was observed that elements such as Mg, K, Co and Ti were on the surface and distributed homogeneously. According to the results obtained from the mapping analysis, enamel coating was obtained as desired.

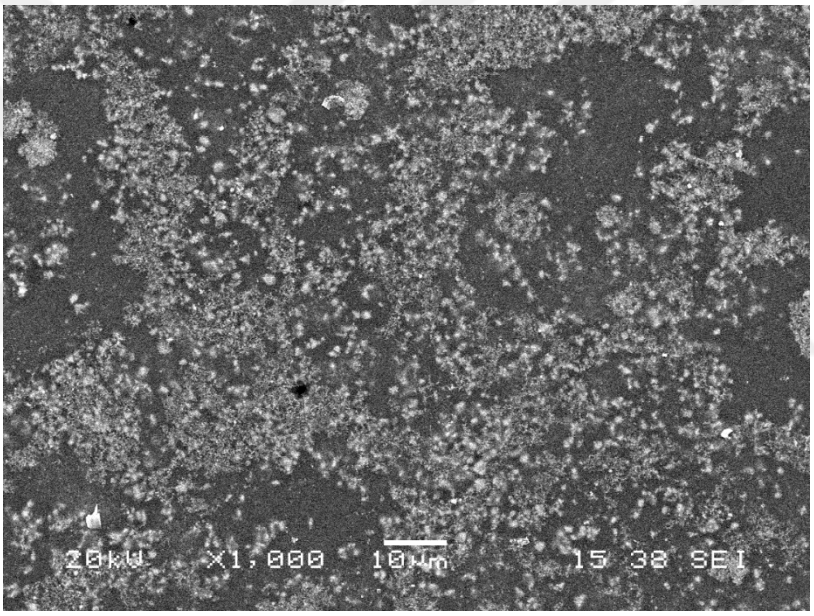


Figure 10.5 Surface SEM image of the studied W10 sample with 1 wt. % nano-WC particles addition

Figure 10.5 shows the surface SEM image of the W10 sample with 1 wt. % nano-WC particles addition. The nano-WC particles added as a mill additive showed an optimal result in the first addition to the structure. As seen on the surface, the nano-WC particles are homogeneously distributed on the surface. Regional spaces are considered to be the vitreous matrix.

Figure 10.6 shows the EDS analysis of the W10 sample with 1 wt. % nano-WC particles addition. As seen in elemental analysis, W peaks in the structure showed a high increase compared to the reference sample. In addition, other peaks observed

in the reference sample survived. A high peak level was not observed at the C peak. The reason for this is thought to be the oxidation of nano-WC particles in the structure during firing. WC particles are thought to turn into WO_3 compound with oxidation. However, it is understood by C peaks that this occlusion is partial.

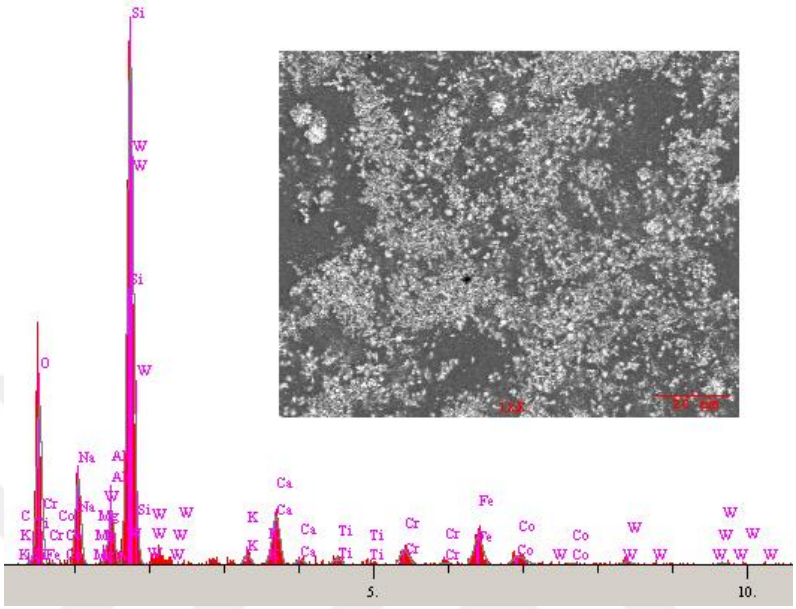


Figure 10.6 EDS analysis of the studied W10 sample with 1 wt. % nano-WC particles addition

Figure 10.7 shows EDS mapping results of the W10 sample with 1 wt. % nano-WC particles addition. As observed in the mapping analysis, there are high levels of elements such as Si, O, Na, Fe, Ca, Ti, Cr and Co. The reason for this is the oxides that already exist in the structure. In W10 sample, W peak image was observed by adding the first WC to the structure. It is understood that they are located in the same area when the W peaks that are homogeneously distributed in the structure are compared to the C peaks. In this way, it can be understood that WC particles are homogeneously distributed in the structure. In terms of oxidation status, it is not possible to make a definitive interpretation since O peaks are high in the whole structure as expected. However, the absence of C peaks in some regions where W peaks are seen sheds light on this issue. In addition, there are possibilities for a new compound to be formed only in regions where W peaks are observed and from the XRD analysis, it is considered that first occurrence of the scheelite phase can be observed.

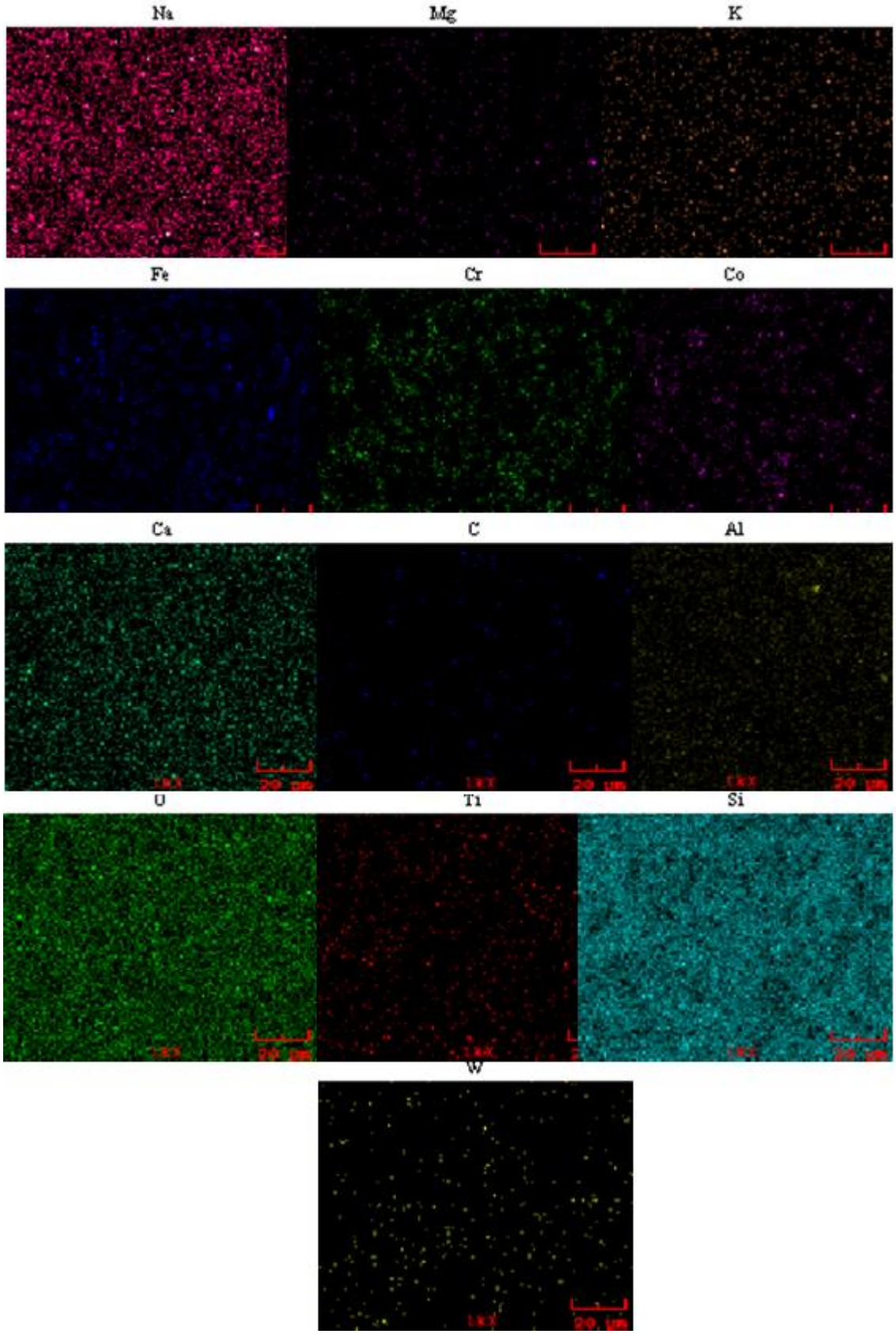


Figure 10.7 EDS mapping results of the W10 sample with addition of 1 wt. % nano-WC particle addition

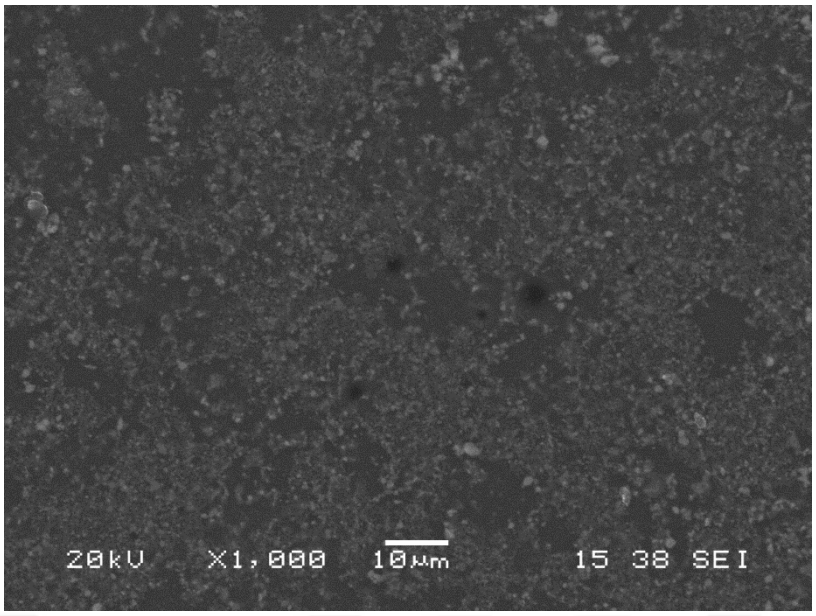


Figure 10.8 Surface SEM image of the studied W25 sample with 2.5 wt. % nano-WC particle addition

Figure 10.8 shows surface SEM image of the W25 after the coating application. When the sample surface is examined, it is observed that the increase of WC particles added on the surface shows a homogeneous distribution. The vitreous matrix can be observed in regional cavities on the sample surface. Light shades are known to be WC particles. However, it is seen that lightness in some regions is more intense and larger. If there are no different particles in these regions, it can be said that WC

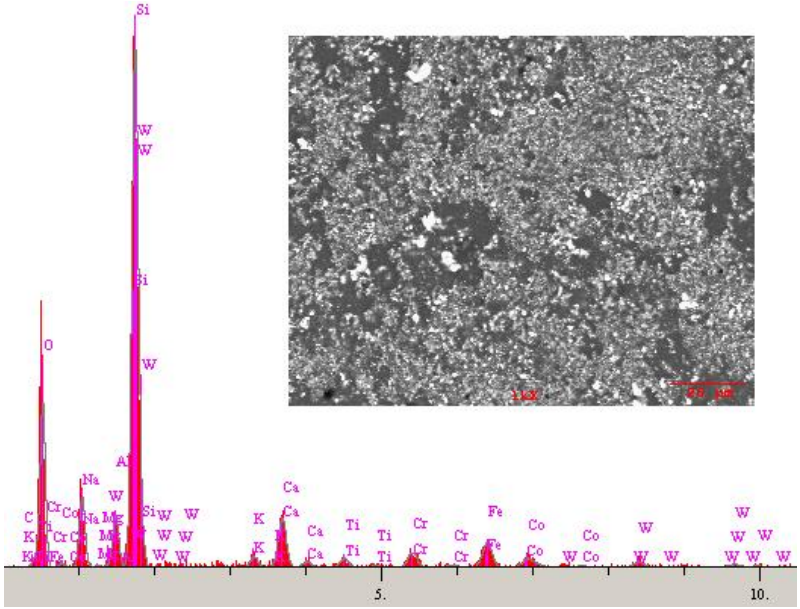


Figure 10.9 EDS analysis of the studied W25 sample with 2.5 wt. % nano-WC particles addition

particles come together and cause agglomeration. This can be explained by the high density of WC particles and the ease of aqueous application for agglomeration.

Figure 10.9 shows the EDS analysis of the W25 sample after the application process. When EDS analysis of the W25 sample is examined, it is observed that Si and W peaks have high intensity. Other peak intensity elements also exist. However, unlike other samples, it can be said that there is a low increase in severity at the Al peak.

Figure 10.10 shows the EDS mapping results of the W25 sample. In the mapping analysis, as in other samples, the severity of elements such as Si, O, Na, Fe, Ca, Ti can be observed. In addition, there is a local increase in Al peaks. This increase is an error that can occur on enamel surfaces, but when it does not have high severity, it is not observed as a macroscopic defect on the surface. When mapping analysis results and SEM analysis results are combined, it is observed that local brightness on the surface is a W element. Considering the distribution of the element C and the distribution of the element W, it is seen that there is no element C in the regions where the element W is severe, but the elements W and C are generally located in the same region. Oxidation is thought to occur in parts where W element is severe. The local oxidation that occurs is usually seen in the parts where the W element is concentrated, that is, agglomerated. It can be said that the surface meets the coating conditions in an elemental sense.

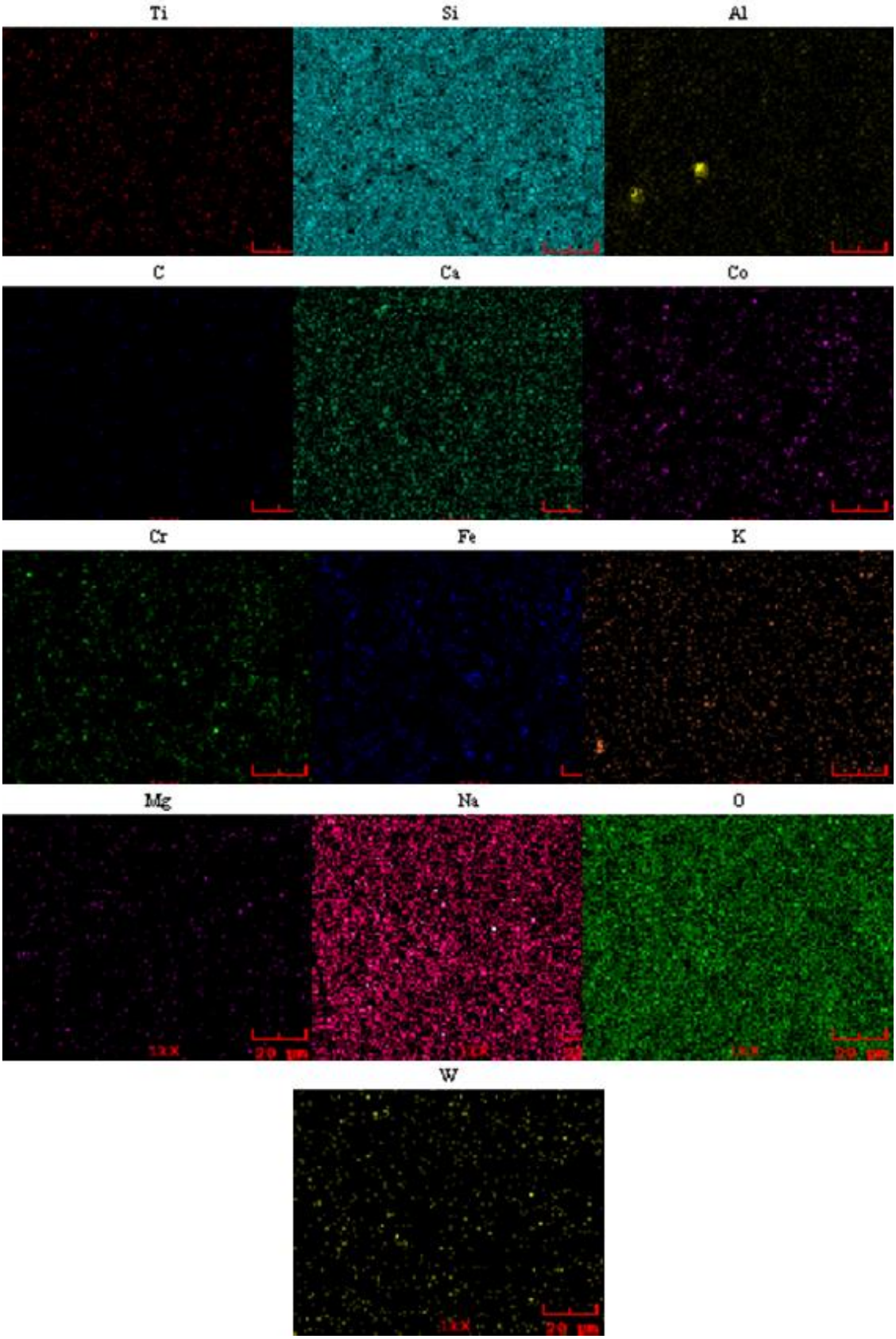


Figure 10.10 EDS mapping results of the W25 sample with 2.5 wt. % nano-WC particles addition

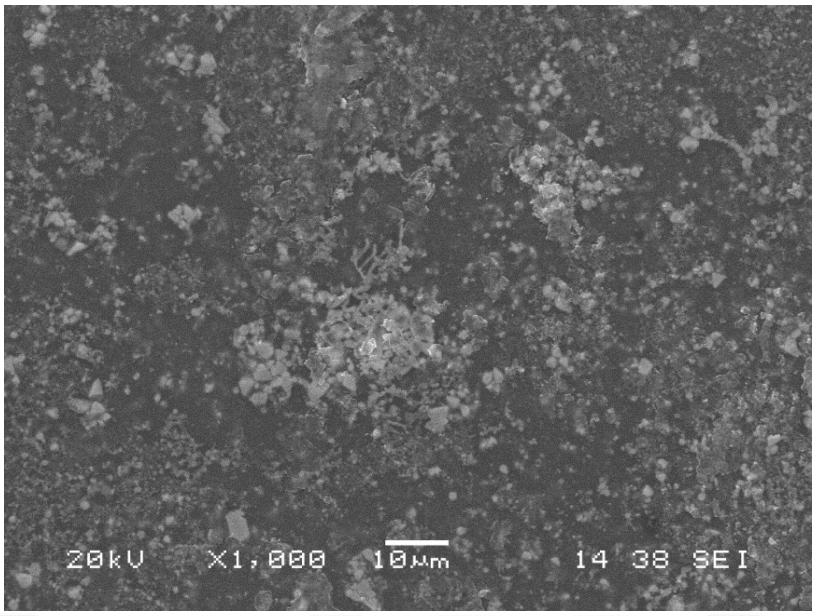


Figure 10.11 Surface SEM image of the studied W50 sample with 5 wt. % nano-WC particle addition

Figure 10.11 shows the surface SEM image of the W50 sample after the coating application. When the surface of the W50 sample is examined, it is observed that the WC particles spread well on the surface. However, as can be understood from the larger size structures and color tone difference, WC particles have become more prone to agglomeration with increasing concentration. The vitreous matrix can

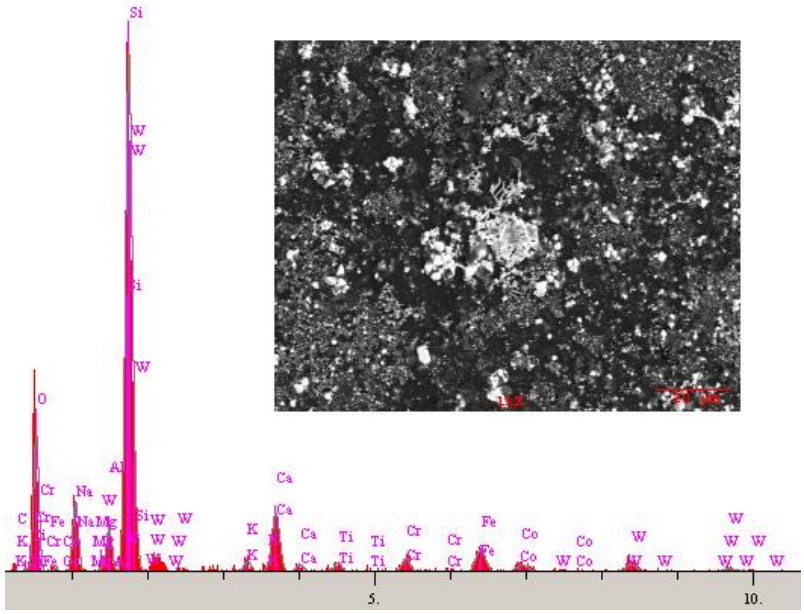


Figure 10.12 EDS analysis of the studied W50 sample with 5 wt. % nano-WC particles addition

appear in smaller areas on the surface. It can be said that the coating surface is suitable.

When the EDS analysis is examined, it can be said that there is an increase in W peaks compared to other samples (Figure 10.12). A decrease in the peak intensity of other elements occurred with increasing concentration of WC particles. However, no peak intensity is observed at the C peaks as much as the W peaks. For this reason, some of the nano-WC particles are thought to be oxidized.

Figure 10.13 shows the EDS mapping results of the W50 sample. When the surface of the W50 sample is examined by mapping analysis after coating, it can be said that, similar to the other samples, there are high amount of elements such as Si, O, Na, Al, Mg and K and it shows a homogeneous distribution. Although W peaks also accumulate in the middle of the image, they show peaks throughout the image in distribution. However, there is a noticeable decrease in the C peaks. Along with the increased WC concentration, the decrease in the C peaks increases the idea of oxidation while W peaks continue to be observed. The different point here is that Ca peaks are observed where W peaks are visible on the surface. SEM and XRD analysis can be correlated in here and stated the scheelite formation is increases with increasing amount of nano-WC addition.

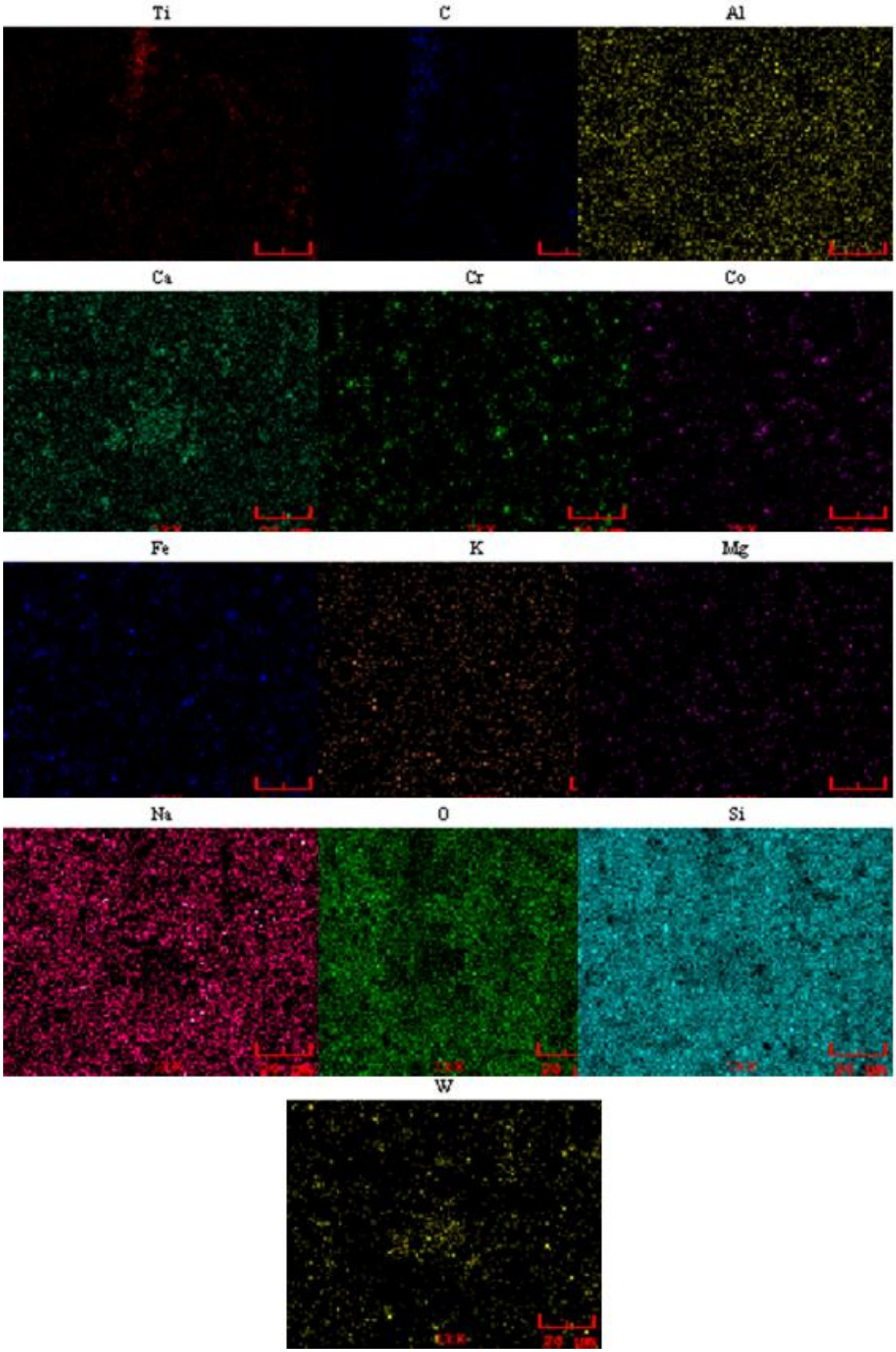


Figure 10.13 EDS mapping results of the W50 sample with 5 wt. % nano-WC particles addition

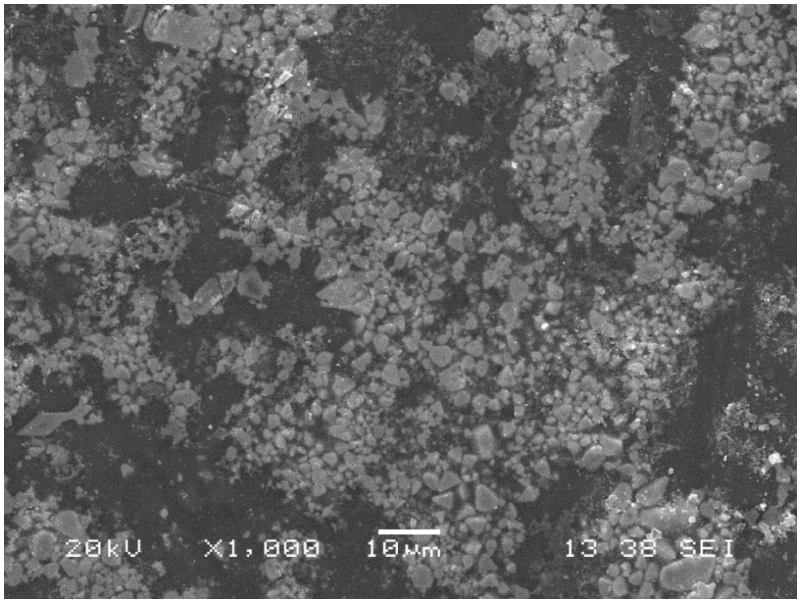


Figure 10.14 Surface SEM image of the studied W75 sample with 7.5 wt. % nano-WC particles addition

Figure 10.14 shows the surface SEM image of the W75 sample. When the surface of the W75 sample is examined after the coating process, the WC particles on the surface are clearly observed. It has been observed that the observed particles come together as a result of agglomeration and are larger in size. Although nano-WC particles spread over the entire surface, they have been agglomerated locally in certain areas and most of the surface. It is known that the gray colored areas are vitreous matrix. The coating was observed to be successful.

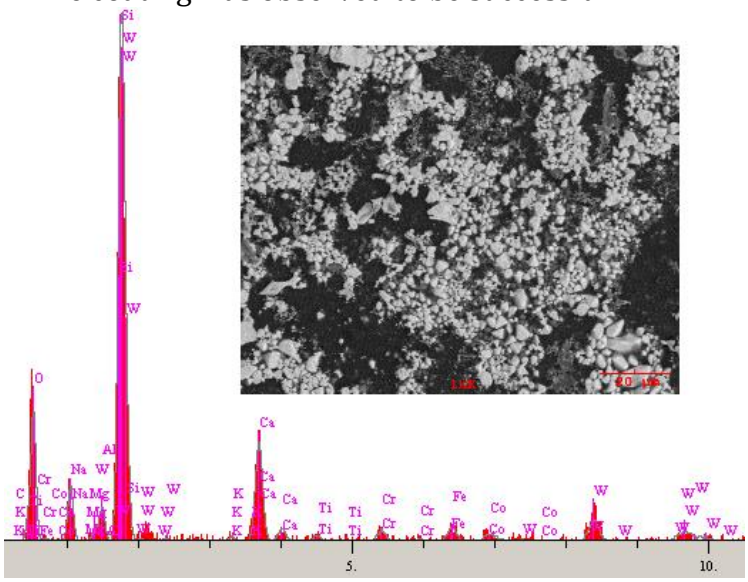


Figure 10.15 EDS analysis of the studied W75 sample with 7,5 wt. % nano-WC particles addition

Figure 10.15 shows EDS analysis of the W75 sample. When EDS analysis was analyzed, a high intensity was observed in Si and W peaks as in other samples. Unlike other samples, there was an increase in the Ca peak and a decrease in the Fe and Na peaks. As in the W50 sample, no intensity was observed in the W75 sample in the C peak as in the W peak. It can be said that there is a certain amount of oxidation in this sample.

Figure 10.16 shows EDS mapping results of the W75 sample. As in other samples, Si, O, Na, K and Mg are observed at a high rate in W75 sample. The remarkable part is the decrease in C peaks despite the increase in W peaks. For this reason, oxidation is considered to be higher than other samples. Another remarkable point is that Ca peaks are generally high in the area where W peaks are. It is thought that this situation, which is observed in the W50 sample, also partially less, is caused by the formation of a new compound or phase between W and Ca, which is scheelite phase. In addition, the high intensity increase in W peaks was seen in the mapping analysis and confirms the oxidation.

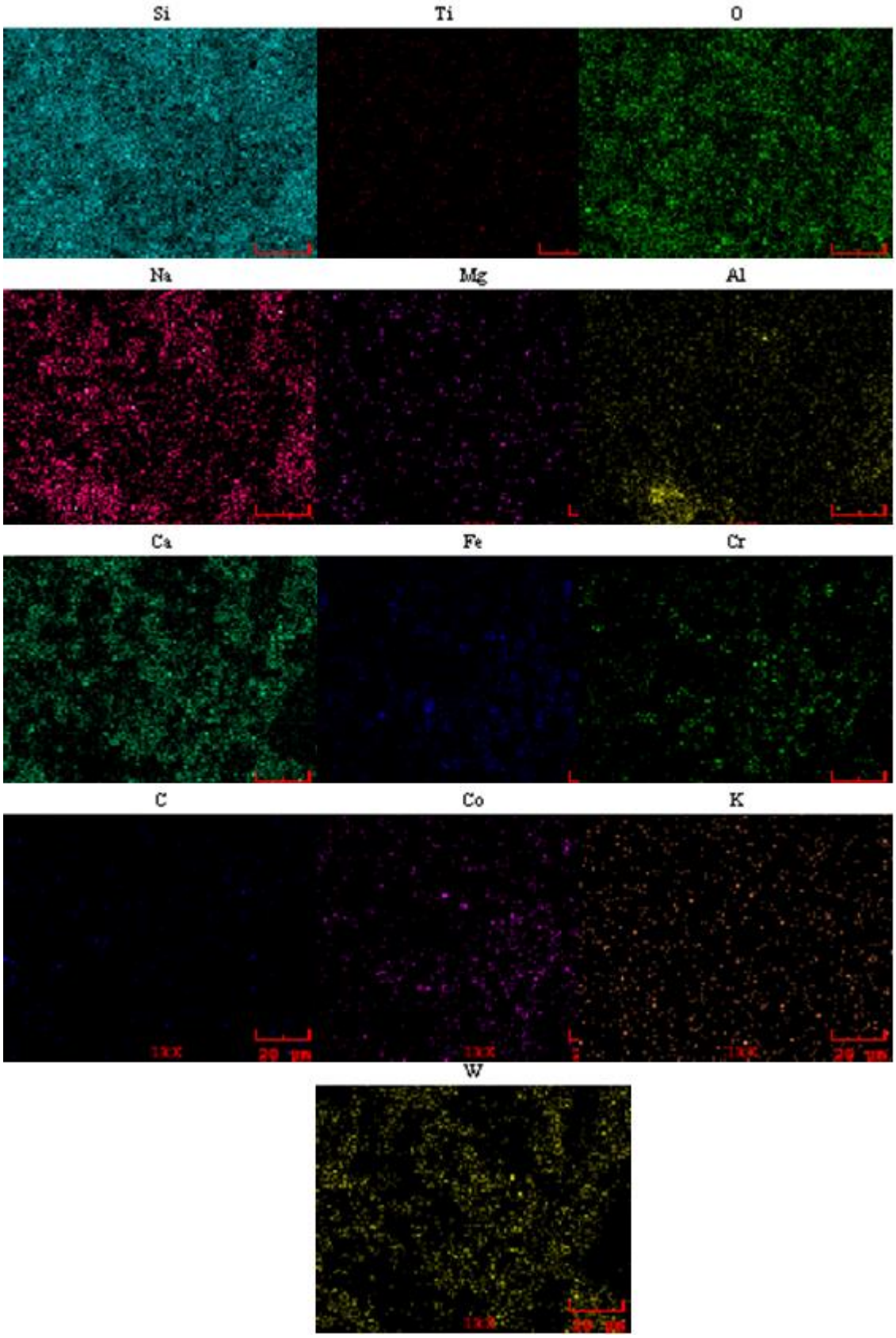


Figure 10.16 EDS mapping results of the W75 sample with 7.5 wt. % nano-WC particle addition

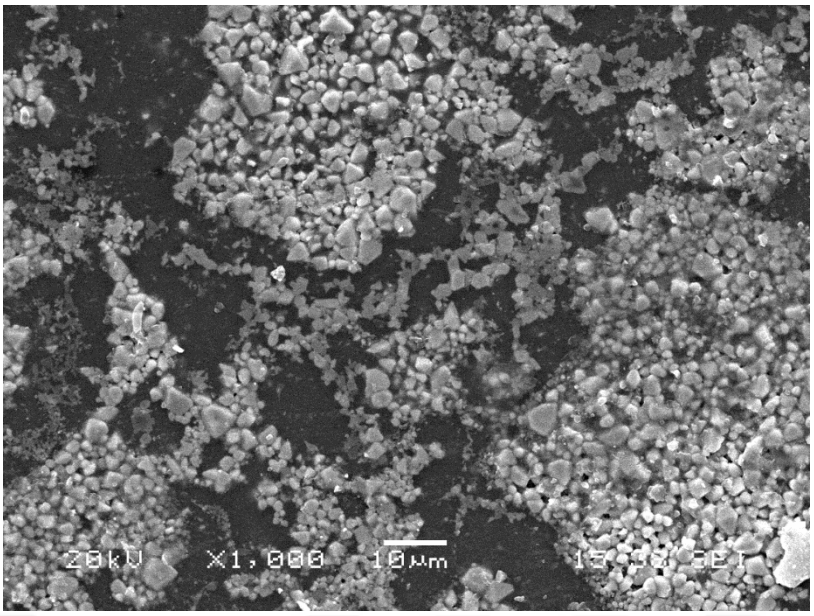


Figure 10.17 Surface SEM image of the studied W100 sample with 10 wt. % nano-WC particles addition

Figure 10.17 shows the surface SEM image of the W100 sample. When the W100 sample was subjected to SEM analysis after the coating process, it was observed that the added nano-WC particles were highly agglomerated. On the observed surface, the vitreous matrix is observed in the black-gray part. Low nano-WC particles are seen in the vitreous matrix. However, it has been observed that most of the particles

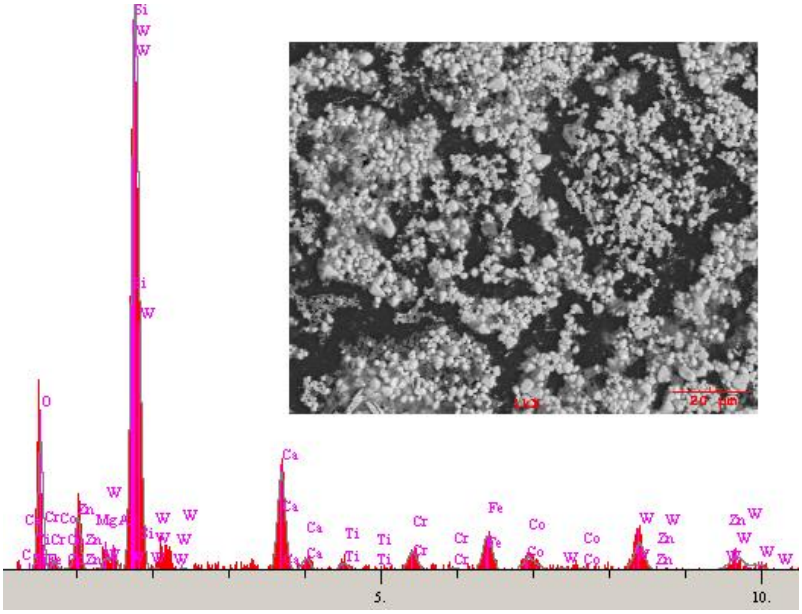


Figure 10.18 EDS analysis of the studied W100 sample with 10 wt. % nano-WC particles addition

come together locally on the surface. In the context of coating, a successful surface is observed.

Figure 10.18 shows the EDS analysis of the W100 sample. When EDS analysis is examined, high intensity Si and W peaks are observed in W100 sample as in other samples with nano-WC additive. As in the W75 sample, an increase in Ca peaks and a decrease in Fe and Na peaks are observed. The drop in the Na peaks is higher than the drop in other samples. This is thought to be due to the presence of high amounts of nano-WC particles on the surface.

Figure 10.19 shows EDS mapping results of the W100 sample. As in other samples, high rate of Si and O peaks were seen in W100 sample. However, there was a significant decrease in Na peaks. The reason for this is thought to be the high amount of nano-WC particles that are added. Unlike other samples with nano-WC additives, there is an increase in Al peaks. W and C peaks are observed to be in almost the same locations locally. However, the intensity of the W peaks is higher than the C peaks. This is thought to be caused by oxidation, as in the W50 and W75 sample. In addition, it is observed that they are concentrated in similar regions where Ca peaks and W peaks are compared. This is considered to be due to the scheelite formation, as in the W75 sample.

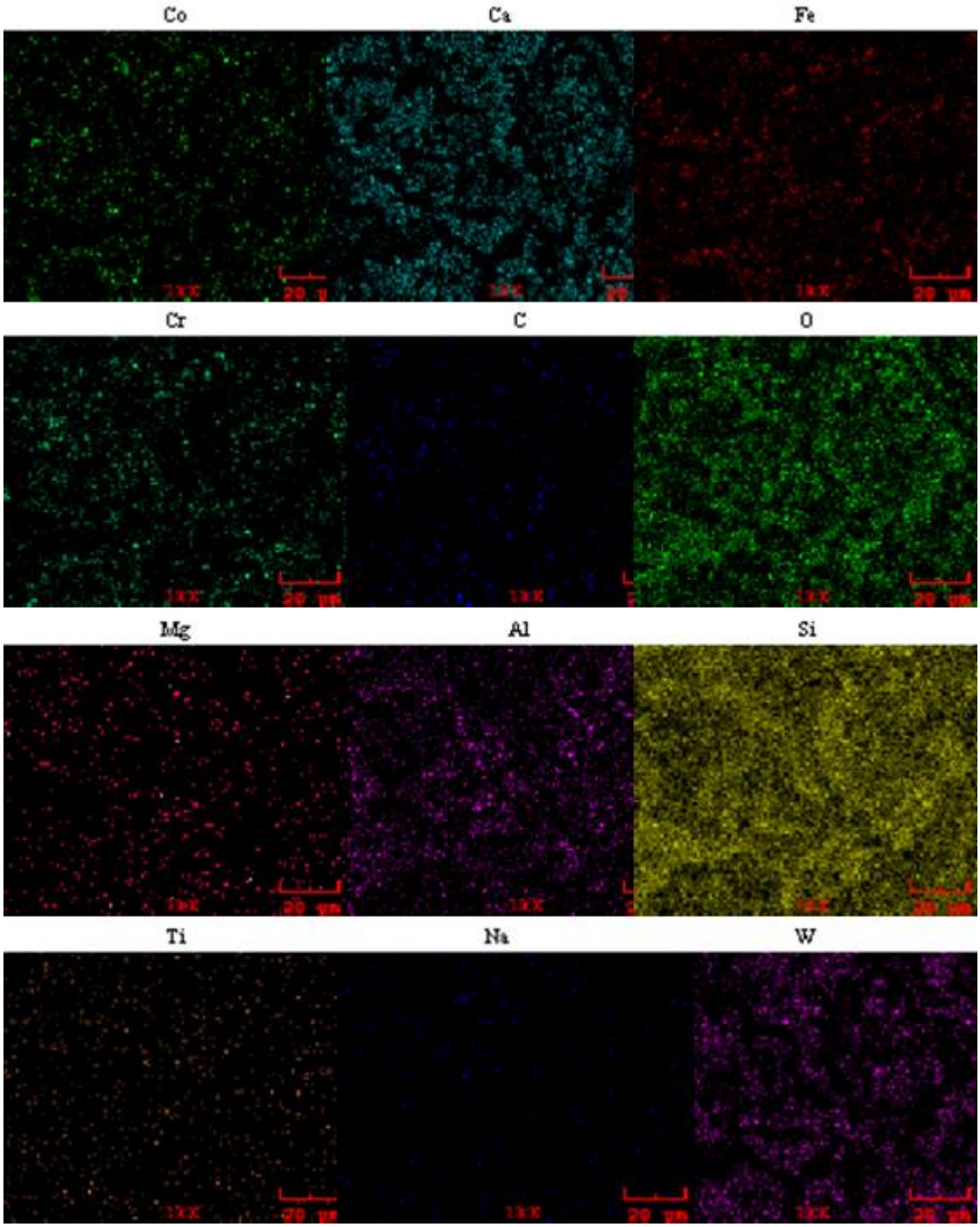


Figure 10.19 EDS mapping results of the W100 sample with 10 wt. % nano-WC particles addition

10.3.2 Cross-Section Analysis Before Abrasion Test

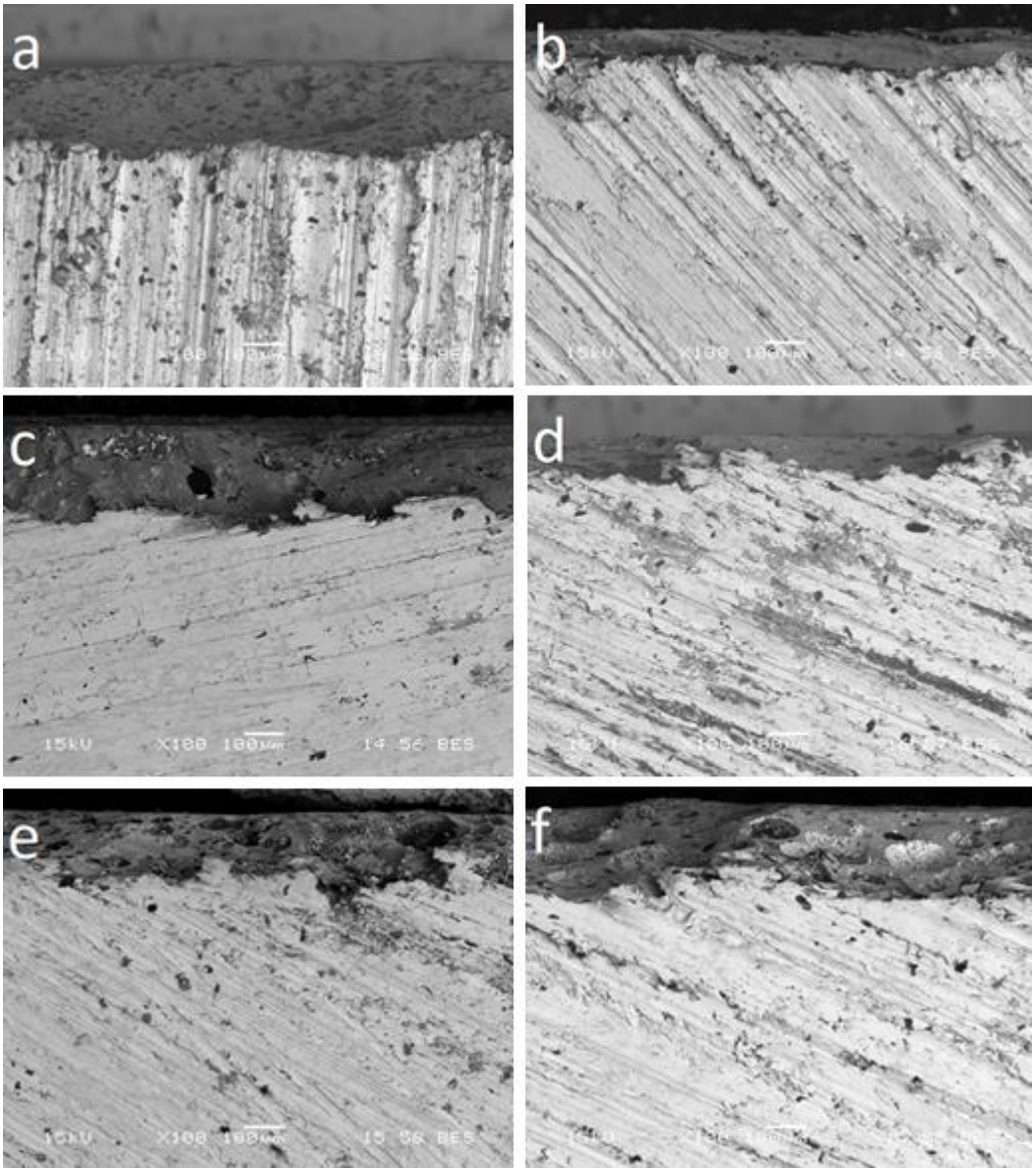


Figure 10.20 Cross-sections of the studied samples after the coating process; (a) reference sample, (b) W10, (c) W25, (d) W50, (e) W75 and (f) W100

Figure 10.20 shows the SEM images of the coatings cross section. For all six samples the adhesion between enamel coating and substrate are excellent [42, 101]. Lack of cohesion has not been observed between particles and glass-ceramic matrix. The porosity inside the coating is a very common defect in enameling [102, 103] which is formed by gas evolution during firing process. The gases can be H_2, CO_2, CO, water vapor and N_2 [104]. However, the shape, size and quantity of the porosities are related to the frit composition.

10.3.3 Surface Analysis After Abrasion Test

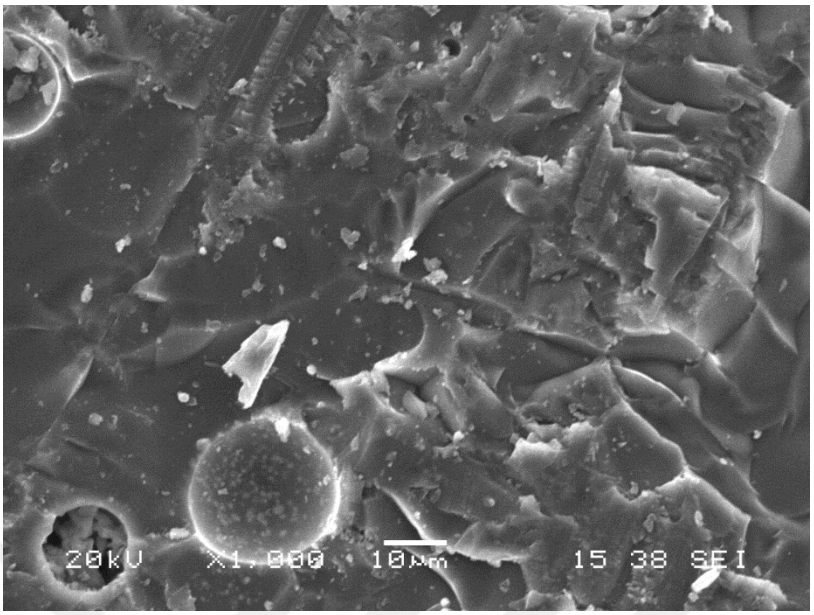


Figure 10.21 Surface SEM image of the studied reference sample without nano-WC particles after the abrasion test.

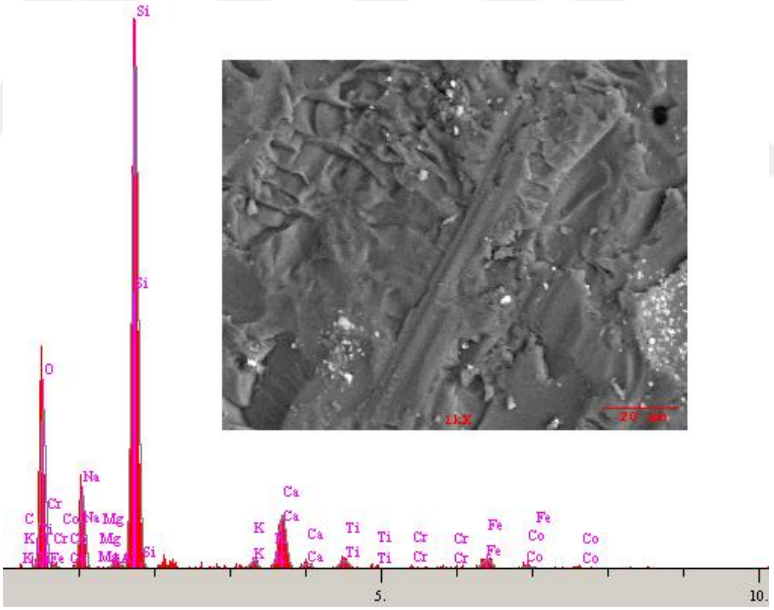


Figure 10.22 EDS analysis of the reference sample without nano-WC particles after the abrasion test

Figure 10.21 shows the surface SEM image of the reference sample after the abrasion test. When the surface is examined, the first signs of abrasion occurring with abrasion behavior can be seen. During the abrasion test, abrasive wheels and mass, along with the surface abrasion, can be seen linearly at the top of the sample.

It can be said that with the abrasion test, micro voids in the surface of the sample are opened. In addition, vitreous flake formation was observed on the surface.

Figure 10.22 shows the EDS analysis of the reference sample. EDS analysis was performed locally, expressing the element density in the whole region and as expected, a high rate of Si and O peaks were observed. The peaks of the elements in the glass-ceramic enamel coating were observed at low rates. When the change in the reference sample before and after abrasion is examined, it is observed that there is no high change in terms of elements. This is explained by the brittle fracture mechanism in the glass-ceramic structure. It can be said that the abrasion is homogeneous since there is no additive to prevent abrasion in the vitreous matrix.

Figure 10.23 shows the EDS mapping results of the reference sample. In the mapping analysis, a comment can be developed in terms of abrasion according to the regions where the elements are concentrated. As expected, a large amount of Si, O and Na elements persist on the surface. It is observed that the content of Vitreous vials formed is higher in Fe, Al and Cr elements compared to other elements. Although no definitive judgment is reached, the local observation of R_2O_3 elements in terms of elements can be explained by the presence of pigment or the idea that R_2O_3 group elements show a local resistance to abrasion. This observation will be compared with tests on other samples.

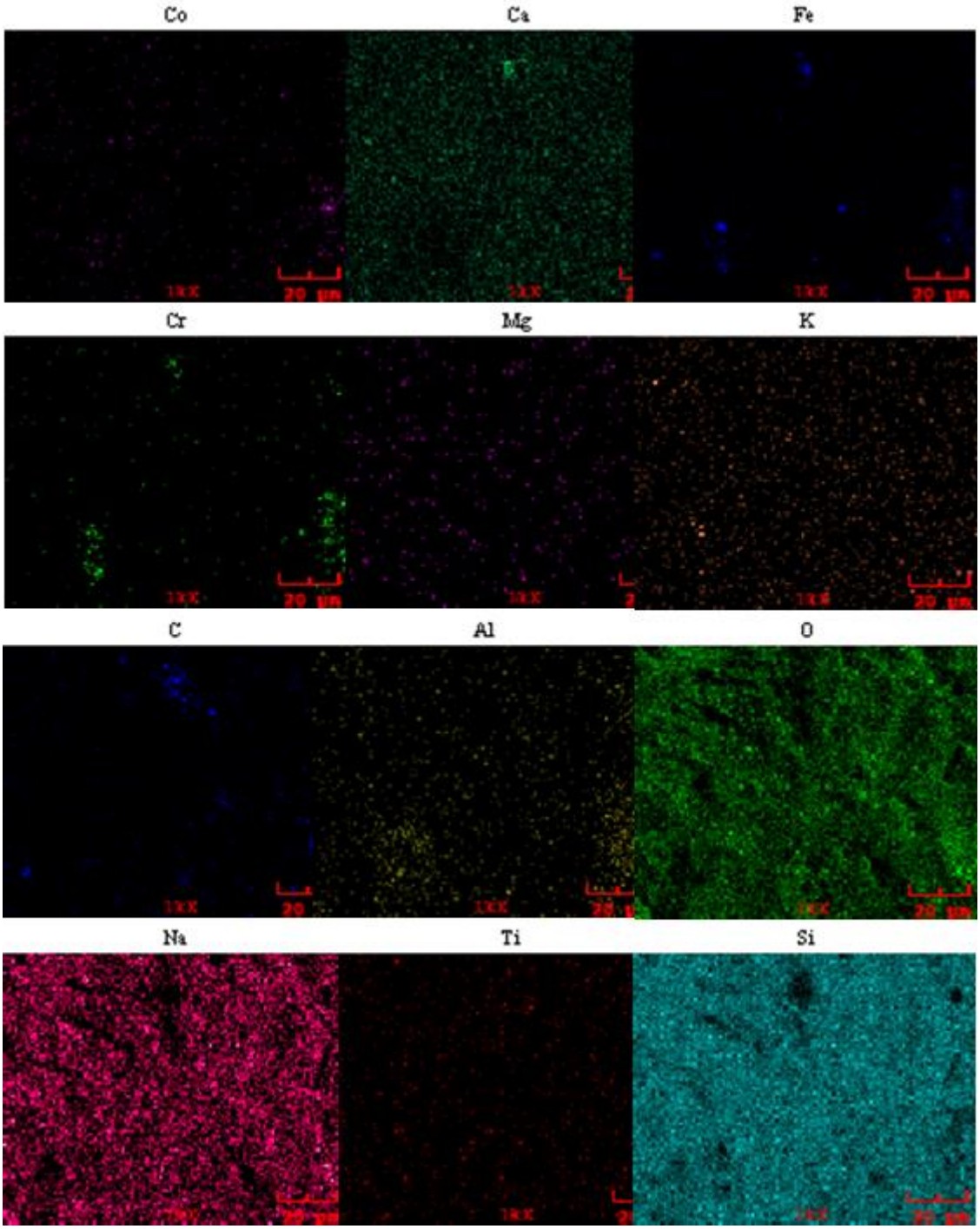


Figure 10.23 EDS mapping results of the reference sample without nano-WC particles after the abrasion test

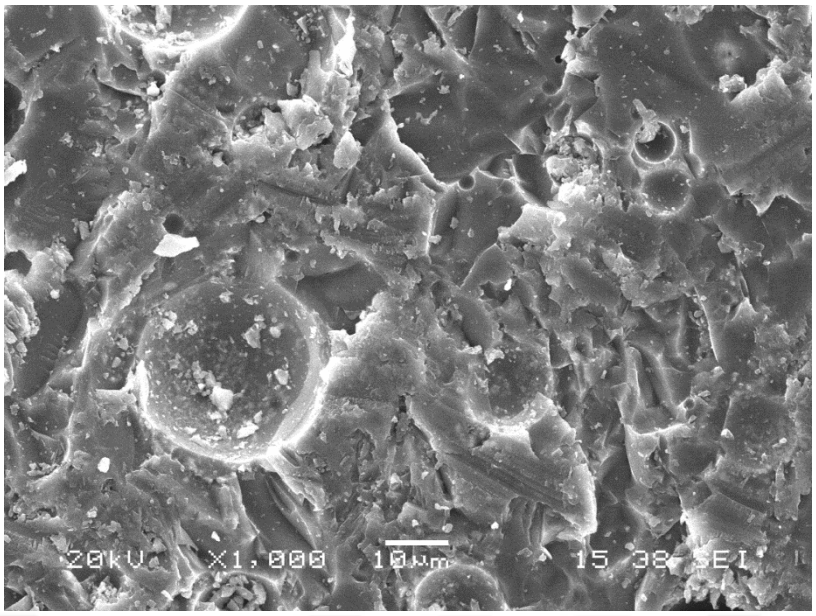


Figure 10.24 Surface SEM image of the studied W10 sample with addition of 1 wt. % nano-WC particles after the abrasion test

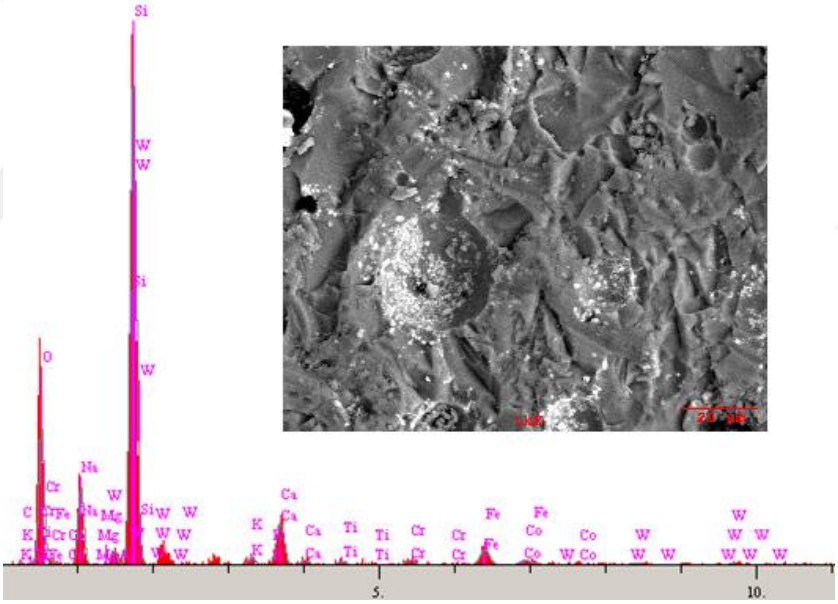


Figure 10.25 EDS analysis of the W10 sample with addition of 1 wt. % nano-WC particles after the abrasion test

Figure 10.24 shows the surface SEM image of the W10 sample after the abrasion test. When the surface is examined, it can be observed that the traces of abrasion are in the lower right part of the sample. With abrasion, it can be observed that the voids under the surface are opened again. In vitreous flake formation, it can be observed that there is a partial particle detachment compared to the reference sample. It can be said that the formation of vitreous flake shows the first resistance of the surface

against abrasion in this part. As it is understood from the surface, it can be said that there is no large abrasion resistance. However, considering the abrasion pattern and flake formation in the surface image of abrasion resistance compared to the reference sample, it can be said that there is a slight increase.

Figure 10.25 shows EDS analysis of the W10 sample after the abrasion test. When the W10 sample is analyzed elementally, it is observed that the intensity in the Si and W peaks continues. It can be said that there is a small decrease in violence in other elements. Especially when Fe peaks are examined, there is a decrease in element intensity. In the case of WC particles, it is seen that W and C peaks are observed in the sample. Thus, it is known that WC particles are in the structure.

Figure 10.26 shows the EDS mapping results of the W10 sample. As with other samples, Si, O, Na, Ti and Mg elements persist in the structure. However, it is observed that the presence of these elements decreases in the void emerging after abrasion in the sample. When the W peaks are examined, it is observed that there is a density in the region where the void in the coating is exposed. However, when the C peaks are examined, it can be said that the C element is found at a normal rate, not high, around the void. It can be said that the void formed here is formed by oxidation of WC particles, but this is not the only reason. Void formation is an expected feature in enamel coating and especially enamel coating produced with aqueous application. These voids may occur during the rapid evaporation of water in the coating during drying and firing after aqueous application. However, the W and C peaks in the formed space and the intensities of these peaks raise the process of oxidation.

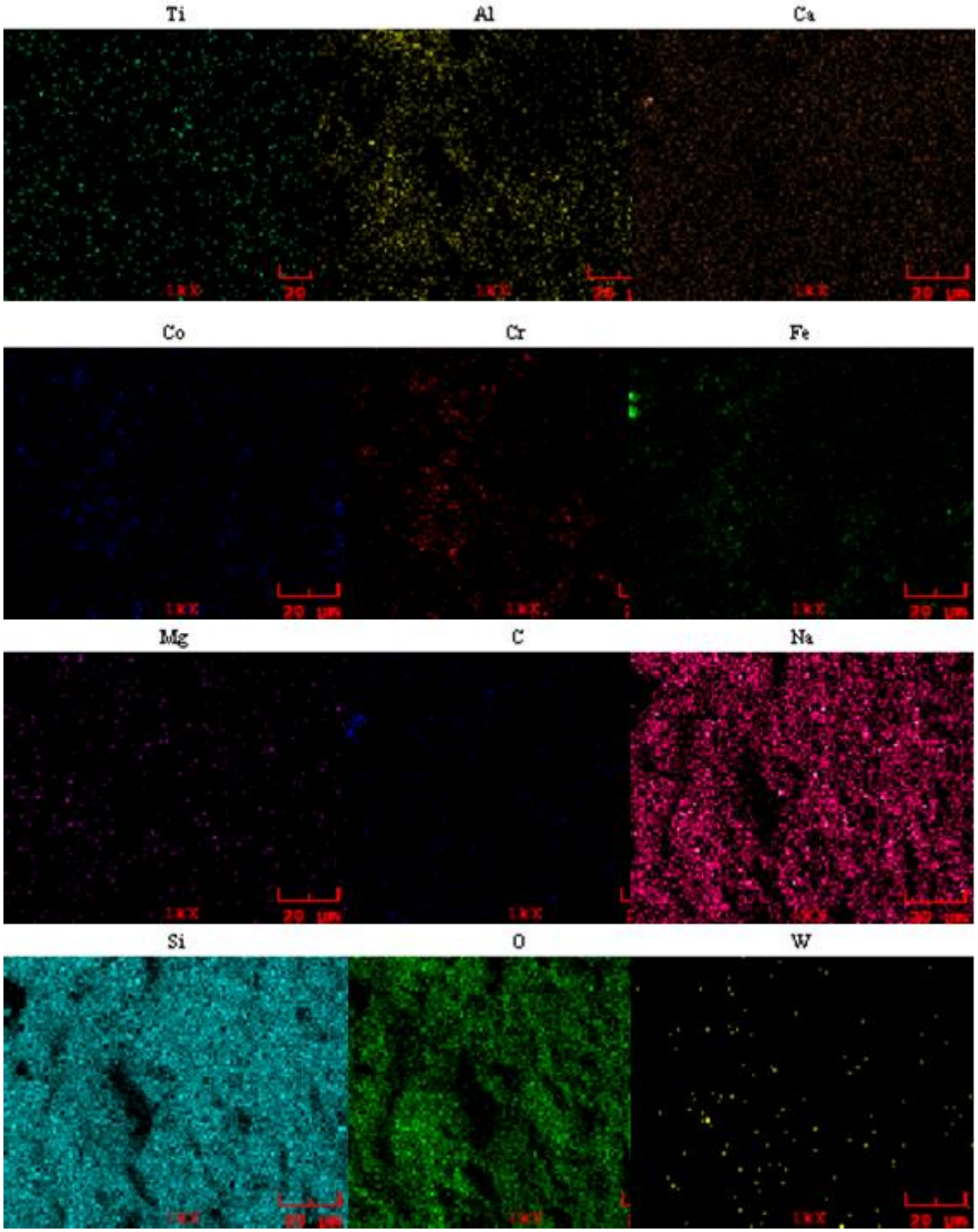


Figure 10.26 EDS mapping results of the W10 sample with addition of 1 wt. % nano-WC particles after the abrasion test

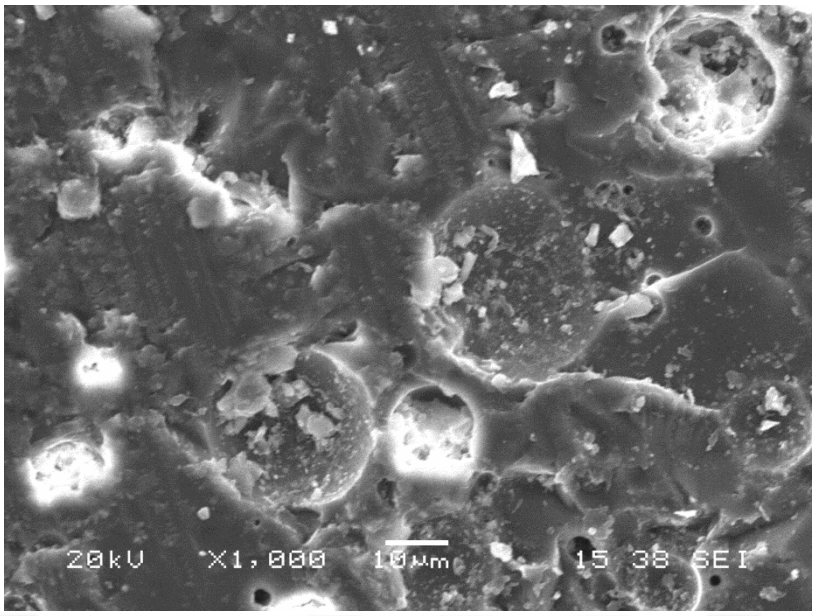


Figure 10.27 Surface SEM image of the studied W25 sample with addition of 2.5 wt. % nano-WC particles after the abrasion test

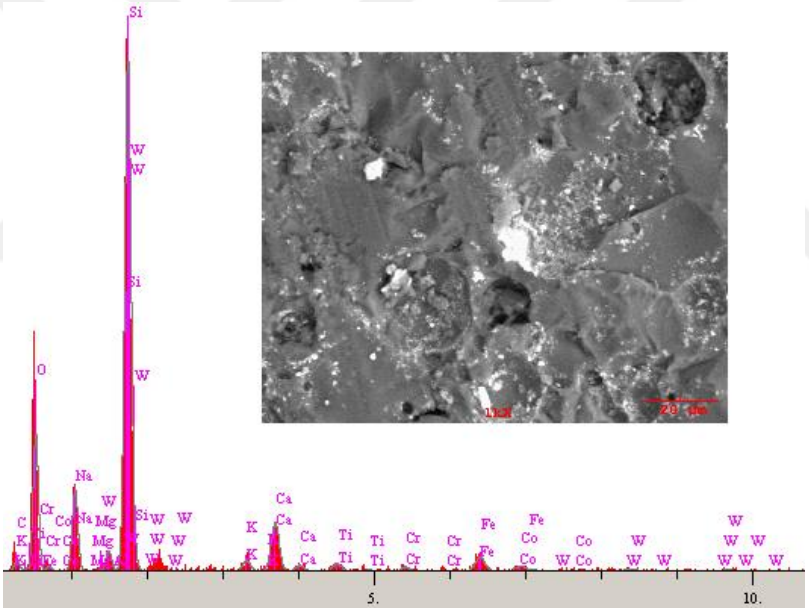


Figure 10.28 EDS analysis of the W25 sample with addition of 2.5 wt. % nano-WC particles after the abrasion test

Figure 10.27 shows the surface SEM image of the W25 sample after the abrasion test. When the surface formed after the abrasion test is examined, the voids and abrasion traces are clearly observed. Compared to the W10 sample, it can be said that the formation of vitreous flake decreases. When abrasion resistance is compared in terms of vitreous flake formation and abrasion traces, it is observed that the effect of abrasion trace formation on resistance is greater. The pieces that

break with the abrasion test are the main reason for flake formation. The non-breaking of the parts can be interpreted as increased abrasion resistance. Wheels that rotate along with the abrasion behavior can not cause a rupture on the surface, but have created a abrasion trace. The traces that occur can be considered as the abrasion cannot continue and locally slip in the same region.

Figure 10.28 shows the EDS analysis of the W25 sample after the abrasion test. In the W25 sample, as in the W10 sample, dense Si and W peaks were observed, while a partial decrease in the peak intensity of other elements was observed. Also, it is understood from the situation that the C peaks are found with W peaks, the WC particles continue to exist in the structure.

Figure 10.29 shows the EDS mapping results of the W25 sample after the abrasion test. As can be seen from elemental mapping analysis, Si, O, Na, Ti and Mg elements are observed to be present in the structure. Elements W and C are located in a similar region. W and C peaks observed in the parts with abrasion traces reveal that the nano-WC particles in these regions prevent the formation of vitreous flake. WC particles fully integrated with the structure develop resistance to abrasion. However, it is observed that there are generally high levels of Fe, Al and Cr elements in large voids opened by abrasion on the surface. Similarly, much smaller voids are formed in the parts where W and C peaks are observed. The gaps formed are the result from oxidation, as in the W10 sample.

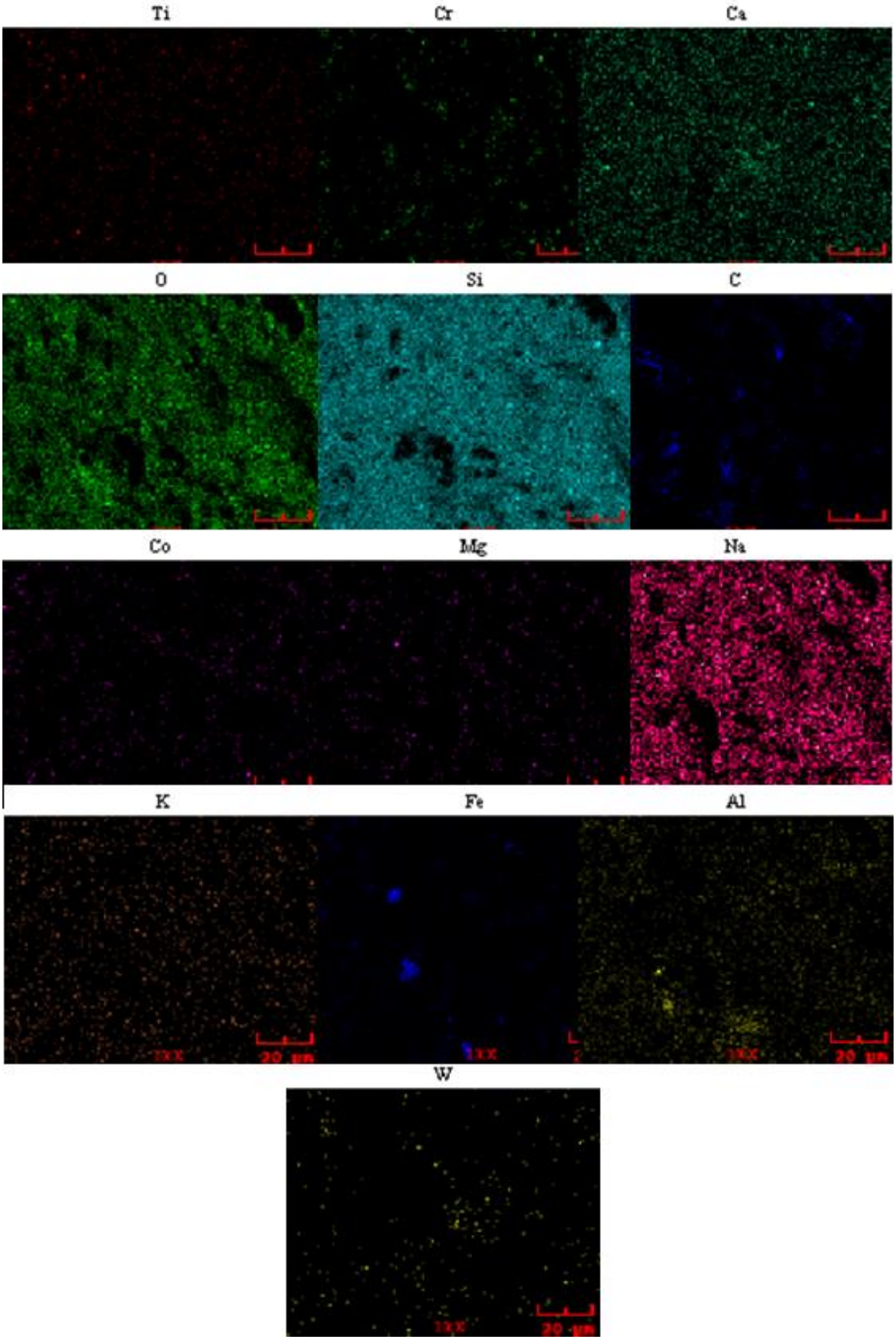


Figure 10.29 EDS mapping results of the W25 sample with addition of 2.5 wt. % nano-WC particles after the abrasion test

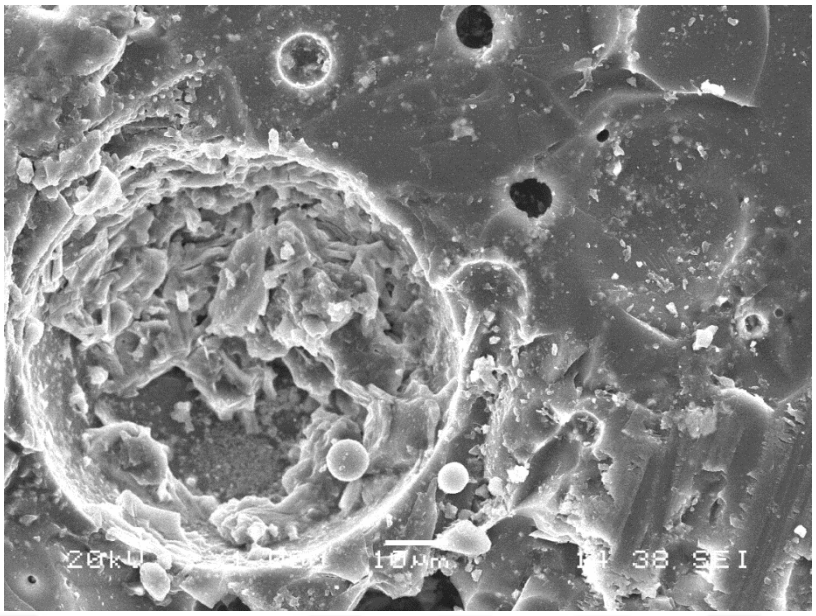


Figure 10.30 Surface SEM image of the studied W50 sample with addition of 5 wt. % nano-WC particles after the abrasion test

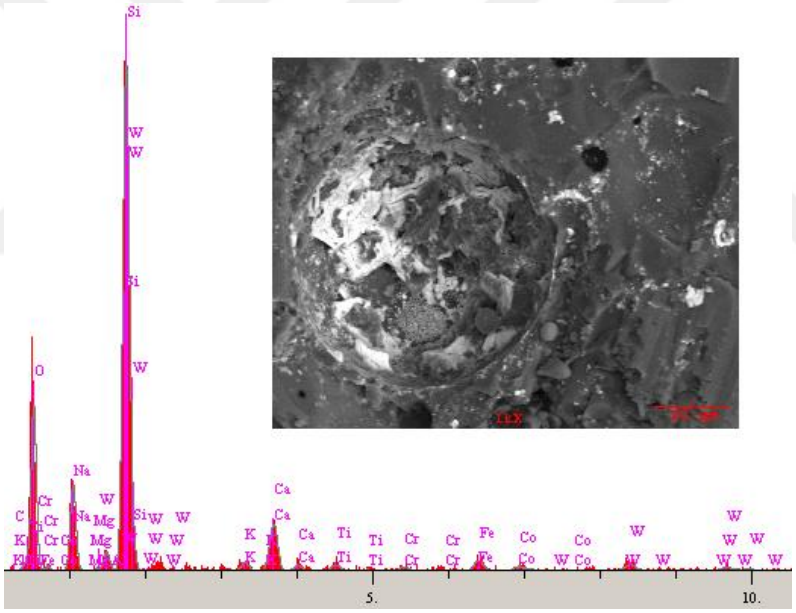


Figure 10.31 EDS analysis of the W50 sample with addition of 5 wt. % nano-WC particles after the abrasion test

Figure 10.30 shows the surface SEM image of the W50 sample after the abrasion test. When the surface of the W50 sample is examined after the abrasion test, traces of abrasion, vitreous flake formation and cavity opening are observed together. However, the gap opened is very large and contains different structures. Crack formation and crack propagation are also clearly observed in the sample. Cracks can be observed to travel through smaller gaps in the upper part of the sample. The

reason for this is that the cracks are stress areas within the structure and progress along the stress with the fragile breaking mechanism observed in the glass-ceramic structure during the abrasion test. When comparing W25 sample and W50 sample, it can be said that W25 sample is superior in terms of crack formation, flake formation and abrasion trace formation.

Figure 10.31 shows the EDS analysis of the W50 sample after the abrasion test. When EDS analysis is analyzed, a high rate of Si, W and Ca peaks are observed in the observed region. It can also be said that there is a high decrease in the ratio of Fe samples to other samples. W peaks were high and C peaks less, indicating that oxidation may occur.

Figure 10.32 shows the EDS mapping analysis of the W50 sample after the abrasion test. Elements such as Si, O, Na and K, which are observed in other samples after the abrasion test, are intensely observed. It is observed that the space in the center of the image contains W peaks. W and C peaks are located in the same regions on the surface but are not in the void. It can be said that such WC particles are on the surface but oxidized during firing. WC particles, which form a void in the structure as a result of oxidation, have not developed a resistance to abrasion. After the abrasion test, the area exposed to high stress was broken. Thus, it can be said that there is an increase in flake formation. Compared to the W25 sample, Ca peaks were observed in some parts of the regions where WC particles were found, as in the majority of the surface. It can be said that oxidation increases when compared with the elemental analysis of W25 sample after abrasion.

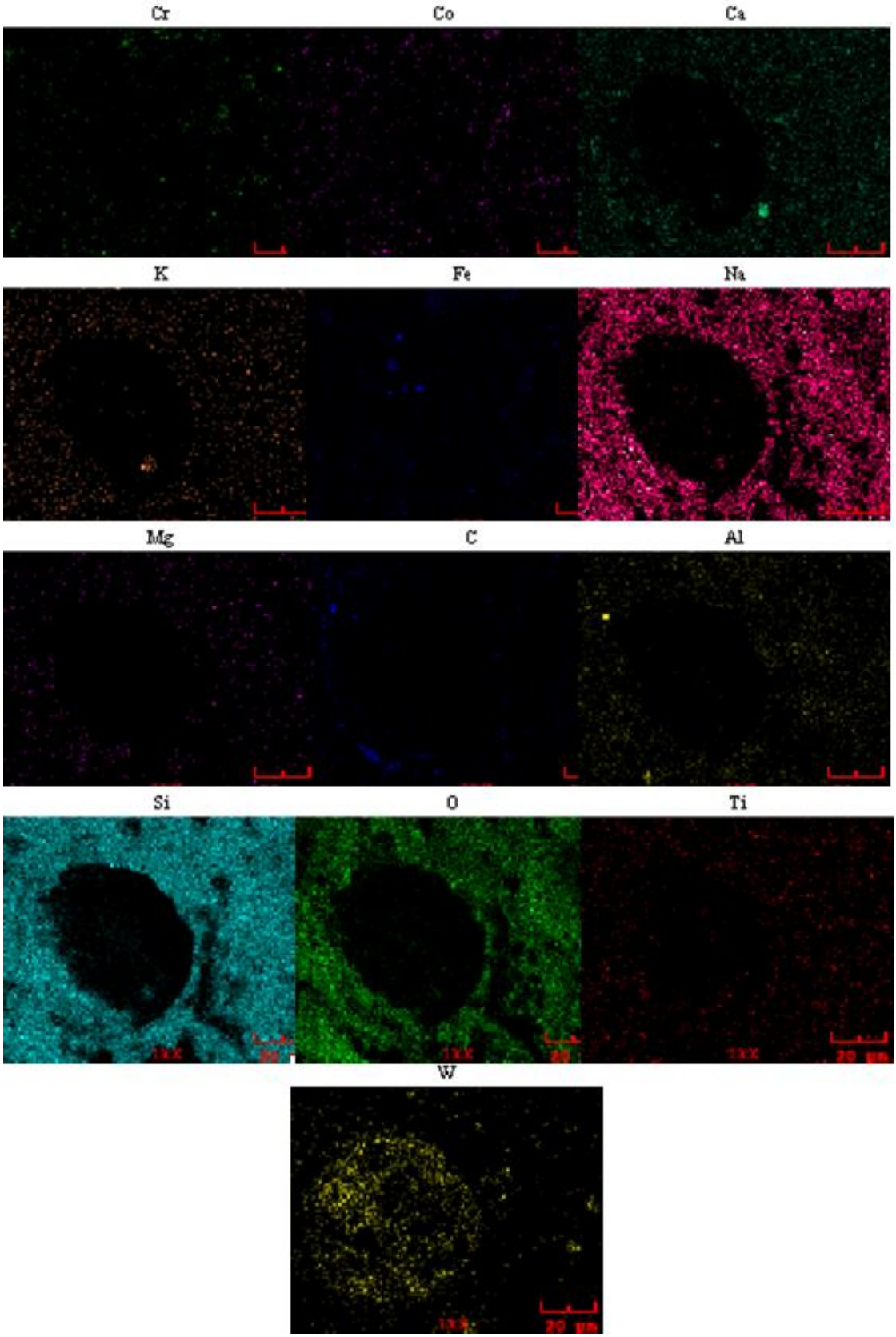


Figure 10.32 EDS mapping results of the W50 sample with addition of 5 wt. % nano-WC particles after the abrasion test

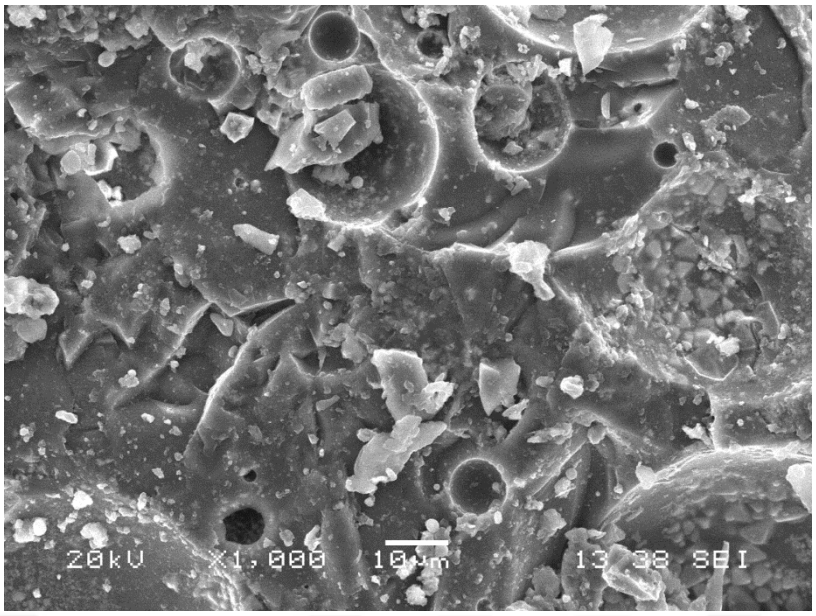


Figure 10.33 Surface SEM image of the studied W75 sample with addition of 7.5 wt. % nano-WC particles after the abrasion test

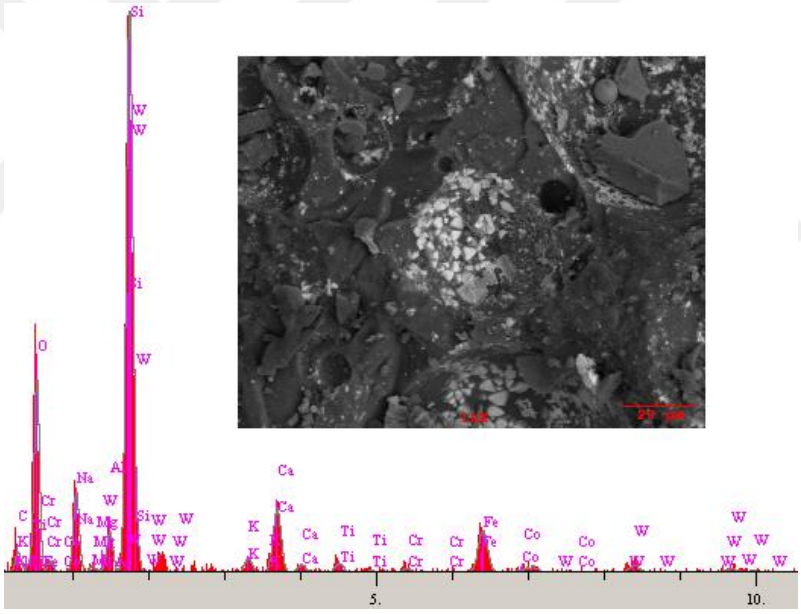


Figure 10.34 EDS analysis of the W75 sample with addition of 7.5 wt. % nano-WC particles after the abrasion test

Figure 10.33 shows the surface SEM image of the W75 sample after the abrasion test. When the surface of the W75 sample was examined after the abrasion test, it was observed that a significant reduction in abrasion traces occurred. It can also be said that the gaps opened increase in number and size. The increase in the number and size of the vitreous flake shows that the sample is similar to the reference sample. Crack formation and crack propagation are also observed on the sample

surface. It can be said that the cracks formed remain in the void areas. The crack propagation that occurs as the stress increases and the vitreous flake formation are quite high in the W75 sample and in this case it can be said in the context of the surface that a significant resistance to abrasion cannot be developed.

Figure 10.34 shows the EDS analysis of the W75 sample after the abrasion test. When the EDS analysis of the sample is examined after the abrasion test, Si and W peaks continue to be seen. Also, the fact that W and C peaks are seen together indicates that WC particles remain in the structure. When other elements are analyzed, the increase in Ca peaks continues. Compared to begore abrasion analysis, intensity in Ca peaks and low in Fe and Na peaks continue.

Figure 10.35 shows the EDS mapping analysis of the W75 sample after the abrasion test. When EDS mapping analysis of W75 sample is examined, the density in Si, O, Na, K and Mg peaks continues as in other samples. In the white part in the middle of the image observed in the surface SEM analysis of the W75 sample after abrasion, a high rate of W peaks were observed. At the same time, when the Ca peaks are examined, it is observed that the Ca concentration spreads to the surface but creates a more severe image in the middle part. The reason of this situation was scheelite formation in the sample as shown in XRD analysis. It is not observed that the new phase formed has a high impact on abrasion. This is understood by the vitreous flakes and voids formed. When the C peaks are examined, it can be said that they are found in most parts where there are W particles on the surface. The parts where W and C peaks are together are WC particles. However, with the increasing nano-WC particle concentration, no desired level abrasion traces were observed on the surface.

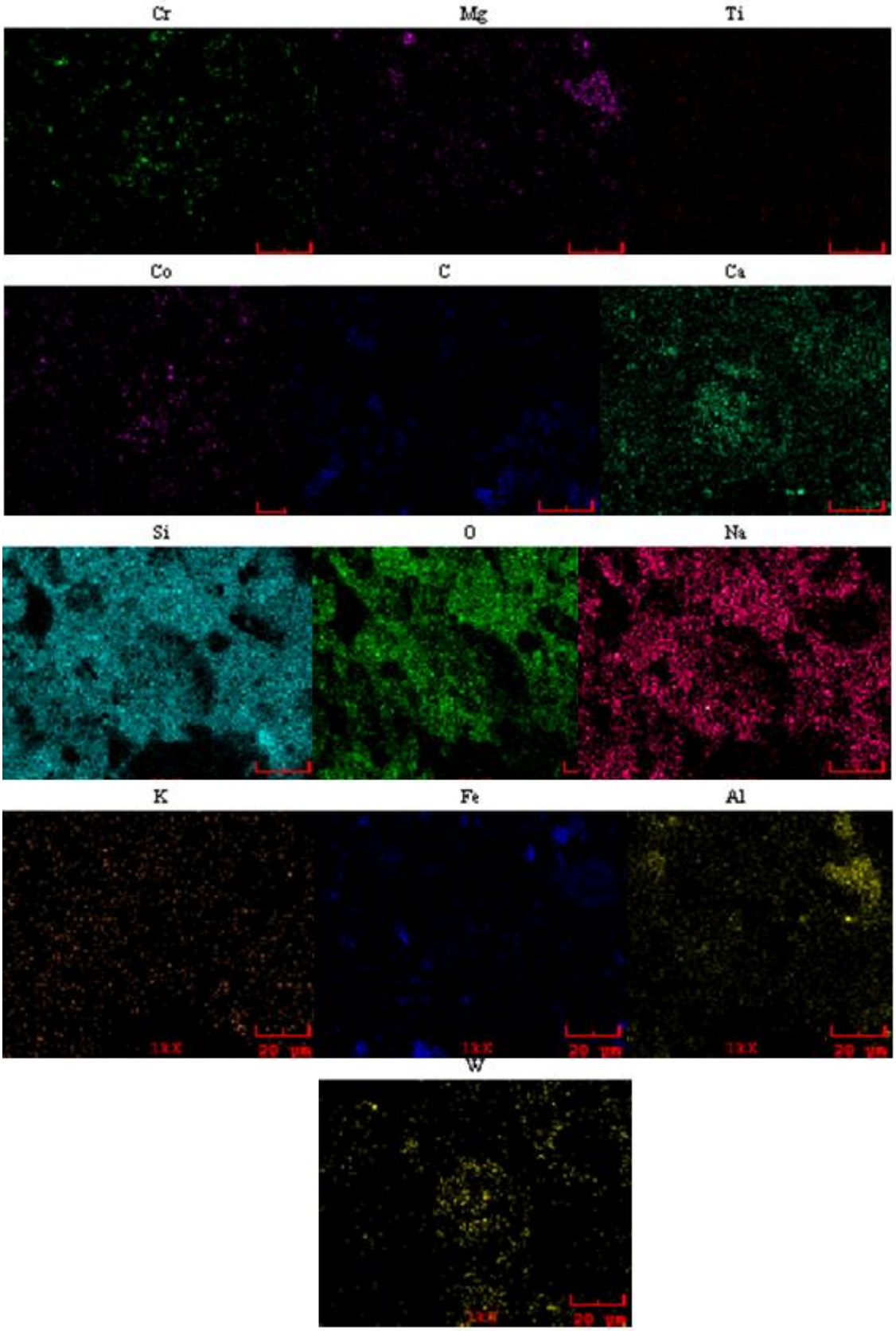


Figure 10.35 EDS mapping results of the W75 sample with addition of 7.5 wt. % nano-WC particles after the abrasion test

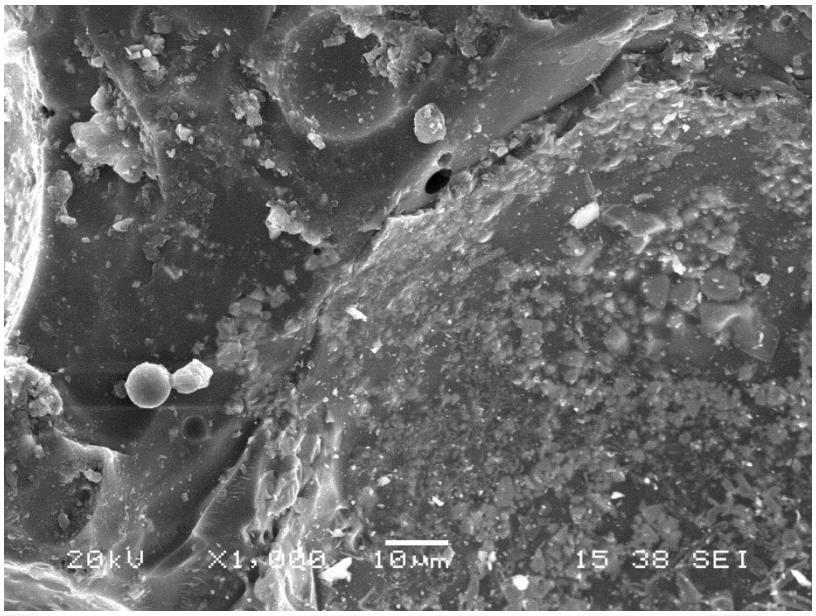


Figure 10.36 Surface SEM image of the studied W100 sample with addition of 10 wt. % nano-WC particles after the abrasion test

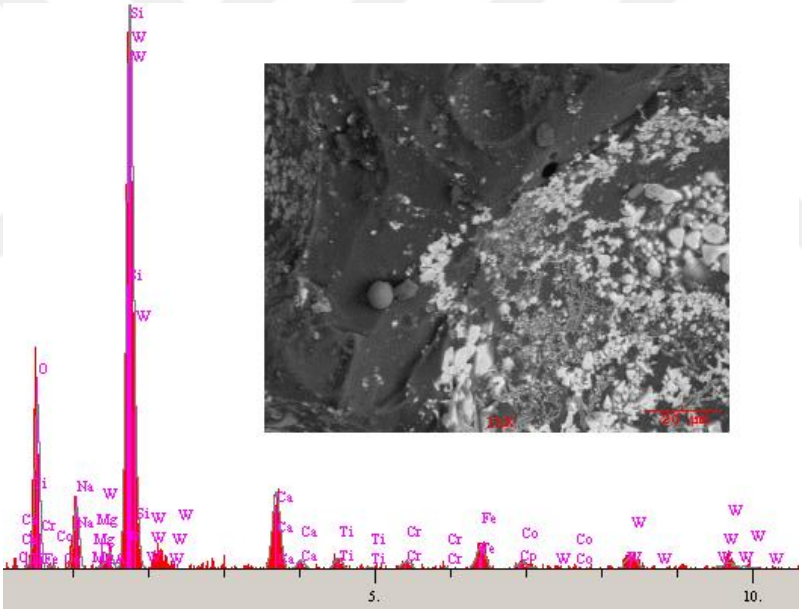


Figure 10.37 EDS analysis of the W100 sample with addition of 10 wt. % nano-WC particles after the abrasion test

Figure 10.36 shows surface SEM image of the W100 sample after the abrasion test. When the surface SEM analysis of the W100 sample was examined after the abrasion test, it was observed that no traces of abrasion were observed on the surface. In addition, the sample with the highest vitreous flake formation is the W100 sample. Besides the vitreous flake formation, the voids are much larger than other samples. When the reference sample and the W100 sample are compared, it is observed that

the W100 sample abrade harsher than the reference sample. Fractures and detachments that occur show this phenomenon.

Figure 10.37 shows the EDS analysis of the W100 sample after the abrasion test. When the EDS analysis of the W100 sample is examined after the abrasion test, it is observed that the high intensity in the Si and W peaks continues. However, decrease in C peaks is thought that WC particles cannot remain in the structure. When examined in other elements, a decrease in peaks is observed.

Figure 10.38 shows the EDS mapping results of the W100 sample after the abrasion test. When the W100 sample is subjected to EDS mapping analysis after the abrasion test, it is observed that there are high Si, O, Na, Al and Mg peaks as in other samples. Although W peaks and C peaks are compared, they show a high similarity in terms of their area, but some of the W peaks do not match the C peaks. In this case, it is thought to be caused by oxidation. Considering the W and Ca peaks scheelite phase has formed, as in the W75 sample. The gap observed in the image with W peaks and occurring in the middle of the image is thought to be due to particle detachment or breakage caused by a brittle fracture mechanism during abrasion.

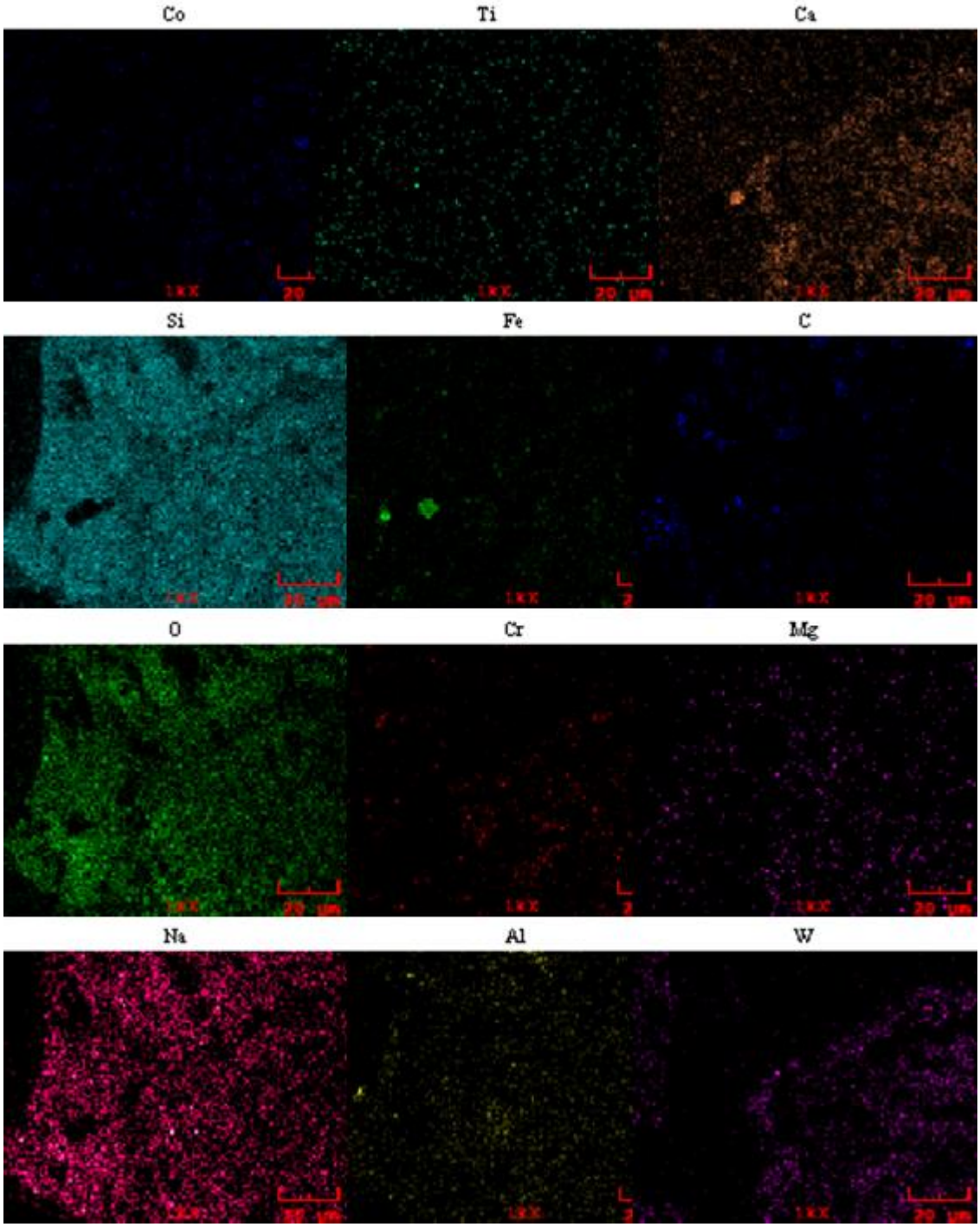


Figure 10.38 EDS mapping results of the W100 sample with addition of 10 wt. % nano-WC particles after the abrasion test

10.3.4 Cross-Section Analysis After Abrasion Test

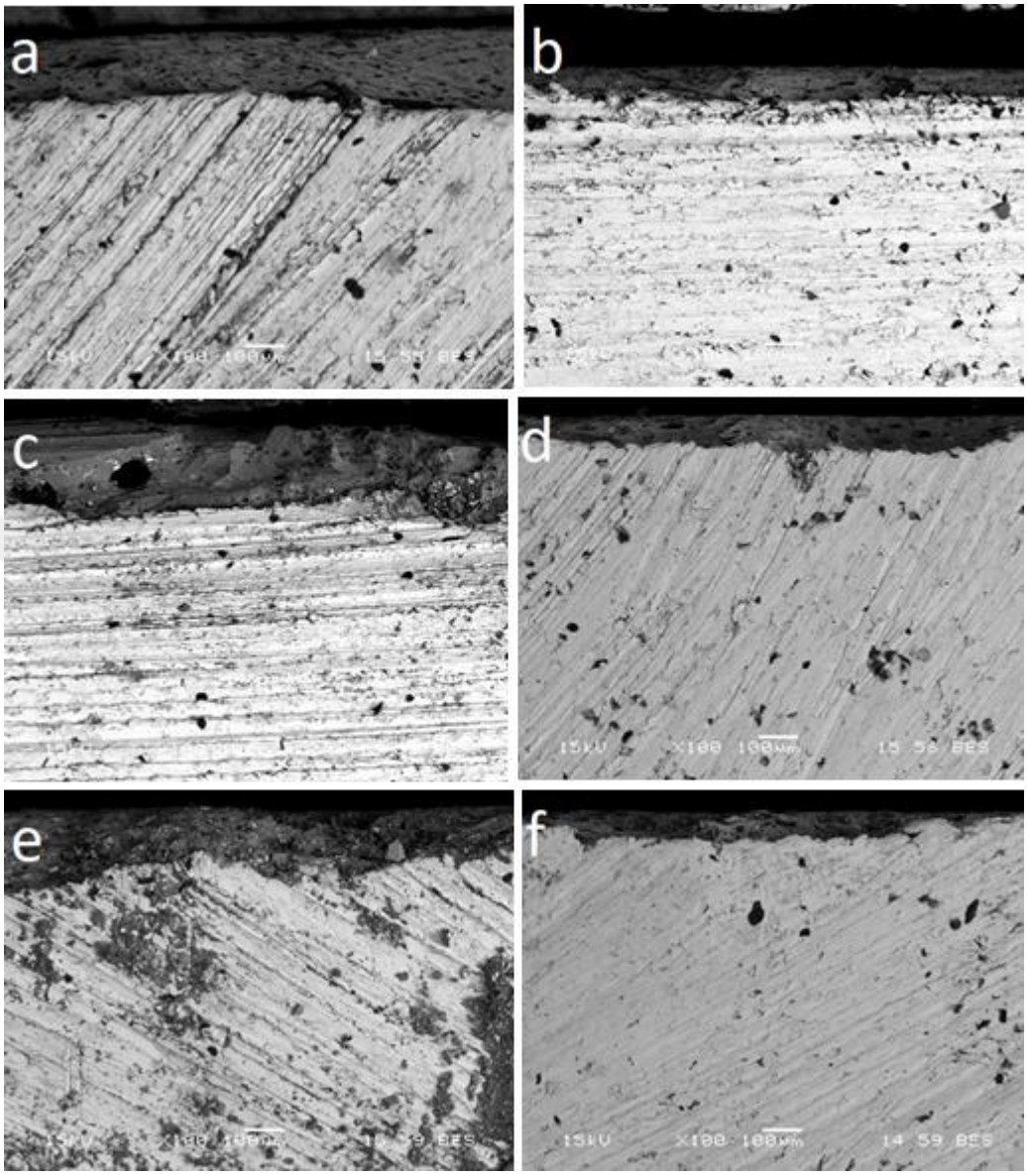


Figure 10.39 Cross-sections of the studied samples after the abrasion test; (a) reference sample, (b) W10, (c) W25, (d) W50, (e) W75 and (f) W100

Figure 10.39 shows the cross-section images of the studied samples after the abrasion test. The coating in the reference sample is more difficult to observe due to errors that may occur while cutting the sample. The coating continues to be present, as the abrasion does not progress towards the sub-surface abrasion. With the abrasion test, only the gaps in the coating became more visible and breaks were observed. The gaps on the surface are also seen in the section analysis. Considering the changes in coating thickness, the lowest change in coating thickness of W25

sample occurred. However, the coating continued to exist in all samples and the coating does not completely separate from the metal surface.

10.4 Thermal Analysis

The prepared samples were subjected to optic dilatometer analysis to examine sintering and thermal behavior. Optical dilatometer results of the samples are given in Figure 10.40. Sintering, softening, half sphere, sphere and melting temperatures of the samples are given in Table 10.2.

When the samples are examined, it is observed that generally close temperatures are obtained. Only in the W25 sample there is a rapid increase in the half sphere and spherical temperatures. Oxidation in the sample analyzed in W75 and W100 samples is thought to have an impact on sphere temperatures. Since the sintering temperature was calculated depending on the volume, very close results were obtained. At softening temperature, temperatures were in the spec of 630 ± 20 ° C. The softening and curing temperature of the W25 sample is highest. Although there was a continuous increase in melting temperatures, the W100 sample did not increase.

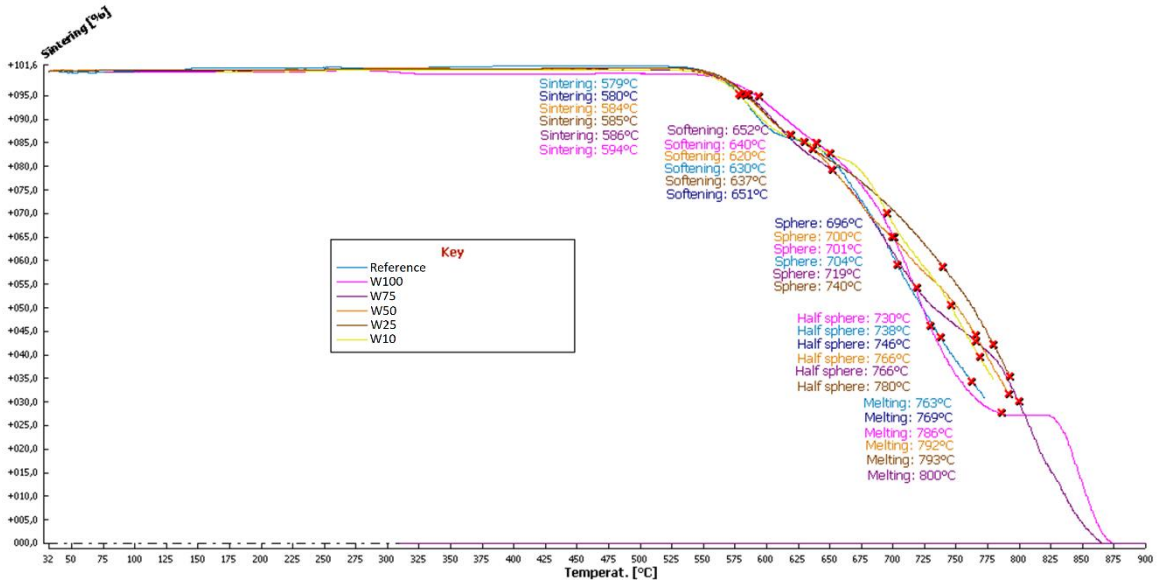


Figure 10.40 Sintering behavior graph of the studied samples

Table 10.2 Sintering, softening, half sphere, sphere and melting temperatures of studied samples

Sample Designation	Sintering (°C)	Softening (°C)	Half Sphere (°C)	Sphere (°C)	Melting (°C)
Reference	579	630	704	738	763
W10	580	651	696	746	769
W25	585	637	740	780	793
W50	584	620	700	766	792
W75	586	652	719	766	800
W100	594	640	701	730	786

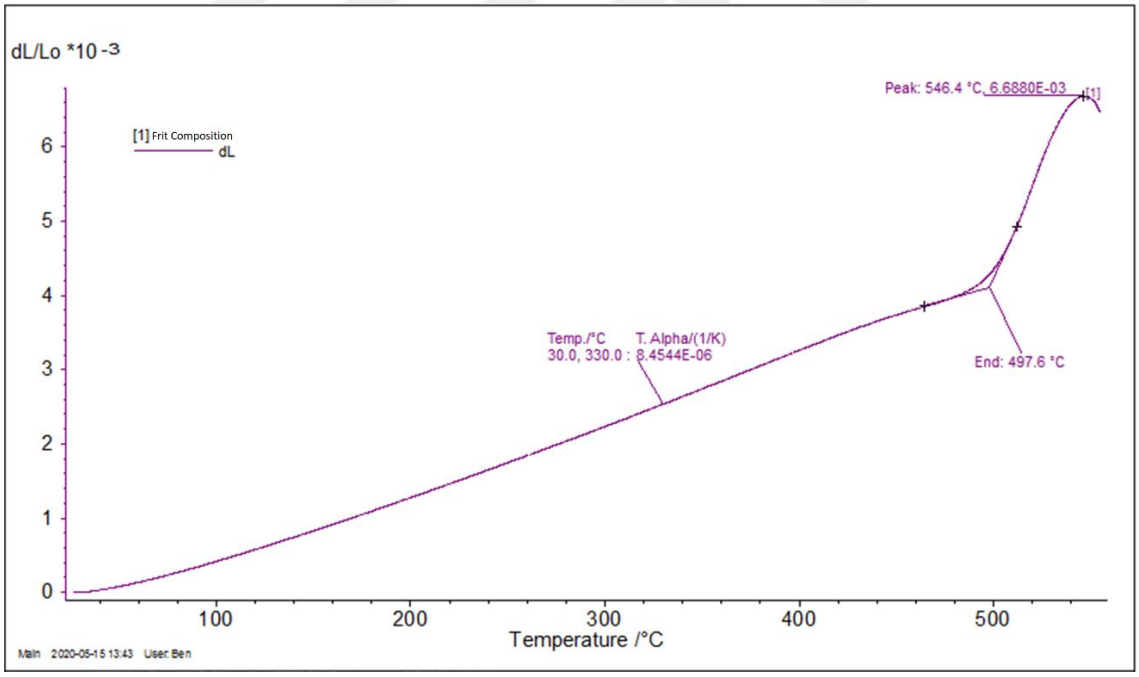


Figure 10.41 Dilatometer results of the studied frit composition

Thermal expansion coefficient of the prepared frit composition prepared for cast iron surfaces are generally desired to be small. The linear thermal expansion coefficient of the frit composition used in this study was found to be 8,4544E-06 (30

– 300 °C), as shown in Figure 10.41, and the volumetric thermal expansion coefficient is 3 times this value, because in isotropic structures, for example amorphous and vitreous materials, there is such a relationship between linear thermal expansion coefficient and volumetric expansion coefficient. Although glass transition temperature (Tg) can be calculated with many methods, it can be calculated mostly with DTA / DSC techniques. With this method, Tg can be calculated from the intersection point. The glass transition temperature of the studied frit composition was calculated as 497.6 ° C. In addition, the point where the curve peaked is defined as the dilatometric softening point and the dilometric softening temperature of the studied frit composition was found to be 546.4 ° C. The resulting composition was observed to be thermally suitable for enamel coating process.

10.5 Impact Resistance Analysis

Impact test results of the samples are given in the Table 10.3. All of the samples had high impact resistance and did not change with the addition of nano-WC in the structure. Adhesion of enamels with metal surface is chemical, mechanical, dendritic and electrolytic as stated in 4 basic theories.

Table 10.3 Impact resistance test results of the studied samples

Sample Designation	**Class**	**Comment**
Reference	1	Excellent
W10	1	Excellent
W25	1	Excellent
W50	1	Excellent
W75	1	Excellent
W100	1	Excellent

Adhesion is very good in all samples since the surface of the sample is subjected to degreasing and sandblasting before enamel coating and there is a CoO that provides electrolytic and chemical bonding in the frit structure.

10.6 Acid Resistance Analysis

The acid resistance of the samples is given in Table 10.4. Acid resistance is an important and desired property in glass-ceramic structures and enamel coatings. For this reason, high acid resistance is preferred. Although the acid resistance of the samples is not high in the initial state, it has become excellent with increasing nano-WC particles. This has been associated with increased WC particles having high chemical resistance. According to the standard, the samples were first visually inspected. The samples are rubbed dry when the trace is seen during visual inspection and if traces are left to remain, they are rubbed moist. If the trace of acid remains in the rubbed sample, it is stated that the sample fails in the acid resistance test.

Table 10.4 Acid resistance of the studied samples

Sample Designation	**Class**	**Comment**
Reference	A	Passed with rubbing test (moist)
W10	A	Passed with rubbing test (moist)
W25	A+	Passed with rubbing test (dry)
W50	A+	Passed with rubbing test (dry)
W75	AA	Passed with visual examination
W100	AA	Passed with visual examination

10.7 Coating Thickness

Although the coating thickness has not a great effect on the abrasion resistance, the coating thickness should be greater than 100 μm and the difference between the samples should not be more than ±50 μm for an optimum comparison.

Table 10.5 Coating thicknesses of the studied samples

Sample Designation	**Coating Thickness (μm)**
Reference	140
W10	140
W25	160
W50	150
W75	170
W100	190

Coating thicknesses of the samples are given in Table 10.5. As can be seen in the table, the average coating thickness of the samples is 165 ± 25 μm.

10.8 Color Measurement

Table 10.6 Color values of the studied samples in terms of D65 SCE

Sample Designation	**Color Values in D65 SCE**
Reference	L: 7,63 a: 0,75 b: -0,94
W10	L: 6,96 a: 0,84 b: -0,67
W25	L: 13,16 a: 0,59 b: -1,88

Table 10.6 Color values of the studied samples in terms of D65 SCE (continue)

W50	L: 18,11 a: 0,24 b: -2,3
W75	L: 23,08 a: 0,07 b: -2,31
W100	L: 28,04 a: 0,07 b: -2,03

Enamel coatings are also important with their aesthetic properties, so coating color is also important. In addition, color measurements were made to examine the effect of the added nano-WC particles macroscopically and shown in Table 10.6. Since the samples are generally black, spectrophotometer measurements were made with the D65 SCE mode.

10.9 Gloss Measurement

The gloss measurements of the samples were made to examine the aesthetic properties and to examine the macroscopic effects of the added nano-WC particles. Subsequent surface roughness tests are also important to understand gloss measurements. The average of the brightness analysis of the samples from 5 different regions at 60 ° is given in the Table 10.7. As can be understood from the analysis result, with the addition of nano-WC particles, the brightness values in the samples decreased and the W100 sample reached a degree that can be considered as matte. The reason for this is thought to be that the added nano-WC particles create micro-roughness on the surface and therefore cause the light to dissipate during the gloss measurement and visibility. The scattered light due to micro-roughness on the surface reduces the gloss values and makes the surface matte.

Table 10.7 Gloss values of the studied samples

Sample Designation	**Gloss (at 60°)**
Reference	107
W10	100

Table 10.7 Gloss values of the studied samples (continue)

W25	85
W50	65
W75	63,5
W100	35

10.10 Surface Roughness Analysis

One of the aesthetic properties of enamel surfaces is their smooth surface, which makes enamel coatings attractive. The low surface roughness also indicates that the vitreous structure is obtained, which is an indication of the success of the coating. Mill additives and other additives have an effect on the surface roughness. Because the materials added except for the frit structure can be dispersed in the structure or can be combined pointwise or regionally. In order to examine the effect of nano-WC particles added on the surface roughness in this study, the Ra values of the studied samples were analyzed. The values are the average of the results from 5 different regions and the analysis results are shown in the Table 10.8.

As it is understood from the table, the added nano-WC particles increased the surface roughness. As expected, the particles added as mill additive had a linear effect on surface Ra values.

Table 10.8 Surface roughness results of the studied samples

Sample Designation	**Surface Roughness – Ra (µm)**
Reference	0,264
W10	0,246
W25	0,314

Table 10.8 Surface roughness results of the studied samples (continue)

W50	0,346
W75	0,389
W100	0,502

10.11 Abrasion Resistance

The abrasion resistance of the samples has been examined using 4 different parameters: color change, brightness change, mass loss and surface roughness change.

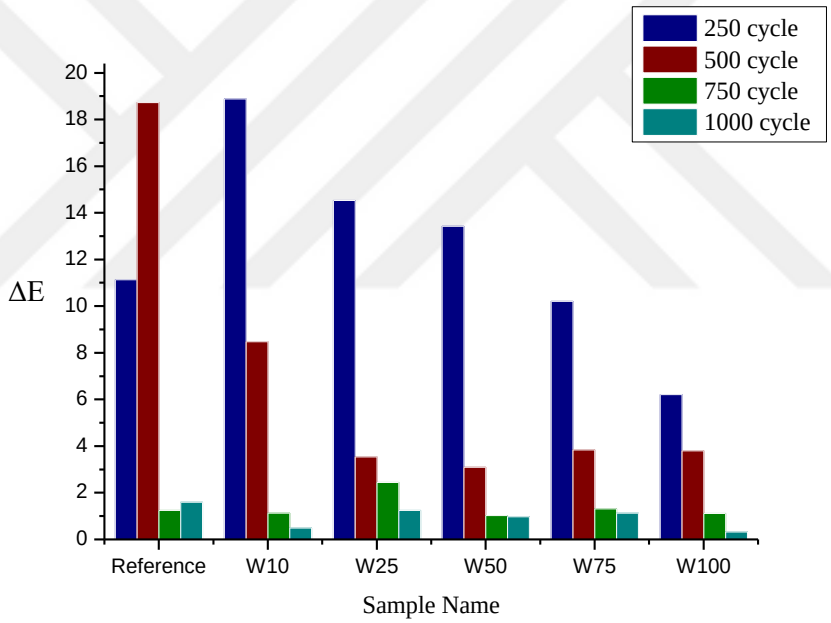


Figure 10.42 Color change of the studied sample at every 250 cycles of abrasion in terms of ΔE

Figure 10.42 shows the color change graph of the studied sample with each 250 cycles of the abrasion test. The color change of the samples was given as "E". In the figure, the reference sample showed a standard color change from the very beginning, while it showed the highest color change after 500 cycles. As a reason, it can be said that the second 250 cycle abrasion shows the highest abrasion. W10 sample showed the highest color change after 250 cycles. Then, the color change

was halved. However, the color change that occurs after 750 and 1000 cycles is below 1. W25 sample, on the other hand, showed high color change at the beginning, then color change decreased rapidly. The color change reached 3, then 2 and 1 after 500 cycles. W50 sample also showed a high color change at the beginning while later color change decreased rapidly. W75 sample also showed a color change at the beginning of 10 levels, while later the color change decreased rapidly. All of the samples added with nano-WC showed the highest color change in the first 250 cycles, and then the color change quickly decreased. Considering the particle refraction and light distribution on the surface with abrasion, it can be said that the color change increases as the resistance to abrasion decreases. In this context, W100 sample showed the lowest color change, but almost no color change in the last 250 cycles or 1000 cycles. Although color change is an important parameter in terms of examining abrasion resistance, it is not sufficient by itself. For this reason, it should be correlated with other parameters.

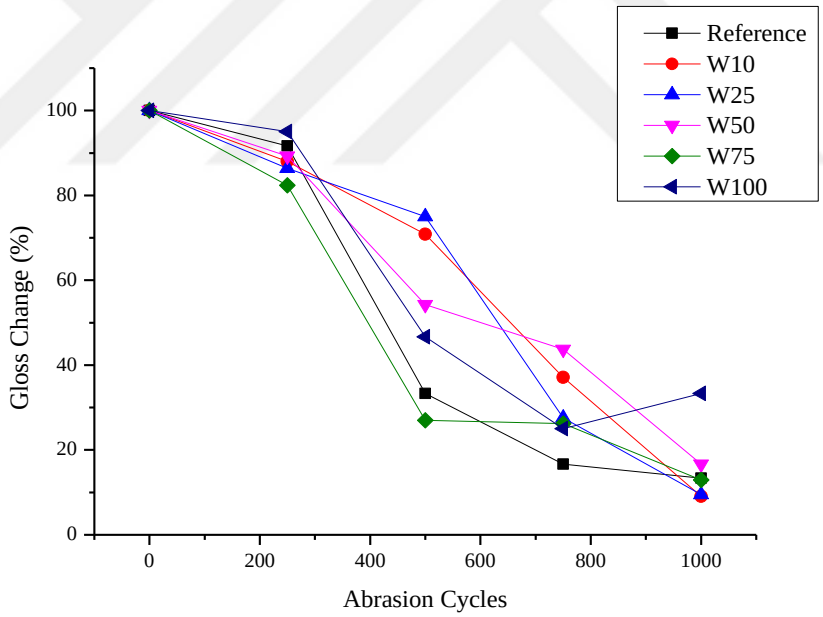


Figure 10.43 Gloss change of the studied samples during the abrasion test

Figure 10.43 shows the gloss change of the studied samples with abrasion test in terms of percentage. The change in gloss on the surface of the samples after abrasion is given in percent. The reference sample initially shows a low gloss loss, while it shows the highest gloss loss at 500 rpm. Later changes in brightness are low. W10

sample shows the highest brightness change after 750 cycles. Then the loss has decreased. W25 sample also shows the highest brightness change after 750 cycles. Then the loss has decreased. W50 sample showed the highest loss after 500 cycles. W75 sample also showed the highest loss after 500 cycles. W100 sample showed the highest abrasion resistance at 500 rpm. The change in gloss is based on the principle that the surface distorted after abrasion diffuses light. In other words, the increased roughness on the abraded surface reduces the brightness of the surface. When the brightness change is associated with the abrasion resistance, it is thought that the brightness change increases as the amount of abrasion increases. For this reason, it is observed that the initial surface abrasion is significantly reduced by increasing nano-WC in W10, W25 and W50 samples. However, the increase in gloss changes with the first abrasion in the reference W75 and W100 samples raises the notion that the abrasion cannot be prevented on the surface. When considered in total, it is observed that the W50 sample has the lowest change in brightness. However, since the change of gloss is not sufficient alone in explaining the abrasion resistance like color change, the surface roughness change and mass loss should also be analyzed.

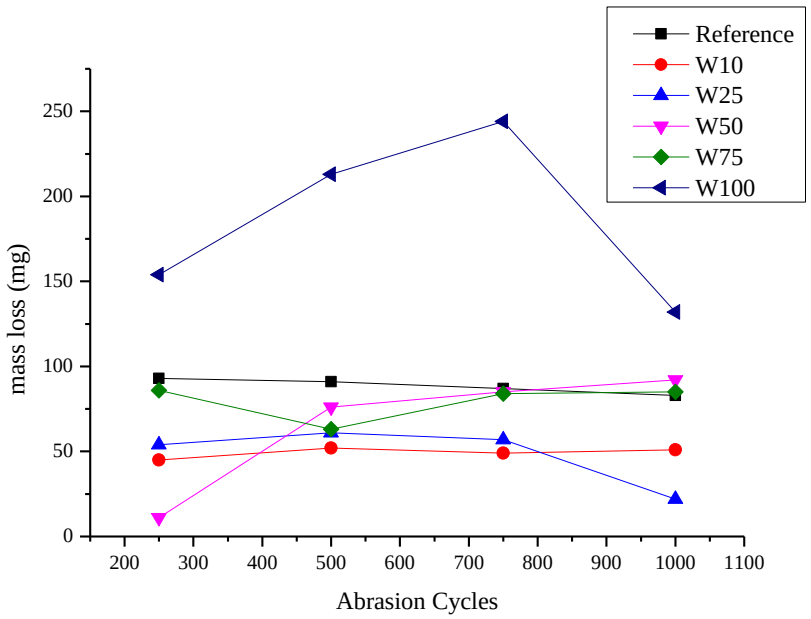


Figure 10.44 Mass loss of the studied samples during abrasion test

Figure 10.44 shows the mass loss of the studied sample during the abrasion test. The mass loss property is the most important parameter in examining the abrasion resistance. Particles separated from the surface with abrasion cause a decrease in the total mass and this change is measured. The important point here is that because the density of nano-WC particles used is high, the abraded nano-WC particles can cause a big change in mass loss. As expected, a constant mass loss is observed when the reference sample is examined. As there is no obstacle against abrasion on the surface, almost every loss of mass occurs with every abrasion cycles. It was observed that the first nano-WC particles added in the W10 sample had a positive effect against abrasion and made the abrasion stable.

Compared to the W25 sample and the W10 sample, there was a slight difference in initial abrasion losses, while the W25 sample with the last abrasion cycle showed resistance to abrasion. Thus, mass loss has been reduced in the last 250 revolutions. W50 sample, on the other hand, had a high resistance to abrasion, while later abrasion resistance gradually decreased, and mass loss increased. The increase in mass loss has become the same as the reference in the last period. W75 sample showed a resistance against abrasion only after 500 cycles. However, when analyzed in total, no major change was observed. W100 sample showed the highest mass loss in terms of mass loss, although it shows superior properties in terms of surface properties. Given the mass loss of the W10, W25 and W50 samples, it can be said to show the highest resistance to abrasion.

Surface roughness is another feature that can show abrasion resistance considering the color change and brightness change properties. Surface roughness may increase with abrasion and surface roughness may decrease with increasing abrasion. Mass and abrasion coming from the abraded surface, along with the increased resistance, may occur on the surface and decrease in roughness. It is observed that the surface roughness of the coatings in the first case is close to each other. This feature was an expected feature because enamels have low surface roughness and smooth surface due to their structure.

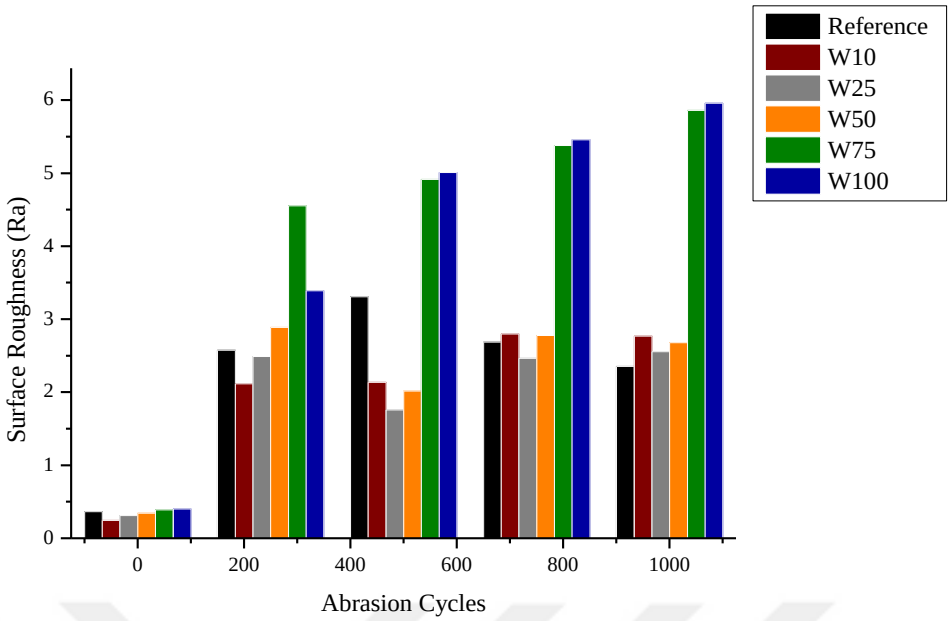


Figure 10.45 Surface roughness (Ra) values of the studied samples at every abrasion cycles

The results of the surface roughness according to the abrasion test cycles are shown in Figure 10.45. The roughness of the reference sample increased with initial abrasion, then continued to increase, and then, after 750 and 1000 cycles, the roughness remained constant and decreased. W10 sample showed the lowest surface roughness with initial abrasion, but later, 750 cycles, roughness increased relatively. W25 sample showed almost the same roughness as the reference sample with the first abrasion, while the roughness was the lowest after 500 cycles. It then increased relatively and remained stable. W75 sample showed the highest roughness with initial abrasion, while later roughness increased with increasing abrasion. Similarly with the increased abrasion on the W100 sample, an increase in roughness occurred. When the samples are examined, it is observed that the W25 and W50 samples show the highest abrasion resistance in terms of roughness.

10.12 Conclusion and Recommendation

As a result of the study, glass-ceramic coatings reinforced with nano-WC particles were achieved with 3 main findings: i) nano-WC particles showed a positive effect on local abrasion resistance and increased the abrasion resistance of the structure by dispersing homogeneously in the vitreous matrix, ii) nano-WC particles When

added to the structure in high concentrations, it should be used in a low amount since the nano carbide particles cause agglomeration and oxidation, iii) glass-ceramic coatings with high abrasion resistance and reinforced with nanoparticle, which do not harm human health and have a long service life, have been successfully developed.

Within the enamel matrix reinforced with 2,5 wt. % nano-WC, WC particles reduced the pore amount and size in the coating while preventing crack formation and progression. It showed the lowest amount of wear (0.223 g) after Taber abrasion test of 1000 cycles in total and showed the most stable color change. The brightness change was higher than other samples (around 90%), while the 1000-cycle test result showed the most stable result (2.5 μm) in surface roughness.

As the ratio of nano-WC particles used in the study increased, it was observed that WC particles were agglomerated. As a result of agglomeration, the stress points in the structure have increased and the abrasion resistance has weakened tremendously and 10 wt. % nano-WC added sample is quite good proof of this statement since the total mass loss after the 1000 cycles abrasion was 0,743 g. In addition, particles formed as a result of agglomeration have been oxidized and caused the scheelite phase to emerge. It was observed that this crystalline phase did not have a major effect on abrasion resistance and also the oxidation products are partially compatible with the vitreous matrix.

In addition, the standard enamel properties of the study were examined, and it was observed that the acid resistance increased from A class to AA class. Nano-WC particles with high chemical resistance also assisted the increase in acid resistance property. The color values of the reference sample were L: 7.63 a: 0.75 and b: -0.94, while the sample with 10 wt. % nano-WC added sample's color values were analyzed as L: 28.04, a: 0.07 and b: -2.03. In other words, as the amount of nano-WC particles in the sample increases, a linear increase in L occurs, while there is no major change in a and b values.

By improving the abrasion resistance, the migration of elements harmful to human health is prevented by elimination of detachment of vitreous matrix and the product life is improved. Glass-ceramic coatings reinforced with the nano particles have met

the standards used by the industry. Thus, a product that is easy to manufacture and apply industrially has also been introduced.

In the future, this study can be explored on the effect of preventing the agglomeration of nano-WC particles, adding different nano or micro ceramic hard particles into the mill additive and into the frit oxidic composition, on the abrasion resistance of the glass-ceramic coatings.

REFERENCES

[1] W. Höland and G. H. Beall, Glass-Ceramic Technology, 3rd Edition, New Jersey: Wiley - American Ceramic Society, 2020.

[2] V. Günay and Ş. Yılmaz, Glass Ceramics: Science and Technology (Cam Seramikler: Bilim ve Teknolojisi), Kocaeli: Tübitak Marmara Araştırma Merkezi, 2010.

[3] A. A. Andrews, S. Pagliuca and W. D. Faust, "Raw Materials for Enamels," in Porcelain Enamels: The Preparation, Application and Properties of Enamels, Mantova, Tipografia Commerciale, 2011, p. 14.

[4] M. Adamiak, Abrasion Resistance of Materials, London: IntechOpen Limited, 2012.

[5] S. Rossi, F. Deflorian, L. Fontanari, A. Cambruzzi and P. L. Bonora, "Electrochemical measurements to evaluate the damage due to abrasion on organic protective system," Progress in Organic Coatings, vol. 52, no. 4, pp. 288-297, 2005.

[6] S. Rossi, N. Parziani ve C. Zanella, Abrasion Resistance of Vitreous Enamel Coatings in Function of Frit Composition and Particles Presence, Wear, vol. 332 - 333, pp. 702 - 709, 2015.

[7] S. Rossi and E. Scrinzi, "Evaluation of the abrasion resistance of enamel coatings," Chemical Engineering and Processing: Process Intensification, vol. 68, pp. 74-80, 2013.

[8] S. Rossi, C. Zanella and R. Sommerhuber, "Influence of Mill Additives on Vitreous Enamel Properties," Materials & Design, vol. 55, pp. 880 - 887, 2014.

[9] S. Rossi, M. Fedel, F. Deflorian ve N. Parziani, Abrasion and Chemical Resistance of Composite Vitreous Enamel Coatings with Hard Particles, Surface and Interface Analysis, vol. 48, no. 8, pp. 827 - 837, 2015.

[10] S. Rossi, M. Calovi, D. Velez ve J. Munoz, Influence of Addition of Hard Particles on The Mechanical and Chemical Behaviour of Vitreous Enamel, Surface & Coatings Technology, vol. 357, pp. 69 - 77, 2019.

[11] J. Deubener, M. Allix, M. J. Davis, A. Duran, T. Höche, T. Honma, T. Komatsu, S. Krüger, I. Mitra, R. Müller, S. Nakane, M. J. Pascual, W. P. Schmelzer, E. D. Zanotto and S. Zhou, "Updated definition of glass-ceramics," Journal of Non-Crystalline Solids, vol. 501, pp. 3-10, 2018.

[12] P. W. McMillan, Glass-Ceramics, Second Edition, London: Academic Press, 1979.

[13] T. J. Headley and R. E. Loehman, "Crystallization of a Glass-Ceramic by Epitaxial Growth," Journal of the American Ceramic Society, vol. 67, pp. 620-625, 1984.

[14] X. Feng and J. Shi, "Laser-induced nonlinear crystalline waveguide on glass fiber format and diode-pumped second harmonic generation," Optical Fiber Technology, vol. 41, pp. 118-124, 2018.

[15] S. Fujita and S. Tanabe, "Fabrication, microstructure and optical properties of Er3+:YAG glass–ceramics," Optical Materials, vol. 32, no. 9, pp. 886-890, 2010.

[16] S. W. Freiman and L. L. Hench, "Effect of Crystallization on the Mechanical Properties of Li2O-SiO2 Glass-Ceramics," Journal of the American Ceramic Society, vol. 55, no. 2, pp. 86-90, 1972.

[17] P. Hing and P. W. McMllan, "The strength and fracture properties of glass-ceramics," Journal of Materials Science, vol. 8, pp. 1041-1048, 1973.

[18] M. Kamnoy, U. Intatha, A. Munpakdee ve S. Eitssayeam, Mechanical Properties and Microstructure of Li2O-SiO2-P2O5-Al2O3-K2O-CaO Glass-Ceramics, Key Engineering Materials, vol. 766, no. 1, pp. 164-169, 2018.

[19] Vitreous Enamel Association, "VEA," Media & Marketing Services and CWN Design, [Online]. Available: https://www.vea.org.uk/what-is-enamel/. [Accessed 15 February 2020].

[20] The Vitreous Enameller's Association, "The Institute of Materials, Minerals and Mining," HM The Queen, [Online]. Available: https://www.iom3.org/vitreous-enamellers-society/concise-history-enamel. [Accessed 15 February 2020].

[21] W. Faust, Procelain (Vitreous) Enamels and Industrial Enamelling Processes, Ohio: The International Enamellers Institue, 2012.

[22] N. Millar and C. Wilson, "Vitreous Enamel Coatings," in Corrosion, Oxford, Butterworth-Heinemann, 1994, pp. 3-12.

[23] E. Scrinzi and S. Rossi, "The aesthetic and functional properties of enamel coatings on steel," Materials and Design, vol. 31, no. 9, pp. 4138-4146, 2010.

[24] ISO, "International Organization for Standardization," [Online]. Available: https://www.iso.org/ics/25.220.50/x/. [Accessed 16 May 2020].

[25] The Porcelain Enamel Institute, Inc., "PEI," AOL, [Online]. Available: http://porcelainenamel.com/501_-_Appearance/. [Accessed 15 February 2020].

[26] The International Enamellers Institute, "IEI," l lova, [Online]. Available: http://www.iei-world.org/pagine/enamel.asp. [Accessed 15 February 2020].

[27] R. A. Eppler ve D. R. Eppler, Formulation of Glazes, Glazes and Glass Coatings, Ohio, The American Ceramic Society, 2000, pp. 15-19.

[28] A. I. Andrews, S. Pagliuca ve W. D. Faust, Enamel Composition, Porcelain (Vitreous) Enamels and Industrial Enamelling Processes The Preparation, Application and Properties of Enamels, Mantova, Gerrard Press, 2011, pp. 293-358.

[29] A. I. Andrews, S. Pagliuca ve W. D. Faust, Enamel Properties and Tests, Porcelain (Vitreous) Enamels and Industrial Enamelling Processes The Preparation, Application and Properties of Enamels, Mantova, Tipografia Commerciale, 2011, pp. 544-584.

[30] A. I. Andrews, S. Pagliuca ve W. D. Faust, Fudamentals and Cosiderations, Porcelain (Vitreous) Enamels and Industrial Enamelling Processes The Preparation, Application and Properties of Enamels, Mantova, Tipografia Commerciale, 2011, pp. 53-64.

[31] ASTM C385-58(2018), Standard Test Method for Thermal Shock Resistance of Porcelain-Enameled Utensils, Pennsylvania: ASTM - American Society for Testing and Materials International , 2018.

[32] V. V. Vargin, Technology of Enamels (Translated from Russian), London : MacLarens & Sons , 1967.

[33] M. Garcia-Valles, H. Hafez, I. Cruz, E. Vergés, M. Aly, J. Nohués, D. Ayala and S. Martinéz, "Calculation of viscosity–temperature curves for glass obtained from four wastewater treatment plants in Egypt," Journal of Thermal Analysis and Calorimetry, vol. 111, no. 1, pp. 107-114, 2013.

[34] M. E. Sumner, "Soil Chemistry," in Handbook of Soil Sciences, London, CRC Press, 2011, pp. 353-363.

[35] A. I. Andrews, S. Pagliuca and W. D. Faust, "Physical and Mechanical Properties," in Porcelain (Vitreous) Enamels and Industrial Enamelling Processes The Preparation, Application and Properties of Enamels, Mantova, Tipografia Commerciale, 2011, pp. 614-669.

[36] M. Shu, H. Yin, Q. Zhong, X. Shi and H. Han, "Effect of Glass Powder on Acid Resistance of Enamel Coating," Surface Review and Letters, vol. 24, no. 3, pp. 1750036-1 - 9, 2017.

[37] A. I. Andrews, S. Pagliuca and W. D. Faust, "Chemical and Electrical Properties," in Porcelain (Vitreous) Enamels and Industrial Enamelling Processes The Preparation, Application and Properties of Enamels, Mantova, Tipografia Commerciale, 2011, pp. 671-689.

[38] DIN 4753-3 Standard, Water heaters, water heating installations and storage water heaters for drinking water - Part 3: Corrosion protection on the water side by enamelling and cathodic protection - Requirements and testing, Berlin: Deutsches Institut Fur Normung, 2017.

[39] A. Conde ve J. J. d. Damborenea, Degradation of Vitreous Enamels, %1 içinde Reference Module in Materials Science and Materials Engineering, Madrid, National Centre of Metallurgical Research, 2016, pp. 1 - 3 .

[40] A. I. Andrews, S. Pagliuca and W. D. Faust, "Metallic Substrate for Enamelling," in Porcelain (Vitreous) Enamels and Industrial Enamelling Processes The Preparation, Application and Properties of Enamels, Mantova, Tipografia Commerciale, 2011, pp. 124-180.

[41] N. I. Min'ko ve T. A. Matveeva, Glass Enamels for Steel and Cast Iron Articles, Glass and Ceramics, vol. 56, no. 11 - 12, pp. 358 - 363, 1999.

[42] J. Wendel, Adherence of Vitreous Enamel on Cast Iron - A Never Ending Story, 20th International Enamellers' Congress, Istanbul, 2005.

[43] Arcelor Mittal, "https://automotive.arcelormittal.com/," Arcelor Mittal, [Online]. Available: https://automotive.arcelormittal.com-/products/flat/HYTSS/IF. [Accessed 16 May 2020].

[44] F. S. Shieu, M. J. Deng, K. C. Lin and J. C. Wong, "Effect of surface pretreatments on the adherence of porcelain enamel to a type 316L stainless steel," Journal of Materials Science, vol. 34, pp. 5265-5272, 1999.

[45] M. Cheng, W. Li, M. Shen, S. Zhu ve F. Wang, Glass coatings on stainless steels for high-temperature oxidation protection: Mechanism, Corrosion Science, vol. 82, pp. 316-327, 2014.

[46] A. I. Andrews, S. Pagliuca ve W. D. Faust, Frit Making, %1 içinde Porcelain (Vitreous) Enamels and Industrial Enamelling Processes The Preparation, Application and Properties of Enamels, Mantova, Tipografia Commerciale, 2011, pp. 360-387.

[47] I. Anzel and A. Goršek, "The use of water atomisation for the production of frits," Metalurgija, vol. 54, no. 3, pp. 485-488, 2015.

[48] A. I. Andrews, S. Pagliuca and W. D. Faust, "Milling and Milling Additions," in Porcelain (Vitreous) Enamels and Industrial Enamelling Processes The Preparation, Application and Properties of Enamels, Mantova, Tipografia Commerciale, 2011, pp. 389-420.

[49] ArcelorMittal Europe – Flat Products, Steel for Enamelling and Enamelled Steel, ArcelorMittal Co., Luxembourg, 2015.

[50] A. I. Andrews, S. Pagliuca and W. D. Faust, "Preparation of the Metal Surfaces for Enamelling," in Porcelain (Vitreous) Enamels and Industrial Enamelling Processes The Preparation, Application and Properties of Enamels, Mantova, Tipografia Commerciale, 2011, pp. 184-254.

[51] A. I. Andrews, S. Pagliuca and W. D. Faust, "Applications and Control," in Porcelain (Vitreous) Enamels and Industrial Enamelling Processes The Preparation, Application and Properties of Enamels, Mantova, Tipografia Commerciale, 2011, pp. 423-492.

[52] T. Zhang, Y. Bao and D. T. Gawne, "Process model of plasma enamelling," Journal of the European Ceramic Society, vol. 23, no. 7, pp. 1019-1023, 2003.

[53] Ditmer Trading & Consulting BV, "Ditmer Trading & Consulting BV," [Online]. Available: https://www.ditmer.nl/EN/Enameling/Process/. [Accessed 16 May 2020].

[54] R. A. Eppler and D. Eppler, Glazes and Glass Coatings, Ohio: The American Ceramic Society, 2000.

[55] A. H. Dietzel, Emaillierung: Wissenschaftliche Grundlagen und Grundzüge der Technologie, Scientific principles and fundamentals of technology, Berlin: Springer, 1981.

[56] B. W. King, H. P. Tripp and W. H. Duckworth, "Nature of Adherence of Porcelain Enamels to Metals," Batelle Memorial Institue, Ohio, 1959.

[57] L. G. Protasova, V. G. Kosenko and E. P. Farafontova, "Corrosion of Steel Under Enamel Coating," Glass and Ceramics, vol. 60, no. 7-8, pp. 229-230, 2003.

[58] L. Samiee, H. Sapoolaky and A. Mirhabibi, "Microstructure and Adherence of Cobalt Containing and Cobalt Free Enamels to Low Carbon Steel," Materials Science and Engineering A, vol. 458, no. 1-2, pp. 88-95, 2007.

[59] V. A. Greenhut and R. A. Haber, "Ceramics, Ceramic-Metal Systems," in Ullmann's Encyclopedia of Industrial Chemistry, Weinheim, Wiley-VCH, 2012, pp. 551-575.

[60] B. W. King, H. P. Tripp and W. H. Duckworth, "Nature of Adherence of Porcelain Enamels to Metals," Journal of the American Ceramic Society, vol. 42, no. 11, pp. 504-525, 1959.

[61] A. S. Kurlov and A. I. Gusev, "Tungsten Carbides and W-C Phase Diagram," Inorganic Materials, vol. 42, no. 2, pp. 121-127, 2006.

[62] G. S. Rohrer, "‘Introduction to Grains, Phases, and Interfaces-an Interpretation of Microstructures" Trans. AIME, 1948, vol.175, pp. 15-51, by C.S. Smith," The Minerals, Metals & Materials Society and ASM International, vol. 41, no. 5, pp. 1063-1100, 2010.

[63] E. Rudy ve S. T. Wındısch, Evidence for Zeta Fe2N-Type Sublattice Order in W2C at Intermediate Temperatures, Journal of the American Ceramic Society, vol. 50, no. 5, pp. 272-273, 1967.

[64] A. Hårsta and S. Rundqvist, "A Neutron Powder Diffraction Study of W2C," Acta Chemica Scandinavica, vol. 32a, no. 9, pp. 891-892, 1978.

[65] H. Okamoto, C-W (Carbon-Tungsten), Journal of Phase Equilibria and Diffusion, vol. 29, pp. 543-544, 2008.

[66] The tungsten-rich region of the system tungsten-carbon, Journal of the Less Common Metals, vol. 5, no. 2, pp. 181-194, 1963.

[67] T. Y. Kosolapova, Carbides, New York: Springer US, 1971.

[68] P. V. Sara, "Phase Equilibria in the System Tungsten—Carbon," Journal of the American Ceramic Society, vol. 48, no. 5, pp. 251-257, 1965.

[69] H. J. Glodschmidt, "Carbides," in Interstitial Alloys, New York, Springer US, 1967, pp. 88-213.

[70] E. K. Storms, The Refractory Carbides, New York-London: Academic Press, 1967.

[71] L. N. Butorina, "An Electron Diffraction Study of the Tungsten Carbide WC," Soviet physics, crystallography, vol. 5, 1960.

[72] A. Y. Liu, R. M. Wentzcovitch and M. L. Cohen, "Structural and electronic properties of WC," Physical Review B, vol. 38, no. 14-15, p. 9483, 1988.

[73] H. O. Pierson, Handnook of Refractory Carbides and Nitrides, Westwood, NJ: William Andrew Publishing, 1996.

[74] V. K. Sarin, "Cemented carbide cutting tools," Advances in Powder Technology, pp. 253-287, 1981.

[75] I. E. Campbell and E. M. Sherwood, High-Temperature Materials and Technology, New York: Wiley, 1967.

[76] R. D. Koester and D. P. Moak, "Hot Hardness of Selected Borides, Oxides and Carbides to 1900 °C," Journal of the American Ceramic Society, vol. 50, no. 6, pp. 290-296, 1967.

[77] M. Lee, "High temperature hardness of tungsten carbide," Metallurgical and Materials Transactions A, vol. 14, no. 8, pp. 1625-1629, 1983.

[78] S. R. Shatynski, "The Thermochemistry of Transition Metal Carbides," Oxidation of Metals, vol. 13, no. 2, pp. 105-118, 1979.

[79] M. V. Frandsen and W. S. Williams, "Thermal Conductivity and Electrical Resistivity of Cemented Transition Metal Carbides at Low Temperatures," Journal of the American Ceramic Society, vol. 74, no. 6, pp. 1411-1416, 1991.

[80] A. Perecherla and W. S. Williams, "Room-Temperature Thermal Conductivity of Cemented Transition-Metal Carbides," Journal of the American Ceramic Society, vol. 71, no. 12, pp. 1130-1133, 1988.

[81] A. S. Kurlov, S. Z. Nazarova and A. I. Gusev, "Magnetic Susceptibility of Tungsten Carbide: Relaxation and Impurity Effects," Journal of Experimental and Theoretical Physics Letters, vol. 82, no. 8, pp. 567-572, 2005.

[82] J. F. Shackelford, Y. Han, S. Kim and S. Kwon, "Ceramics," in CRC Materials Science and Engineering Handbook, Cleveland, Ohio, CRC Press, 2016, pp. 344-370.

[83] J. R. Turnlund, R. A. Jacob, C. L. Keen ve S. S. Strain, Long-term high copper intake: Effects on indexes of copper status, antioxidant status, and immune function in young men, American Journal of Clinical Nutrition, vol. 79, no. 6, pp. 1037-1044, 2004.

[84] N. Andrews, The iron transporter DMT1, International Journal of Biochem Cell Biol., vol. 31, no. 10, pp. 991-994, 1999.

[85] P. Gustavsson, R. Jakobsson, H. Johansson, F. Lewin, S. Norell ve L. E. Rutkvist , Occupational exposures and squamous cell carcinoma of the oral cavity, Occup Environ Med, vol. 55, no. 6, pp. 393-400, 1998.

[86] C. K. Abrams, S. M. Siram, C. Galsim, H. Johnson-Hamilton, F. L. Munford ve H. Mezghebe, Selenium deficiency in total parenteral nutrition, Nutr Clin Pract, vol. 7, no. 4, pp. 175-178, 1992.

[87] ASTM International, Standard Test Methods for Abrasion Resistance of Porcelain Enamels, Pennsylvania: American Society for Testing and Materials, 2016.

[88] Taber Industries, "Taber Abraser," [Online]. Available: https://www.-taberindustries.com/content/Data%20Sheets/Taber%201700%20Abraser%20Data%20Sheet_v8.pdf. [Accessed 16 May 2020].

[89] ISO, Cold rolled low carbon steel flat products for vitreous enameling. Technical delivery conditions, International Organization for Standardization, Geneva, 2013.

[90] ISO, "Vitreous and porcelain enamels — Determination of resistance to chemical corrosion — Part 2: Determination of resistance to chemical corrosion by boiling acids, boiling neutral liquids, alkaline liquids and/or their vapours," International Organization for Standardization, Geneva, 2017.

[91] ISO 2178:2016 - Non-magnetic coatings on magnetic substrates — Measurement of coating thickness — Magnetic method, International Organization for Standardization, Geneva, 2016.

[92] ISO, Textiles — Tests for colour fastness — Part J03: Calculation of colour differences, International Organization for Standardization , Geneva, 2009.

[93] ISO, ISO 2813 - Paints and varnishes. Determination of gloss value at 20 degrees, 60 degrees and 85 degrees, International Organization for Standardization, Geneva, 2014.

[94] Taber Indutries, Taber Abrading Wheels Data Sheet, [Çevrimiçi]. Available: https://www.taberindustries.com/content/Data%20Sheets/Taber%20Abrading%20Wheels%20Data%20Sheet_v6.pdf. [Erişildi: 16 May 2020].

[95] A. Warren, A. Nylund and I. Olejford, "Oxidation of Tunsgten and Tunsgten Carbide in Dry and Humid Atmospheres," International Journal of Refractory Metals & Hard Materials, vol. 14, no. 5-6, pp. 345-353, 1996.

[96] A. E. Newkirk, "The Oxidation of Tunsgten Carbide," Journal of the American Ceramic Society, vol. 77, no. 17, pp. 4521-4522, 1955.

[97] A. V. Kurlov and A. I. Gusev, "Oxidation of tungsten carbide powders in air," International Journal of Refractory Metals and Hard Materials, vol. 41, pp. 300-307, 2013.

[98] A. M. Abdel-Rehim, "Thermal Analysis and X-ray Diffraction of Synthesis of Scheelite," Journal of Thermal Analysis and Calorimetry, vol. 64, no. 3, pp. 1283-1296, 2001.

[99] L. L. Chang, M. G. Scroger and B. Phillips, "Alkaline-Earth Tungstates: Equilibrium and Stability in the M-W-O Systems," Journal of the American Ceramic Society, vol. 49, no. 7, pp. 385-390, 1966.

[100] S. Kobayashi, M. Misawa and K. Suzuki, "A Structural Study of Glass Formation of a Na2O-WO3 System," Journal of Non-Crystalline Solids , vol. 91, no. 2, pp. 180-190, 1987.

[101] B. W. King, H. P. Tripp ve W. H. Duckworth, Nature of Adherence of Porcelain Enamels to Metals, Journal of American Ceramic Society, vol. 42, no. 11, pp. 504 - 525, 1959.

[102] H. Sarpoolaky and A. Mirhabibi, "Influence of bubble structure on adherence and chemical durability of porcelain enamel," Advances in Applied Ceramics, vol. 107, no. 1, pp. 27-33, 2008.

[103] E. Scrinzi ve R. S., The aesthetic and functional properties of enamel coatings on steel, Materials & Design, vol. 31, no. 9, pp. 4138-4146, 2010.

[104] R. Brook, Processing of ceramics, Weinheim: Wiley-VCH, 1996.

PUBLICATIONS FROM THE THESIS

Contact Information: nurullah.copoglu@gmail.com

Conference Papers

1. N. Çöpoğlu, Ş. M. Gülen, M. Kaya, B. Tanış, T. Cengiz and B. Çiçek, "Abrasion Resistance of Vitreous Enamel Coatings with Addition of Boron Carbide (B_4C) Particles," in *International Boron Symposium*, Nevşehir, 2019.